WDL-TR2629
30 OCTOBER 1965

INTERPLANETARY NAVIGATION AND GUIDANCE STUDY

VOLUME II — TECHNICAL REPORT

GPO PRICE $ _____

CFSTI PRICE(S) $ _____

CONTRACT NO. NAS8-11198

Hard copy (HC) 4.00

Microfiche (MF) .65

ff 653 July 65

PREPARED FOR:

MARSHALL SPACE FLIGHT CENTER
HUNTSVILLE, ALABAMA

WDL-TR2629
30 October 1965

INTERPLANETARY NAVIGATION AND GUIDANCE STUDY

VOLUME II

TECHNICAL REPORT

Prepared by

PHILCO CORPORATION
A Subsidiary of Ford Motor Company
WDL Division
Palo Alto, California

Contract No. NAS 8-11198

Prepared for

MARSHALL SPACE FLIGHT CENTER
Huntsville, Alabama

FOREWORD

This volume contains the detailed results of the navigation and guidance analysis performed uncer contract NAS 8 11198 for Marshall Space Flight Center. These results are summarized in Volume I of this report. The tables and figured referenced in this volume are contained in Volume III of this report.

ABSTRACT

The primary objective of Contract NAS 8-11198 is to establish the basic requirements for an Advanced Spaceborne Detection, Tracking, and Navigation System capable of performing interplanetary missions. The study has been restricted to an analysis of navigation and guidance requirements during the midcourse and orbital phases of a 1975 round-trip Mars mission. The guidance and navigation requirements for the powered flight and/or atmospheric maneuvering phases have not been analyzed. The 532 day round-trip trajectory which is used has high energies on both the Earth-to-Mars leg and the return. A low energy Earth-Mars trajectory is also used to determine the influence of the trajectory itself on the results which are obtained. Four navigation system configurations are evaluated under the assumption that the observation data are processed with a minimum variance Kalman filter to estimate the vehicle state.

The results of this evaluation for the Deep Space Instrumentation Facility (DSIF) Tracking network (System I), shows that this system is capable of an ultimate guidance accuracy at Mars of approximately $\pm$100 km. This accuracy is obtained with present-day DSIF measurement capabilities and under the assumption that uncertainties in bias error sources (e.g., tracking station locations and physical constants) will have been removed by their estimation on earlier missions. Bias errors in the tracker station locations of 100 meters east and north degrade the DSIF accuracy at Mars to $\pm$250 km. These results are quite trajectory-dependent. The DSIF tracking accuracy at Mars on the low-energy trajectory is $\pm$25 km.

The use of onboard theodolite or sextant navigation data in addition to the DSIF data (System II) improves the guidance accuracy at Mars by approximately two orders of magnitude. The onboard observations taken with this system are restricted in time to allow for (1) Earth-based

computations of state from the data, and (2) ground command of midcourse connections. A 12-arc-second instrument with the DSIF is capable of a guidance accuracy at Mars of ± 3.5 km. This system accuracy provides a three sigma confidence of hitting a 21 km atmospheric entry corridor at Mars. These results are obtained under the restrictions of the particular observation schedule which is used and the assumption of no uncertainties in the physical constants. Relaxing the instrument accuracy to 60 arc seconds results in a guidance accuracy at Mars of ± 9.1 km. The results for this system are not highly trajectory-dependent.

System III is similiar to System II, but it assumes the addition of an onboard computer which is capable of performing the navigation and guidance computations. As a result, the period of time required to transmit guidance commands from Earth can be used to obtain a better estimate of the state before the maneuver is executed. This type of system, which utilizes Earth-based tracking with a complete onboard navigation system, could be used as a primary system for a manned mission to Mars. The results indicate that System III is capable of a guidance accuracy of ± 3.5 km at Mars with an 18-arc-second instrument. The guidance accuracy with a 60-arc-second is ± 7.9 km. On the Mars-Earth return trajectory, the use of DSIF tracking alone provides a guidance accuracy at perigee of ±2.2 km. This perigee accuracy is sufficient to hit an atmospheric entry corridor if it is required. In fact, the results indicate that, on the return trajectory, there is no requirement for an onboard instrument with this system. Also, these results are not highly trajectory-dependent.

The last navigation system which is evaluated (System IV) is representative of the type of system which could be used as a backup in the event of a ground communication failure on a manned mission. It has a complete onboard navigation system with no reliance on Earth-based tracking

facilities. The results which are presented have been obtained with an ideal physical model and a particular onboard observation schedule for a theodolite. The techniques used to select the schedule are presented in the report. This system requires a 4-arc-second instrument on both the outboard and return trajectories to achieve ± 3.5 km end point guidance accuracies at Mars and Earth. With a 60-arc-second instrument, the guidance deviations at Mars and Earth are ± 36 km and ± 39 km, respectively.

The requirement of a 4-arc-second instrument to hit an entry corridor can be altered significantly by including additional measurements or changes in the observation schedule. If subtended angle range measurements are taken during the approach to Mars and Moon observations are added to the schedule on the Earth return, the instrument accuracy can be relaxed to approximately 10-arc-seconds and a ± 35 km guidance accuracy can still be maintained at both Mars and Earth. The guidance accuracy of System IV is slightly better on the low-energy outbound trajectory and the Venus swingby return than on the nominal round-trip trajectory.

The guidance accuracies which are stated above, assume impulsive velocity changes and have been obtained with a "nominal" guidance system. The error magnitudes of this system are: (1) 0.5 degrees pointing error, (2) 1 percent proportional error, and (3) 0.1 meter/second resolution error. Using this guidance system and three corrections with Systems II and III and four corrections with Systems IV, the deviations in the end constraints are 10-20 percent larger than the error in estimate of the constraints. A parametric analysis of the guidance system error sources indicates that the resolution error limits the performance after the final correction.

The midcourse velocity corrections for System IV, with a 10-arc-second instrument require 23 meters/second on the outhoused trajectory

and 110 meters/second on the return trajectory. These velocity requirements are quite dependent on the initial velocity state deviations that are assumed at injection from the Earth park orbit and upon leaving the Mars orbit for the return phase.

The results which are obtained on a Venus swingby return trajectory indicate that this type of trajectory does not require any special navigation requirements. The midcourse velocity requirements are approximately 250 meters/second, which is twice as large as is required on the direct return trajectory. These velocity requirements are obtained by using a fixed time-of-arrival guidance law at both Venus and Earth.

The navigation capabilities of three of the basic systems are also determined for the Martian orbit phase. The results are presented in terms of components of position and velocity uncertainties that are in the orbit plane and normal to it, as well as in terms of the six orbital elements. A study of DSIF tracking for various angles between the Earth-Mars line and its projection in the orbit plane, shows that the best accuracy for this system is obtained when the angle is 90 degrees.

The best overall accuracies for any of the systems are obtained with DSIF tracking and sextant observations. This results in position and velocity uncertainties of 0.2 km and 0.15 m/sec, respectively, at the end of 72 hours of tracking. The onboard navigation system (System IV) with only sextant observations can achieve accuracies of 0.8 km and 0.6 m/sec. The other navigation systems with DSIF and onboard radar, subtended angle, and radar measurements result in significantly poorer estimates in position and velocity. These results have been obtained using the nominal park orbit. The angle between the Earth-Mars line and its projection in the nominal park orbit plane is 6.0 degrees.

LIST OF SYMBOLS

MATRICES

$B(t)$	input matrix for variational equations.
$C(T)$	transformation from state vector to constraint vector.
C	correlation matrix between estimated state and unknown random parameters.
$D(T,t)$	matrix relating changes in the state at time t to changes in the end-constraints at time T.
$F(t)$	state matrix for the variational equations.
H	gradient of the measurement with respect to the state.
I	identity matrix.
K	Optimal gain for the Kalman filter.
M	covariance matrix of unknown parameters in equations of motion.
P	covariance matrix of the error in estimate of the vehicle state after a measurement.
Q	covariance matrix of measurement errors.
$\Phi(t_1;t_o)$	state transition matrix (relates changes in the state at t_o to changes in the state at t_1).
$\Phi_u(t_1;t_o)$	control transition matrix (relates changes in the control at t_o to changes in the state at t_1).
PAR	covariance matrix of the deviation state.
DEV	third-order covariance matrix of end-constraint deviations.
EST	third-order covariance matrix of error in estimate of end-constraints.

VECTORS

$\vec{B}$	target miss vector.
ϵ	guidance system execution error vector.
$\hat{N}$	unit vector in orbit plane normal to V
$\hat{V}$	unit vector along vehicle velocity vector.
$\hat{W}$	unit vector normal to orbit plane.

VECTORS

$\hat{R}$, $\hat{S}$, $\hat{T}$	unit vectors of the target constraint coordinates.
$\hat{t}$	direction of zero LOS rate.
$\hat{u}$	direction of maximum LOS rate.
U	nominal control vector.
u	deviation control vector.
V	inertial velocity vector of vehicle relative to body of greatest attraction.
$\hat{X}$, $\hat{Y}$, $\hat{Z}$	unit vectors of target centered coordinate system.
X	nominal state vector.
$\underline{x}$	third-order position deviation state vector.
x	sixth-order deviation state vector.
$\bar{x}$	mean value of x.
$\hat{x}$	estimate of deviation state
$\tilde{x}$	error in estimate of deviation state.
$\underline{\hat{x}}_g$	optimal estimate of the state after an observation.
Y	measurement.
y	measurement deviation.
z	expanded deviation state vector which includes equation of motion and measurement error constants.

SCALAR CONSTANTS, VARIABLES AND FUNCTIONS

a	semi-major axis of an orbit.
$E\left(f(x)\right)$	expected value of the function of x.
e	eccentricity of an orbit.
i	orbit plane inclination.
L	loss function minimized by the Kalman filter.
$P(x)$	probability density function
q	radius of closest approach for an orbit.

SCALAR CONSTANTS, VARIABLES AND FUNCTIONS

V_{inf}	vehicle velocity at an infinite distance from a body.
ΔV	RMS values of required velocity at a guidance correction $= \sqrt{\text{trace } E(\hat{\underline{x}}_g \hat{\underline{x}}_g^T)}$
α	a constant used to account for an onboard monitor for guidance corrections.
β	separation angle for two star-planet measurements.
δ	reference direction for sextant measurements.
θ	true anomaly angle.
u	gravitational constant.
σ	standard deviation (when used with a subscript, the subscript denotes the quantity for which σ is obtained).
ω	argument of perifocus.
Ω	longitude of ascending node.
σ_P	standard deviation of pointing error.
σ_R	standard deviation of resolution error.
σ_v	standard deviation of proportional error.

TABLE OF CONTENTS

Section		Page
1	INTRODUCTION	1-1
	1.1 General Objectives and Scope	1-1
	1.2 Study Format	1-2
2	THEORETICAL ANALYSIS OF THE NAVIGATION AND GUIDANCE SYSTEMS	2-1
	2.1 Equations of Motion	2-2
	2.2 Coordinate Systems	2-4
	2.3 General Descriptions of Deterministic Midcourse Guidance Laws	2-5
	2.4 Error Analysis	2-14
	2.5 Determining the State	2-19
	2.6 Complete Midcourse Guidance Analysis	2-31
3	DESCRIPTION OF THE DIGITAL COMPUTER SIMULATION	3-1
	3.1 The Nominal Trajectory	3-2
	3.2 The Transition Matrix	3-3
4	ONBOARD MEASUREMENT TECHNIQUES	4-1
	4.1 Introduction	4-1
	4.2 Significance of the Measurement Gradient	4-1
	4.3 Onboard Navigation Instruments	4-4
	4.4 Measurement Accuracy	4-7
	4.5 Body Selection	4-8
	4.6 Star Selection	4-13
5	EARTH-MARS MIDCOURSE STUDY	5-1
	5.1 Introduction	5-1
	5.2 Midcourse Study Restrictions	5-2
	5.3 Navigation Analysis	5-4
	5.4 Guidance Analysis	5-20

TABLE OF CONTENTS (CONT'D.)

Section		Page
6	MARS-EARTH MIDCOURSE STUDY	6-1
	6.1 Introduction	6-1
	6.2 Study Restrictions	6-2
	6.3 Navigation Analysis	6-3
	6.4 Guidance Analysis	6-10
	6.5 Summary	6-14
7	MARS ORBITAL ANALYSIS	7-1
	7.1 Introduction	7-1
	7.2 Study Restrictions	7-2
	7.3 Navigation Analysis	7-3
	7.4 Comparison of Systems Performance	7-10
8	RECOMMENDATIONS	8-1

Appendix		
A	DERIVATION OF THE COVARIANCE MATRIX $\lceil \rceil_v$	A-1
B	MEASUREMENT GRADIENT	B-1
C	INTERPLANETARY TRAJECTORIES	C-1
D	DERIVATION OF ORBITAL ELEMENT GRADIENTS	D-1

SECTION 1

INTRODUCTION

1.1 GENERAL OBJECTIVES AND SCOPE

The primary objective of contract NAS8-11198 is to establish the basic requirements for an Advanced Spaceborne Detection, Tracking and Navigation System capable of performing future interplanetary missions. To achieve this objective, the following tasks had to be completed:

a. Organize the study such that information is obtained which shows tradeoff between performance and system complexity, and can be used to select a system for a given mission.

b. Derive suitable mathematical techniques for calculation of performance.

c. Develop methods for data presentation which indicate accuracy tradeoffs between various subsystems and components within a particular system.

d. Determine the areas and components which require future research.

The scope of the study includes an evaluation of systems which utilize Earth-based and onboard navigation, and combinations of the two systems. The results which were obtained can be used to establish the capabilities of these systems to perform various missions. In order to make the problem amenable to study, however, certain restrictions on the scope of the study had to be made. The following restrictions were either suggested by or approved by MSFC personnel:

a. Primary emphasis and calculations are for the 1975 opportunity for a round-trip to Mars. The trajectory includes a stay time of about 40 days in orbit about Mars at an altitude higher than the sensible

Martian atmosphere (500 Km). The outbound flight time is 235 days, and the return flight time is 297 days. This restriction was made at the start of the study because obtaining data for all possible missions would not be feasible.

b. The covariance matrix of injection errors at the Earth is not studied as a parameter. This matrix, which is a function of the time in park orbit at the Earth, is intended to be representative of the capabilities of future launch vehicle guidance systems. The primary influence of this matrix is on the magnitude of the midcourse velocity requirements at the first guidance correction.

c. The study emphasized the following phases of the mission:
   1. Midcourse from Earth to Mars
   2. Orbital navigation at Mars
   3. Midcourse from Mars to Earth.

   These phases are probably the most demanding on the sensor requirements if one neglects the inertial components required during the accelerating (or decelerating) positions of the total mission.

1.2 STUDY FORMAT

The requirements of the navigation and guidance systems may vary considerably depending on the mission itself. This study is designed to obtain data that shows the tradeoff between onboard system complexity and the guidance and navigation system performance that can be achieved. Four navigation system configurations are considered; they vary in complexity from one that depends entirely on Earth-based tracking and computations to one that has a total onboard navigation capability. These four systems could be used for missions that vary from a simple planetary flyby mission to a round-trip manned mission.

The four navigation and guidance systems whose performance are analyzed in this study are:

a. System I

1. Onboard Equipment

(a) An attitude control system with a reference alignment procedure

(b) Rocket motor for thrusting

(c) Command system for receipt of command signals for midcourse maneuvers.

2. Earth-based Equipment

(a) DSIF Tracking Network

(b) Computation facilities

3. Typical Mission

(a) Planetary flyby

(b) Planetary orbiter

b. System II

1. Onboard Equipment

(a) Same as System I

(b) Sextant or theodolite - Measurements restricted near maneuver times to permit Earth-based computation

2. Earth-Based Equipment

(a) Same as System I

3. Typical Missions

(a) Close Approach Flyby

(b) Planetary Orbiter

c. System III

1. Onboard Equipment

(a) Same as System II

(b) Onboard radar

(c) Digital Computer which will be used during the terminal part of the outbound midcourse phase, orbital navigation phase, and the initial part of the midcourse return phase. This system would allow rapid onboard calculations when they are required during the rapidly changing portions of the flight which occur at great distances (and consequently cause command time delays) from the Earth.

2. Earth-Based Equipment
   (a) Same as System II
3. Typical Mission
   (a) Manned round trip to Mars
   (b) Planetary orbiter
   (c) Lander

d. System IV
1. Onboard Equipment
   (a) Same as System III with the exception of the command system; System IV places no reliance on Earth-based facilities.
2. Earth-based Equipment
   (a) None; complete onboard system for all phases of the mission.
3. Typical Mission
   (a) Manned Round trip to Mars

In order to make this report self-contained, a certain amount of introductory material has been included in Sections 2, 3, and 4, including the theory of the guidance and navigation analysis; a description of the computer simulation; and a description of special onboard navigation techniques that have been developed in conjunction with this study. The principal results of this study that are presented in Sections 5, 6, and 7 have been obtained from statistical error analyses of the outbound midcourse phase, the return midcourse phase, and the orbital phase, respectively. Each of the four systems is evaluated for the outbound phase; however, only systems III and IV are considered for the return leg since these systems are representative of systems that could be used on a round-trip manned mission to Mars. The orbital phase is studied independently of the two midcourse phases. Systems I, III, and IV are evaluated for this phase.

The instrument error data and the results of the different analyses presented in this report are all one-sigma standard deviations. The figures and tables that are discussed in this report are presented in Volume III.

SECTION 2

THEORETICAL ANALYSIS OF THE NAVIGATION AND GUIDANCE SYSTEMS

The function of the navigation system, as defined in this report, is to obtain an estimate of the vehicle state based on either direct observations of the vehicle (Earth-based tracking) or observations of celestial bodies whose positions are known (onboard tracking). Since only midcourse guidance corrections are studied in this document the function of the guidance system is to eliminate state deviations from the nominal trajectory at the end of the midcourse phase, according to a specific guidance law. The complete analysis of both of these systems requires the use of advanced techniques. It is the purpose of this section, therefore, to introduce the theoretical concepts and notations that will be used throughout the report.

The use of linear analysis about a nominal trajectory is described at the beginning of this section, and will be applied to all phases of the study. This assumption permits the derivation of the state transition matrix, which is essential in propagating both navigation and guidance system errors along the nominal trajectory. This matrix is also useful in deriving guidance laws. Three midcourse guidance laws are derived in this section based on deterministic deviations in the state. However, since the state deviations in general, are not deterministic quantities, the guidance corrections must be made on the basis of estimates of the state.

Furthermore, it is the statistical errors in the navigation and guidance systems that will be studied in this report. Therefore, the statistical concepts of state estimation are introduced in this section. The derivation of the Kalman filter, which is used to obtain a best estimate of the state, is included. In addition, a method of propagating statistical errors is discussed. Finally, the derivation of specific guidance laws that are based on statistical estimates of state are derived, and the guidance execution errors are discussed.

2.1 EQUATIONS OF MOTION

It is assumed in this report that the trajectory of the space vehicle can be defined by a set of nonlinear differential equations of the form

$$\dot{X} = f(X, U, t) \tag{2-1}$$

The n^{th}-order vector X defines the state of the vehicle, U is an ℓ^{th}-order vector defining the control motions, and t is the running-time variable. In general, X will consist of the vehicle's position and velocity some particular three-dimensional coordinate system. Rarely, however, can these quantities be measured directly. Instead, quantities such as range, range-rate, azimuth, etc., are observed by tracking stations. It will therefore be assumed that the observed quantities can be related to the original state X by

$$Y = G(X, t) \tag{2-2}$$

In order to perform an analysis of systems represented by (2-1) it is necessary to linearize these equations about a nominal trajectory. The total state is then defined as the sum of the nominal state and a state composed of deviations about the nominal, that is,

$$\left.\begin{aligned} X &= X_{Nom} + x \\ U &= U_{Nom} + u \end{aligned}\right\} \tag{2-3}$$

If (2-1) is now written as

$$\dot{X}_{Nom} + \dot{x} = f(X_{Nom} + x, U + u), \tag{2-4}$$

and expanded in a Taylor series, the result is

$$X_{Nom} + x = f(X, U, t) + \frac{\partial f}{\partial X} x + \frac{\partial f}{\partial U} u + \ldots, \tag{2-5}$$

where higher-order terms have been neglected and the partial derivatives are evaluated for numerical values on the nominal trajectory. Subtracting (2-1) from (2-5) yields the time-varying state equation for the deviations,

$$\dot{x} = \frac{\partial f}{\partial X} x + \frac{\partial f}{\partial U} u, \tag{2-6}$$

or

$$\dot{x} = F(t)\ x + B(t)\ u. \tag{2-7}$$

For n states and ℓ controls, F(t) is an n × n matrix and B(t) is an n × ℓ. Equation (2-7) is referred to as the variational equation.

Similarly, expanding (2-2) as

$$Y + y = G(X,t) + \frac{\partial G}{\partial X} x(t) \tag{2-8}$$

and subtracting (2-2), gives the linear relationship between the deviation state and the measurement deviation,

$$y = \frac{\partial G}{\partial X} x = H(t)\ x \tag{2-9}$$

The solution of (2-7) and (2-9), for constant control increments over the interval $t_1 \leq t \leq t_2$, may be expressed as

$$(t_2) = \Phi(t_2;t_1)\ x(t_1) + \Phi_u(t_2,t_1)\ u(t_1), \tag{2-10}$$

and

$$y(t_2) = H(t_2)\ x(t_2), \tag{2-11}$$

where Φ is the n × n transition matrix which relates the deviation of the state at t_1 to that at t_2, and Φ_u is a n × ℓ matrix which relates the deviation of the state at t_2 to a unit variation in control at t_1. The

elements of Φ and Φ_u are referred to as sensitivity coefficients. In general, Φ_u will be computed for large time intervals by numerical integration.

2.2 COORDINATE SYSTEMS

All simulations which are done on the digital computer for the trajectory computations are done in the Earth equator and equinox of 1950 coordinates system. In order to permit a better physical interpretation of the results that are obtained, however, these results will be presented in a number of other coordinate frames. These coordinate systems are described below.

2.2.1 Target Coordinates

This coordinate frame was used to define the nominal trajectory end constraints for the Earth-Mars trajectory. It is target-centered at the time of the trajectory arrival (as shown in Figure 2-1) and is oriented such that the $\hat{x}$ axis is directed toward the Sun, the $\hat{z}$ axis is normal to the target planet's orbit plane, and the $\hat{y}$ axis is in the direction of $\hat{z} \times \hat{x}$. The $\hat{x}$-$\hat{y}$ plane in this coordinate system is, therefore, nearly in the ecliptic plane.

2.2.2. N V W Coordinates

This coordinate system is useful for describing the data which are obtained in the study in terms of the trajectory plane. The coordinates are shown in Figure 2-2A. The unit vectors $\hat{N}$, $\hat{V}$, and $\hat{W}$ are defined as follows:

$$\hat{V} = \frac{\vec{V}}{|\vec{V}|} \qquad \text{(along the velocity vector)} \qquad (2\text{-}12)$$

$$\hat{W} = \frac{\vec{R} \times \vec{V}}{|\vec{R} \times \vec{V}|} \qquad \text{(normal to the orbit plane)} \qquad (2\text{-}13)$$

$$\hat{N} = \hat{V} \times \hat{W} \qquad \text{(in the orbit plane normal to the velocity)} \qquad (2\text{-}14)$$

where $\vec{R}$ and $\vec{V}$ are, respectively, the instantaneous position and velocity relative to the central body. The $\hat{N}$-$\hat{V}$ plane is the trajectory plane, and $\hat{W}$ is normal to the trajectory plane in the direction of the momentum.

These coordinates are used to define the terminal constraints on the Mars-Earth trajectory at perigee. At this point, $\hat{R}$ and $\hat{V}$ are normal to each other so that the N, V, W coordinates become altitude (ALT), down-range (DR), and cross-range (CR), respectively, Figure 2-2B.

2.2.3 B Vector Coordinates

For certain types of guidance laws, it is convenient to express the miss constraints at the target in terms of the $\vec{B}$ vector.* As shown in Figure 2-3A, the origin of the B vector is the center of the target, and its direction is such that it is normal to the incoming asymptote. The S vector is directed along the asymptote. The plane containing the $\vec{B}$ is normal to $\hat{S}$ and is the target miss plane. The orthogonal coordinates in this plane are $\hat{T}$ and $\hat{R}$ (Figure 2-3B). The orientation of $\hat{T}$ and $\hat{R}$ in the miss plane may be chosen arbitrarily. For the end-point $\vec{B}$ vector data presented in this report, the $\hat{T}$ vector was selected so that it was in the trajectory plane, and $\hat{R}$ was normal to the trajectory plane. The end constraints for both the outbound and return trajectories were, therefore, $\vec{B}\cdot\hat{T} = |\vec{B}|$ and $\vec{B}\cdot\hat{R} = 0$. Deviations in these constraints are therefore related to radius of closest approach and inclination, respectively.

2.3 GENERAL DESCRIPTIONS OF DETERMINISTIC MIDCOURSE GUIDANCE LAWS

The purpose of a midcourse maneuver is to correct a trajectory so that it will satisfy a set of nominal end-point constraints. The corrections are required because of the error in the guidance system at injection. In this section, three guidance laws are derived based on the state-vector notation of the previous section and the assumption that the state deviations are

*The $\vec{B}$ vector is described and defined in Reference 3.

known quantities. In practice, these deviations are not known exactly and therefore the guidance corrections are based on statistical estimates of the deviations. The statistical analysis of the midcourse guidance system will be shown in later sections based on the results of this section.

A typical midcourse situation for an interplanetary mission is shown in Figure 2-4, where the true trajectory of the spacecraft at time B has been determined by Earth-based tracking stations and it is desired to compute the magnitude and direction of a correction at B so that the vehicle misses the target by the same distance as the nominal. As an added precaution for preventing the case where the deviation at C is zero, but the vehicle collides with the target, additional correction may often be used. For example, the correction at B may be applied to reduce the position error at D, and a second correction may be applied to D to eliminate the velocity deviation at C.*

For the purpose of deriving midcourse guidance laws, the equations of motion for the vehicle are written as**

$$\ddot{\underline{X}} = f(\underline{X}, t) \tag{2-15}$$

Where the function, f, involves the inverse square law for the number of bodies whose gravitational attraction is significant enough to effect the trajectory, as well as gravitational anomalies (oblateness of Earth, etc.) and possible external forces (solar pressure, etc.).

Equation (2-15) is linearized about a nominal trajectory to obtain the variation equations by expanding (2-15) in a Taylor series and neglecting higher-order terms. This results in an expression of the form

$$\ddot{\underline{X}} + \ddot{\underline{x}} = f(\underline{X}, t) + \frac{\partial f}{\partial \underline{X}}\,\underline{x} \tag{2-16}$$

* A tutorial example is included in Reference 2, where guidance laws are developed for a two-dimensional problem.

** An underline vector will in general denote a three-dimensional state vector, whereas one that is not underlined will denote a six-dimensioned state vector consisting of position and velocity components.

By subtracting nominal trajectory equation (2-15) from (2-16) the variational equations are obtained as

$$\ddot{\underline{x}} = \frac{\partial \underline{f}}{\partial \underline{X}} \underline{x} = F_1(t)\, \underline{x} \tag{2-17}$$

These equations may be written as a set of first-order differential equations by defining the following states:

$$\underline{x}_1 = \underline{x} \quad \underline{x}_2 = \dot{\underline{x}} \quad \dot{\underline{x}}_1 = \dot{\underline{x}} \quad \dot{\underline{x}}_2 = \ddot{\underline{x}}$$

Equation (2-17) may then be written as

$$\begin{bmatrix} \dot{\underline{x}}_1 \\ \dot{\underline{x}}_2 \end{bmatrix} = \begin{bmatrix} 0 & I \\ F_1(t) & 0 \end{bmatrix} \begin{bmatrix} \underline{x}_1 \\ \underline{x}_2 \end{bmatrix} \equiv F(t) \begin{bmatrix} \underline{x}_1 \\ \underline{x}_2 \end{bmatrix} \tag{2-18}$$

It is now possible to compute the transition matrix, $\Phi(t_2 t_1)$, by integration of the variational equations (2-18) along the nominal trajectory defined by (2-15). The transition matrix is the sensitivity of the state at some time, t_2, to deviations in the state at an earlier time t_1.

2.3.1 Fixed Time-of-Arrival Guidance Law

The guidance correction at a time when the spacecraft is at point B in Figure 2-4 that will correct for deviations in the nominal trajectory when it reaches D, can be derived in terms of the transition matrix $\Phi(T_D, T_B)$, and is partitioned into

$$\Phi(T_D, T_B) = \begin{bmatrix} \Phi_1 & \Phi_2 \\ \Phi_3 & \Phi_4 \end{bmatrix}, \tag{2-19}$$

then the deviation in position at T_D due to deviation errors at T_B, ($\underline{x}(T_B)$ and $\dot{\underline{x}}(T_B)$), is given by

$$\underline{x}(T_D) = \begin{bmatrix} x_1 \\ x_2 \\ x_3 \end{bmatrix} = \Phi_1(T_D,T_B)\ \underline{x}(T_B) + \Phi_2(T_D,T_B)\ \dot{\underline{x}}(T_B) \qquad (2\text{-}20)$$

Also, the effect of a velocity guidance correction applied at T_B on the position vector at T_D is

$$\underline{x}_g(T_D) = \Phi_2(T_D,T_B)\ \dot{\underline{x}}_g(T_B) \qquad (2\text{-}21)$$

Since the purpose of the velocity correction at T_B is to eliminate the position error at T_D the desired velocity corrections is found by equating the sum of (2-20) and (2-21) to zero, and solving for $\dot{\underline{x}}_g(T_B)$,

$$\dot{\underline{x}}_g\ (T_B) = -\Phi_2^{-1}\ \Phi_1\ \underline{x}(T_B) - \dot{\underline{x}}(T_B) \qquad (2\text{-}22)$$

The derivation state at time T_B after the correction then becomes

$$x'(T_B) = \begin{bmatrix} \underline{x}(T_B) \\ \\ \dot{\underline{x}}(T_B) + \dot{\underline{x}}_g(T_B) \end{bmatrix} \equiv \begin{bmatrix} \dot{\underline{x}}(T_B) \\ \\ \dot{\underline{x}}'(T_B) \end{bmatrix} \qquad (2\text{-}23)$$

Therefore, the required velocity correction at T_D to zero the velocity deviation at T_C is given by

$$\dot{\underline{x}}g(T_D) = -\dot{\underline{x}}(T_D) = -\left[\Phi_3\ \underline{x}'(T_B) + \Phi_4\ \dot{\underline{x}}'(T_B)\right] \qquad (2\text{-}24)$$

Thus the application of the guidance correction in (2-22) at T_B and the guidance correction in (2-24) at T_D insures that the actual trajectory will coincide with the nominal trajectory at point C. This is neglecting the errors in the computation and execution of the maneuvers. This type of fixed time-of-arrival guidance law, which controls the trajectory to the nominal end position at the nominal arrival time, is used in the study.

An alternate set of contraints which would provide a fixed time of arrival guidance law is

$$\begin{bmatrix} \vec{B} \cdot \hat{T} \\ \vec{B} \cdot \hat{R} \\ t \end{bmatrix} = \text{constraint vector} \qquad (2\text{-}25)$$

where t = time.

The $\vec{B} \cdot \hat{T}$ and $\vec{B} \cdot \hat{R}$ constraints will control the approach asymptote of the trajectory. The time constraint will cause the periapsis distance to vary from the nominal value so that the arrival time is controlled. This type of FTA guidance law would control the trajectory to arrive at the nominal time, but the end position would not be the nominal value. This FTA guidance law was not used in the study.

2.3.2 Variable Time-of-Arrival Guidance Law

A second type of guidance law can be derived such that the vehicle will pass the target in a prescribed manner but not necessarily at the same time as the nominal trajectory. In fact, allowing the time of arrival to be a variable generally requires smaller velocity corrections. A reasonable set of contraints for use with a variable time of arrival guidance law is

$$\begin{bmatrix} \vec{B} \cdot \hat{T} \\ \vec{B} \cdot \hat{R} \\ V_{INF} \end{bmatrix} = \text{constraint vector} \qquad (2\text{-}26)$$

where

$$V^2_{INF} = V^2 - \frac{2\mu}{R}$$

R = Radius to center of target body

μ = Gravitational constant of target body

V = Vehicle speed at distance R

The $\vec{B} \cdot \hat{T}$ and $\vec{B} \cdot \hat{R}$ components of (2-26) will control the approach asymptote relative to the target. The use of V_{INF} as the third constant will then control the radius of closest approach.*

The nominal trajectory constraint vector (2-26) is a function of the end-point state and the end time

$$\begin{bmatrix} \vec{B} \cdot \hat{T} \\ \vec{B} \cdot \hat{R} \\ V_{INF} \end{bmatrix} = f(X,T) \qquad (2\text{-}27)$$

where X = Nominal end-point state

T = Nominal end-point time.

The constraint vector on an adjacent trajectory is obtained by making a Taylor Series expansion of (2-27) and retaining only first-order terms.

$$\begin{bmatrix} B \cdot T \\ B \cdot R \\ V_{INF} \end{bmatrix} + \begin{bmatrix} \delta B \cdot T \\ \delta B \cdot R \\ \delta V_{INF} \end{bmatrix} = f(X,T) + \frac{\partial f}{\partial X}\bigg|_T x(T) + \frac{\partial f}{\partial T}\bigg|_T \Delta T \qquad (2\text{-}28)$$

Subtracting the nominal constraint vector (2-27) from (2-28) yields the deviation constraint vector,

* Reference 4, Page 152.

$$\begin{bmatrix} \delta B \cdot T \\ \delta B \cdot R \\ \delta V_{INF} \end{bmatrix} = \left.\frac{\partial f}{\partial X}\right|_T x(T) + \left.\frac{\partial f}{\partial T}\right|_T \Delta T \qquad (2\text{-}29)$$

If the nominal trajectory passes close to the target body with the choice of miss parameters given in (2-27) it is likely that f(X,T) will be independent of T. This would be certain if the trajectory relative to the target obeyed Kepler's equation and is expressed mathematically by

$$\left.\frac{\partial f}{\partial T}\right|_T = 0. \qquad (2\text{-}30)$$

As a result of (2-30), Equation (2-29) can be expressed as

$$\begin{bmatrix} \delta B \cdot T \\ \delta B \cdot R \\ \delta V_{INF} \end{bmatrix} = \left.\frac{\partial f}{\partial X}\right|_T x(T) \equiv C(T)\ \Phi(T;t)\ x(t) \equiv D(T,t)\ x(t) \qquad (2\text{-}31)$$

where C(T) is a 3 x 6 matrix of sensitivity coefficients relating the deviation in the constraints to deviations in the state at time (T). Equation (2-31) may also be written as

$$\begin{bmatrix} \delta B \cdot T \\ \delta B \cdot R \\ \delta V_{INF} \end{bmatrix} = \left(D_1 \mid D_2\right) x(t) = D_1\, \underline{x}(t) + D_2\, \dot{\underline{x}}(t) \qquad (2\text{-}32)$$

The effect of a velocity correction at time (t) would be to produce a deviation in the constraint vector equal to $D_2\, \dot{\underline{x}}_g(t)$. Therefore the guidance correction is found by equating the sum of $D_2\, \dot{\underline{x}}_g(t)$ and (2-32) to zero and solving for $\dot{\underline{x}}_g(t)$.

The result is

$$\dot{\underline{x}}_g(t) = -D_2^{-1} \begin{bmatrix} \delta B \cdot T \\ \delta B \cdot R \\ \delta V_{INF} \end{bmatrix} = -D_2^{-1} D_1 \underline{x}(t) - \dot{\underline{x}}(t) \qquad (2\text{-}33)$$

Equation (2-33) is the expression of the velocity correction required for the variable time-of-arrival guidance law.

The quantity ΔT, which is the variation in the arrival time, can be computed in the following manner. The constraint parameter θ is added; this is associated with the nominal end-time T when the target constraint parameters are calculated. θ is the true anomaly which is a function of the end time T. The variation in θ from its nominal value may be related to deviations from the trajectory at any previous time as well as the variation in the end time, T , itself by the expression

$$\Delta \theta = \frac{\partial \theta}{\partial \underline{X}(T)} \Phi(T,t)\, x(t) + \frac{\partial \theta}{\partial T} \Delta T \qquad (2\text{-}34)$$

By adding the constraint $\Delta \theta = 0$ for all perturbed trajectories (i.e., the miss vector for all perturbed trajectories will be evaluated at the same value of θ as the nominal), one may write equation (2-34) for ΔT.

$$\Delta T = -\left(\frac{\partial \theta}{\partial T}\right)^{-1} \left(\frac{\partial \theta}{\partial \underline{X}(T)}\right) \Phi(T,t)\, x(t) \equiv A\Phi(T,t)\, x(t) \qquad (2\text{-}35)$$

where $A = \left(\frac{\partial \theta}{\partial T}\right)^{-1} \left(\frac{\partial \theta}{\partial \underline{X}(T)}\right)$ a 1 x 6 row vector.

2.3.3 Guidance Law for Minimum Midcourse Maneuver

The previous guidance law can be modified by computing a numerical value for V_{INF} such that the required ΔV maneuver is a minimum, rather than controlling it to the nominal value. The velocity correction as a function of δV_{INF} is shown in equation (2-33) and is repeated here with the matrix D_2^{-1} written in terms of its elements,

$$\dot{\underline{x}}_g = -D_2^{-1} \begin{pmatrix} \delta\underline{B} \cdot \hat{T} \\ \delta\underline{B} \cdot \hat{R} \\ \delta V_{INF} \end{pmatrix} = \begin{bmatrix} a_{11} & a_{12} & a_{13} \\ a_{21} & a_{22} & a_{23} \\ a_{31} & a_{32} & a_{33} \end{bmatrix} \begin{pmatrix} \delta\underline{B} \cdot \hat{T} \\ \delta B \cdot \hat{R} \\ \delta V_{INF} \end{pmatrix} \qquad (2\text{-}36)$$

The magnitude of the correction is

$$\left[\dot{\underline{x}}_g^T \dot{\underline{x}}_g\right]^{\frac{1}{2}} = \Big[\left(a_{11}\ \delta\underline{B} \cdot \hat{T} + a_{12}\ \delta\underline{B} \cdot \hat{R} + a_{13}\ \delta V_{INF}\right)^2 + \left(a_{21}\ \delta\underline{B} \cdot \hat{T} + a_{22}\ \delta\underline{B} \cdot \hat{R} + a_{23}\ \delta V_{INF}\right)^2 + \left(a_{31}\ \delta\underline{B} \cdot \hat{T} + a_{32}\ \delta\underline{B} \cdot \hat{R} + a_{33}\ \delta V_{INF}\right)^2\Big]^{\frac{1}{2}} \qquad (2\text{-}37)$$

Taking the partial derivative of (2-37) with respect to δV_{INF} and setting the result, zero gives

$$\begin{aligned} 0 = {} & 2\left(a_{11}\ \delta B \cdot \hat{T} + a_{12}\ \delta\underline{B} \cdot \hat{R} + a_{13}\ \delta V_{INF}\right) a_{13} \\ & +2\left(a_{21}\ \delta B \cdot \hat{T} + a_{22}\ \delta B \cdot \hat{R} + a_{23}\ \delta V_{INF}\right) a_{23} \\ & +2\left(a_{31}\ \delta B \cdot \hat{T} + a_{32}\ \delta B \cdot \hat{R} + a_{33}\ \delta V_{INF}\right) a_{33} \end{aligned} \qquad (2\text{-}38)$$

Solving for δV_{INF} in (2-38) yields

$$\delta V_{INF} = \frac{-\left(a_{11}a_{13} + a_{21}a_{23} + a_{31}a_{33}\right)\delta\underline{B} \cdot \hat{T} + \left(a_{12}a_{13} + a_{22}a_{23} + a_{32}a_{33}\right)\delta\underline{B} \cdot \hat{R}}{a_{13}^2 + a_{23}^2 + a_{33}^2} \qquad (2\text{-}39)$$

If the value of δV_{INF} from (2-39) is substituted into (2-36), then the resultant correction is the value required for a variable time of arrival guidance law with a minimum ΔV correction.

The three guidance laws that have been discussed in this section are illustrated in Figure 2-5.

2.4 ERROR ANALYSIS

The success of most missions depends on whether the expected deviation from the desired objective is within allowable bounds. An essential part of the guidance analysis, therefore, is to determine the effect of guidance component errors on the deviation of the vehicle state. By use of the sensitivity coefficients, the error sources can be propagated to various objectives in the missions. It is thus possible to determine which error sources are significant and thereby improve the system design such that the mission objectives are attained. The propagation of deterministic deviations in the state have already been used to derive guidance laws. However, since the errors in a guidance system may often be of a radom nature, it is random necessary to introduce certain statistical notations and definitions in order to derive the propagation of these errors in a linear system.

2.4.1 Statistical Definitions and Notations

The expected value of the scalar function $f(x)$ is given by

$$E\left(f(x)\right) = \int_{-\infty}^{+\infty} f(x)\, p(x)\, dx \qquad (2\text{-}40)$$

where $p(x)$ is the probability density function which has the properties

$$\int_{-\infty}^{+\infty} p(x)\, dx = 1 \qquad (2\text{-}41)$$

and

$$\int_A^B p(x)\,dx = \text{probability that } x \text{ lies in the interval } A \le x \le B \tag{2-42}$$

For a gaussian or normal distribution, the density function p(x) is given by

$$p(x) = \frac{1}{\sqrt{2\pi}\sigma} e^{\frac{-(x-\bar{x})^2}{2\sigma^2}} \tag{2-43}$$

where

$\bar{x} = E(x)$ = mean or average value of x

$\sigma^2 = E(x^2) - \bar{x}^2$ = variance

$\sigma = \sqrt{\sigma^2}$ = standard of deviation.

For the vector function $f(\underline{x})$, the expected value is

$$E\left(f(x)\right) = \begin{bmatrix} E\left(f_1(x)\right) \\ E\left(f_2(x)\right) \\ E\left(f_n(x)\right) \end{bmatrix} \tag{2-44}$$

and the gaussian or normal probability density function of $\underline{x}$ is given by

$$p(x_1, x_2 \cdots x_n) = \frac{1}{(2\pi)^{n/2}\left|P\right|^{\frac{1}{2}}} e^{-\frac{1}{2}(\underline{x}-\underline{\bar{x}})^T(P^{-1})(x-\bar{x})} \tag{2-45}$$

where

$$\bar{x} = \begin{bmatrix} E(x_1) \\ E(x_2) \\ \cdot \\ \cdot \\ \cdot \\ E(x_n) \end{bmatrix} = E(\underline{x}) \qquad (2\text{-}46)$$

and P is the covariance matrix

$$P = E(x\,x^T) - (\bar{x}\,\bar{x}^T)$$

$$P = \begin{bmatrix} (E(x_1^2) - (\bar{x}_1^2) & (E(x_1x_2) - \bar{x}_1\bar{x}_2) \cdots\cdots (E(x_1x_n) - \bar{x}_1\bar{x}_n) \\ \vdots & \\ & (E(x_2^2) - \bar{x}_2^2) \cdot \\ & \quad \cdot \quad \cdot \\ & \quad \cdot \quad \cdot \quad \cdot \\ (E(x_1x_n) - (\bar{x}_1\bar{x}_n) & \cdots\cdots\cdots\cdots (E(x_n^2) - \bar{x}_n^2) \end{bmatrix} \qquad (2\text{-}47)$$

P is a symmetric matrix, i.e., $(P_{ij} = P_{ji})$. Along the diagonal of P are the variances of each of the components of x. The off-diagonal terms are $E(x_n x_m) - \bar{x}_n \bar{x}_m \triangleq \rho_{nm}\,\sigma_n\,\sigma_m$ where ρ_{nm} is the correlation between the n and m components of x. The correlation ranges between the values $-1 \leq \rho_{nm} \leq +1$. $|P|$ is the determinant of the covariance matrix P.

If x is a sixth-order vector consisting of three position states and three velocity states, then the RMS errors in position and velocity are given by

$$\text{RMS Position} = \sigma_x = \text{trace } P_x \qquad (2\text{-}48)$$

and

$$\text{RMS Velocity} = \sigma_{\dot{x}} = \text{trace } P_{\dot{x}} \qquad (2\text{-}49)$$

where P_x and $P_{\dot{x}}$ are the upper-left and lower-right 3 x 3 submatrices of P in Equation (2-47).

2.4.2 Propagation of Errors in Linear Systems

Although the actual orbit equations are nonlinear, it is again assumed that for small perturbations about the nominal, the variational equations can be written as

$$\dot{\underline{x}} = F(t)\underline{x} + B(t)\underline{u}(t) \tag{2-50}$$

The solution may be written as

$$\underline{x}(t_1) = \Phi(t_1;t_o)\ \underline{x}(t_o) + \Phi u\ (t_1;t_o)\ \underline{u}(t_o) \tag{2-51}$$

for $\underline{u}(t_o)$ constant in the interval $t_o \leq t \leq t_1$.

The initial errors for this system are statistically defined by

$$E\left(x(t_o)\right) = \bar{x}(t_o) \tag{2-52}$$

$$E\left\{\left(x(t_o) - \bar{x}(t_o)\right)\left(x(t_o) - \bar{x}(t_o)\right)\right\}^T = P(t_o) \tag{2-53}$$

$$E\left(u_\ell(t_o)\ x_k(t_o)\right) = 0 \text{ for all } \ell \text{ and } k \tag{2-54}$$

$$E\left(u(t_o)\right) = 0 \tag{2-55}$$

$$E\left(u(t_o)\ u^T(t_o)\right) = M \tag{2-56}$$

The effect of these errors at some later time (t_1) is then specified by the mean value of $\bar{x}(t_1)$ and the covariance matrix $P(t_1)$. By (2-51) $\bar{x}(t_1)$ is given by

$$E\left(x(t_1)\right) = \bar{x}(t_1) = \Phi(t_1;t_o)\, E\left(\underline{x}(t_o)\right) + \Phi u(t_1;t_o)\, E\left(\underline{u}(t_o)\right) \qquad (2\text{-}57)$$

which, as a result of (2-52) and (2-55), is

$$\bar{x}(t_1) = \Phi(t_1;t_o)\, \bar{x}(t_o) \qquad (2\text{-}58)$$

also, if the error in estimate x, defined as

$$\tilde{x} = x - \bar{x}, \qquad (2\text{-}59)$$

then by (2-59) and (2-51) $\tilde{x}(t_1)$ is

$$\tilde{x}(t_1) = \Phi(t_1;t_o)\, \tilde{x}(t_o) + \Phi_u(t_1;t_o)\, u(t_o), \qquad (2\text{-}60)$$

and the covariance matrix $P(t_1)$ is

$$P(t_1) = E\left(\tilde{x}(t_1)\, \tilde{x}^T(t_1)\right) = \Phi E\left(\tilde{x}(t_o)\, \tilde{x}^T(t_o)\right) \Phi^T \qquad (2\text{-}61)$$

$$+ \Phi E\left(\tilde{x}(t_o)\, u^T(t_o)\right) U^T + \Phi u E\left(u(t_o)\, \tilde{x}^T(t_o)\right) \Phi^T$$

$$+ \Phi u\, E\left(u(t_o)\, u^T(t_o)\right) \Phi u^T$$

Finally, since the cross product terms in (2-61) are zero, substituting (2-53) and (2-56) into (2-61) results in

$$P(t_1) = \Phi P(t_o)\, \Phi^T + \Phi_u M\, \Phi_u^T \qquad (2\text{-}62)$$

Equation (2-62) provides a relationship for updating the covariance matrix in a linear system. This is an important result, and will be used extensively throughout the report.*

2.5 DETERMINING THE STATE

The discussion of guidance laws and error analysis in the previous section has assumed that the vehicle state vector is known at discrete points in time. The problem of determining the state from Earth-based observations or onboard equipment is considered in detail in this section. Since, in general, one set of observations is not sufficient to define the state, it is necessary to make a number of observations and then solve for the equations of motion which give a "best" fit to the observed data. The solution to this filtering or estimation problem is given by Kalman (Reference 5) for linear systems. A derivation of the Kalman filter that can be applied to nonlinear systems has been developed by Schmidt et al (References 6, 7, and 8), and is included for the case where measurement errors exist. In addition, solutions are included for determining the effect of unknown parameters without actually solving for them. These unknown parameters may include bias errors in the equations of motion, or bias errors in the measurements.

2.5.1 Kalman Filter Derivation

It has been shown that an error analysis of a navigation system can be performed if the estimate of the state vector and the covariance matrix of the errors in the estimate are known. This section will derive these quantities on the basis that a Kalman filter is used in the estimation process. The state deviations $x(t)$, the estimate of the state deviations $\hat{x}(t)$, and the error in estimate of the state deviations $\tilde{x}(t)$ are shown pictorially in Figure 2-5. The problem can be defined mathematically** as follows:

---

* A detailed example which illustrates the use of the projected covariance matrix for midcourse corrections is given in Reference 2.

** Although P has been defined in (2-47) as the covariance matrix of $(x-\bar{x})$ to illustrate the propagation of this quantity, it will henceforth be used to denote $(x-\hat{x})$, the error in estimate.

Given:

$\hat{x}(t_1)$ = estimate of x

$P(t_1) = E\left((x-\hat{x})(x-\hat{x})^T\right) = E(\tilde{x}\tilde{x}^T)$ Covariance matrix of the error in the estimate

$y(t_1) = Hx(t_1) + q(t_1)$

$q(t_1)$ = random error in the measurement $y(t_1)$

$E\left(q(t_1)\right) = 0$

$E\left(q(t_1)q^T(t_1)\right) = Q$

Find:

a new estimate of the state, $\hat{x}_n(t_1)$, so the following loss function is minimized:

$$L = E(x-\hat{x}_n)^T(x-\hat{x}_n) \tag{2-63}$$

It should be noted that an initial covariance matrix of the error in the estimate $P(t_1)$ and the initial estimate of x ($\hat{x}(t_1)$) are required. These quantities may be determined by a least-squares fit (described in Reference 1). Also the derivation in this section assumes that the random variables are gaussian.

The loss function may be written as

$$L = \int (x-\hat{x}_n)^T(x-\hat{x}_n)\ p(x|y, \hat{x})\ dx \tag{2-64}$$

Taking the gradient of (2-64) with respect to $\hat{x}_n$ and interchanging order of differentiation and integration gives

$$\nabla L = \int 2(x-\hat{x}_n)^T\ p\ (x|y, \hat{x})\ dx \tag{2-65}$$

Since $\hat{x}_n$ is a constant, the integration of (2-65) results in

$$\nabla L = 2 \int x^T p(x|y, \hat{x})\, dx - 2\hat{x}_n^T \tag{2-66}$$

By definition, the term under the integral is the conditional mean; therefore, setting ∇L equal to zero and solving for $\hat{x}_n$ yields

$$\hat{x}_n = E(x|y, \hat{x}). \tag{2-67}$$

Equation (2-64) shows that the conditional mean is the optimum estimate of $\hat{x}_n$ for the loss function L of (2-63)

The conditional mean can be determined from the probability density function $p(x|y,\hat{x})$. $p(x)$ has been derived in (2-45) as

$$p(x) = \frac{1}{(2\pi)^{n/2}|P(t_1)|^{\frac{1}{2}}}\, e^{-\frac{1}{2}(x-\hat{x})^T \left[P^{-1}(t_1)\right] (x-\hat{x})} \tag{2-68}$$

where n = number of states and $P(t_1)$ is the covariance matrix of $(x-\hat{x})$. Also, the deviation of the observation y from its estimate is given by

$$y - \hat{y} = H(x-\hat{x}) + q, \tag{2-69}$$

the covariance matrix of this deviation is

$$E(y-\hat{y})(y-\hat{y})^T = HPH^T + Q, \tag{2-70}$$

from the assumption

$$E\left\{(x-\hat{x})\,[q^T]\right\} = 0, \tag{2-71}$$

P(y) is therefore given by

$$p(y) = \frac{1}{(2\pi)^{n/2}\left|HPH^T + Q\right|^{\frac{1}{2}}} e^{-\frac{1}{2}(y-\hat{y})^T\left[HPH^T + Q\right]^{-1}(y-\hat{y})} \qquad (2\text{-}72)$$

where

n = number of observations. Similarly, $P(y|x)$ is

$$p(y|x) = p(q) = \frac{1}{(2\pi)^{n/2}|Q|^{\frac{1}{2}}} e^{-\frac{1}{2}q^TQ^{-1}q} \qquad (2\text{-}73)$$

By use of Baye's equation,

$$P(x|y,\hat{x}) = \frac{P(y|x)\ P(x)}{p(y)} \qquad (2\text{-}74)$$

Substituting (2-68), (2-72), and (2-74) yields

$$p(x|y,\ \hat{x}) = Ae^{-\frac{1}{2}\left[(x-\hat{x})^T P^{-1}(x-\hat{x}) + q^TQ^{-1}q - (y-\hat{y})^T(HPH^T + Q)^{-1}(y-\hat{y})\right]}, \qquad (2\text{-}75)$$

where

$$A = \frac{\left|HPH^T + Q\right|^{\frac{1}{2}}}{(2\pi)^{n/2}|Q|^{\frac{1}{2}}|P|^{\frac{1}{2}}} \qquad (2\text{-}76)$$

For gaussian random variable, the conditional mean given by (2-67) is at the maximum of the density function (2-75). Therefore, taking the gradient of the exponent in (2-75) with respect to x, setting the resultant equal to zero and letting $x = x_n$ gives

$$\left[(\hat{x}_n - x)^T P^{-1} - (y-\hat{y})^T (HPH^T + Q)^{-1} \nabla_x (y-\hat{y})\right] = 0 \qquad (2\text{-}77)$$

Also since

$$y = Hx + q, \tag{2-78}$$

and

$$\nabla_x y = H, \tag{2-79}$$

solving (2-77) for $\hat{x}_n$ gives the desired result

$$\hat{x}_n = \hat{x} + PH^T (HPH^T + Q)^{-1} (y-\hat{y}), \tag{2-80}$$

where $\hat{y} = H\hat{x}$ and y is the observation. Equation (2-80) shows the optimum new estimate.

It is also desired to determine P_n, the new covariance matrix of the error in estimate, which can be expressed as

$$E(x-\hat{x}_n)\ (x-x_n)^T = E\left((x-\hat{x}) - K(y-\hat{y})\right)\left((x-\hat{x}) - K(y-\hat{y})\right), \tag{2-81}$$

where the filter gain K is given by

$$K = PH^T (HPH^T + Q)^{-1} \tag{2-82}$$

Expanding (2-81) yields

$$\begin{aligned} E(x-\hat{x}_n)(x-\hat{x}_n)^T = {} & E(x-\hat{x})(x-\hat{x})^T - E(x-\hat{x})(y-\hat{y})^T K^T \\ & - E\,K(y-\hat{y})(x-\hat{x})^T + E\,K(y-\hat{y})(y-\hat{y})^T K^T, \end{aligned} \tag{2-83}$$

and letting $y-\hat{y} = H(x-\hat{x}) + q$, the terms of (2-83) are

$$
\left.
\begin{aligned}
E(x-\hat{x})(x-\hat{x})^T &= P \\
E(x-\hat{x})(y-\hat{y})^T K^T &= E\left((x-\hat{x})\right)\left((x-\hat{x})^T H^T + q^T\right) K^T \\
&= PH^T K^T \quad (\text{since } E(x-\hat{x})(q)^T = 0) \\
E\ K(y-\hat{y})(x-\hat{x})^T &= KE\ (H(x-\hat{x}) + q)\ (x-\hat{x})^T = KHP \\
E\ K(y-\hat{y})(y-\hat{y})^T K^T &= K\left[HPH^T + Q\right] K^T
\end{aligned}
\right\} \qquad (2\text{-}84)
$$

Substitution of the value of K from (2-82) gives

$$
\begin{aligned}
PH^T K^T &= PH^T (HPH^T + Q)^{-1} H\ P \\
KHP &= PH^T (HPH^T + Q)^{-1} H\ P \\
K(HPH^T+Q)K^T &= PH^T (HPH^T + Q)^{-1} (HPH^T + Q)(HPH^T + Q)^{-1} H\ P \\
&= PH^T (HPH^T + Q)^{-1}\ H\ P. \qquad (2\text{-}85)
\end{aligned}
$$

Thus, Equation (2-85) may be written as

$$
E(x-\hat{x}_n)(x-\hat{x}_n)^T = P_n = P - PH^T (HPH^T + Q)^{-1} H\ P \qquad (2\text{-}86)
$$

The two results, Equations (2-80) and (2-86) are repeated below for convenience.

$$
\hat{x}_n = \hat{x} + PH^T (HPH^T+Q)^{-1} (y-\hat{y}) \qquad (2\text{-}87)
$$

$$
P_n = P - PH^T (HPH^T + Q)^{-1} H\ P \qquad (2\text{-}88)
$$

Equation (2-87) shows how the estimate of the state is modified by each new observation y, and (2-86) shows how the covariance matrix of the error in the estimate is reduced by each new observation. A second derivation of these quantities which assumes a linear filter is given in Reference 2 together with an example problem.

2.5.2 Parameter Estimation

In addition to estimating the position and velocity of the vehicle, it is often desired to estimate unknown parameters. Some of the important parameters which are applicable to this study are bias errors, which include:

a. Station location errors
b. Speed-of-light uncertainty
c. Biases in measuring instruments and physical constant and forces, which include:

   1. The Astronomical Unit (A.U.)
   2. Gravitational constants for planetary bodies
   3. Solar pressure.

These unknown parameters may be determined by writing the equations of motion as

$$\dot{\mathbf{X}} = F(\mathbf{X},U,t) \tag{2-89}$$

where $\mathbf{X}$ = vector of positions and velocities

U = vector of forcing functions plus unknown parameters in the equations of motion.

The observations or measurements are, in general, related to $\mathbf{X}$ by

$$Y = G(\mathbf{X},V,t) + q^{*}(\mathbf{X},V,t) \tag{2-90}$$

where

V = a vector of unknown parameters

q^{*} = random errors in measurement

Linearization of (2-89) and (2-90) about a nominal trajectory gives

$$\dot{\mathbf{x}} = \left[\frac{\partial F}{\partial \mathbf{X}}\right] \mathbf{x} + \left[\frac{\partial F}{\partial U}\right] u \tag{2-91}$$

$$y = \left[\frac{\partial G}{\partial X}\right] x + \left[\frac{\partial G}{\partial V}\right] v + q(t) \qquad (2\text{-}92)$$

The random error in measurement has been called q in (2-92).

Since a constant c obeys the differential equation

$$\frac{dc}{dt} = 0, \qquad (2\text{-}93)$$

any unknown constants in the equations of motion or the measurements may be described be defining an expanded state vector

$$\underline{z} = \begin{bmatrix} x \\ u \\ v \end{bmatrix} = \begin{bmatrix} 6 \times 1 \\ m \times 1 \\ n \times 1 \end{bmatrix} \qquad (2\text{-}94)$$

where u has m unknowns and v has n unknowns. The differential equations for z which include unknowns as defined by (2-93) are therefore

$$\dot{z} = \begin{bmatrix} \frac{\partial F}{\partial X} & \frac{\partial F}{\partial U} & 0 \\ 0 & 0 & 0 \\ 0 & 0 & 0 \end{bmatrix} z \qquad (2\text{-}95)$$

The solution of Equation (2-95) may be written as

$$z(t) = \begin{bmatrix} \Phi_x(t,t_o) & \Phi_u(t,t_o) & 0 \\ 0 & I & 0 \\ 0 & 0 & I \end{bmatrix} z(t_o) = \Phi(t,t_o)\, z(t_o) \qquad (2\text{-}96)$$

With this definition of state, as many unknowns as desired may be included.

The solution to the estimation problem is the same as given previously, that is

$$\left.\begin{aligned} \hat{z}_n &= \begin{pmatrix} \hat{x}_n \\ u_n \\ v_n \end{pmatrix} = \hat{z} + P_z H_z^T (H_z P_z H_z^T + Q)^{-1} (y - \hat{y}) \\ P_{zn} &= P_z = P_z H_z^T (H_z P_z H_z^T + Q)^{-1} H_z P_z \end{aligned}\right\} \qquad (2\text{-}97)$$

$$\left.\begin{aligned} \hat{z}(t) &= \hat{z}(t_o) + \left[\int_{t_o}^{t} F(\hat{x},\hat{u},t)\,dt\right] \\ P_z(t) &= \Phi(t;t_o)\, P_z(t_o)\, \Phi^T(t;t_o) + B_z \end{aligned}\right\} \qquad (2\text{-}98)$$

Equation (2-97) is for the improvement in estimate and the covariance matrix of the error in estimate as a results of the observation y, and Equation (2-98) is for updating the estimate and error in estimate between the observations. B_z is for inclusion of any random forcing functions which have occurred in the time interval ($t_o \rightarrow t$). Φ is calculated by numerical integration of the variational equations along the current best estimate of X and U. It should also be noted that P_Z is now an $(6 + n + m)$ by $(6 + m + n)$ matrix and includes not only the covariance matrix of the error in estimate for x but also for u and v.

2.5.3 Effects of Unknown Parameters

As shown in the preceding section, there are no theoretical difficulties encountered in actually solving for unknown parameters. The order of the state vector, however, may become extremely large and thereby limit the soltuions by onboard computers. It is therefore very useful to determine the effect of these unknown parameters, without actually solving for them. A solution to this problem has been developed by Schmidt (reference 2) and the results of this method are summarized in this section for equation of motion unknowns, or measurement unknowns, or both.

For equation of motion unknowns, it is desired to determine the effect of the unknown part of U in (2-89). The problem is mathematically defined as

Given: (1) $E(x-\hat{x})(x-\hat{x})^T = P(t_o)$

(2) $x(t) = \Phi(t;t_o)\, x(t_o) + U(t;t_o)\, u(t_o)$

(3) $E(x-\hat{x})\, u^T = C(t_o)$

(4) $E(u) = 0$

(5) $E(uu^T) = M$

Find: (1) $P(t) = E\left((x(t) - \hat{x}(t))\,(x(t) - \hat{x}(t))^T\right)$

(2) $C(t) = E\left((x(t) - \hat{x}(t))u^T\right)$

From (2-91) and (2-98) it is clear that the only influence of u will be during the propagation of the covariance matrix of errors in the estimate between observations.

The solution is summarized as follows:

Between observations

$$\hat{x}(t) = \hat{x}(t_o) + \int_{t_o}^{t} F(\hat{x}, \underline{U}_o, t)dt$$

$$P(t) = \Phi P(t_o)\, \Phi^T + \Phi C(t_o)\, \Phi_u^T + \Phi_u C^T(t_o)\Phi^T + \Phi_u M \Phi_u^T$$

$$C(t) = \Phi C(t_o) + \Phi_u M \qquad (2\text{-}99)$$

At an observation Y

$$\hat{x}_n = \hat{x} + PH^T(HPH^T + Q)^{-1}\,(y-\hat{y})$$

$$P_n = P - PH^T(HPH^T + Q)^{-1}(HP)$$

$$C_n = C - PH^T(HPH^T + Q)^{-1}HC \qquad (2\text{-}100)$$

As can be seen from (2-99), correlation exists for any value of time other than t_o even when $C(t_o) = 0$. This is a result of the fact that the estimate of the state $\hat{x}$ is dependent upon the unknown parameters in the equations of motion.

The effect of quantities such as measurement bias errors, station location errors, etc., affect the observation, as seen by (2-90). Therefore, these errors would influence estimates of the vehicle position and velocity. The problem of how to determine the effect of measurement errors is defined as

Given: (1) $\hat{x}$ = an estimate of the state

(2) P = the covariance matrix of the error in estimate
$= E\left((x-\hat{x})\,(x-\hat{x})^T\right)$

(3) C = the correlation between the error in estimate and unknown parameters ($C = E(x-\hat{x})v^T$)

(4) An observation y where
$y = H(t)x + G(t)v + q(t)$
v = unknown parameter (constant)
q(t) = random error in measurement

(5) The covariance matrix and mean value of the parameters v
$E(v) = 0$
$E(vv^T) = W$

(6) The covariance matrix and mean value of the random errors which are not correlated with either v or x
$E(q) = 0$
$E(qq^T) = 0$

Find: (1) A new estimate of the state $\hat{x}_n$ such that
$L = E(x-\hat{x}_n)^T(x-\hat{x}_n)$ is minimized

(2) The covariance matrix of the error in the new estimate
$P_n = E(x-\hat{x}_n)(x-\hat{x}_n)^T$

(3) The correlation between the new estimate and the parameters
$C_n = E(x-\hat{x})v^T$

The solution of this problem was derived in Reference 2, and is summarized as follows:

At an observation:

$$\left.\begin{aligned} \hat{x}_n &= \hat{x} + (PH^T + CG^T)y^{-1}\,(y-\hat{y}) \\ P_n &= P - (PH^T + CG^T)y^{-1}(HP + GC^T) \\ C_n &= C - (PH^T + CG^T)y^{-1}\,(HC + GW) \\ y &= HPH^T + HCG^T + GC^TH^T + GWG^T + Q \end{aligned}\right\} \qquad (2\text{-}101)$$

For updating between measurements:

$$\left.\begin{aligned} \hat{x}(t) &= \hat{x}(t_o) + \int_{t_o}^{t} \dot{\hat{x}}\,dt \\ P(t) &= \Phi(t;t_o)\,P(t_o)\,\Phi^T(t;t_o) \\ C(t) &= \Phi(t;t_o)\,C(t_o) \end{aligned}\right\} \qquad (2\text{-}102)$$

It is also possible to include the effects of both equation of motion unknowns and unknown parameters in the measurements. These results for u and v uncorrelated, $E(u\,v^T) = 0$, are:

For updating between measurements:

$$\left.\begin{aligned} \hat{x}(t) &= \hat{x}(t_o) + \int_{t_o}^{t} F(\hat{x}, \underline{U}_o, t)\,dt \\ P(t) &= \Phi P(t_o)\Phi^T + \Phi C_{ux}(t_o)\,\Phi_u^T + \Phi_u C_{ux}(t_o)\Phi^T + \Phi_u M \Phi_u^T \\ C_{ux} &= \Phi C_{ux}(t_o) + \Phi_u M \\ C_{vx} &= \Phi C_{vx}(t_o) \end{aligned}\right\} \qquad (2\text{-}103)$$

where

$$\begin{aligned} C_{ux} &= E\,((x(t) - \hat{x}(t))u^T) \\ C_{vx} &= E\,((x(t) - \hat{x}(t))v^T) \end{aligned} \qquad (2\text{-}104)$$

At an observation

$$\left.\begin{aligned}
\hat{x}_n &= \hat{x} + (PH^T + C_{vx}G^T)(y^{-1})(y-\hat{y}) \\
P_n &= P - (PH^T + C_{vx}G^T)(\bar{Y}^{-1})(HP + GC_{vx}^T) \\
C_{vx_n} &= C_{vx} - (PH^T + C_{vx}G^T)(\bar{Y}^{-1})(HC_{vx} + GW) \\
C_{ux_n} &= C_{ux} - (PH^T + C_{vx}G^T)(\bar{Y}^{-1})(HC_{ux})
\end{aligned}\right\} \qquad (2\text{-}105)$$

where

$$y = HPH^T + HC_{vx}G^T + GC_{vx}^TH^T + GWG^T + Q$$

$$H = \frac{\partial Y}{\partial X}\Big|_{X=\hat{X}} \qquad G = \frac{\partial Y}{\partial V}\Big|_{V=V_o}$$

$$W = E(vv^T) \qquad M = E(uu^T)$$

$$\Phi = \left(\frac{\partial x(t)}{\partial x(t_o)}\right) \qquad \Phi_u = \left[\frac{\partial x(t)}{\partial u(t_o)}\right] \qquad (2\text{-}106)$$

2.6 COMPLETE MIDCOURSE GUIDANCE ANALYSIS

In the preceding sections, deterministic guidance laws have been derived and the statistical concepts of state estimation and error propagation have been presented. These concepts are now used to derive the velocity requirements based on the estimate of state deviations. The definition of state deviations after a guidance correction and the guidance execution errors that cause these deviations are also discussed.

2.6.1 Midcourse Velocity Requirements

In general, the precise deviation from the nominal trajectory is not known. As a results, the guidance correction must be calculated on the basis of the best estimate of the deviation $\hat{x}(t)$. The estimated velocity correction $\hat{\dot{x}}_{\bar{g}}(t)$ based on equation (2-33) is therefore

$$\dot{\underline{\hat{x}}}_g(t) = - \left[D_2^{-1} D_1 \mid I \right] \hat{x}(t) \equiv G(T,t)\ \hat{x}(t) \qquad (2\text{-}107)$$

where $\hat{x}(t)$ is the six-dimensional state deviation estimate.

The covariance matrix of the expected guidance correction at time t is

$$E\left(\dot{\underline{\hat{x}}}_g \dot{\underline{\hat{x}}}_g^T\right) = G(T,t)\ E(\hat{x}(t)\hat{x}(t)^T)\ G^T(T,t) \qquad (2\text{-}108)$$

The covariance matrix of state estimate, $E(\hat{x}(t)\hat{x}(t)^T)$, may be expanded in the following manner:

$$\begin{aligned} E(\hat{x}(t)\hat{x}(t)^T) &= E\left[(x(t) - \tilde{x}(t))\ (x(t) - \tilde{x}(t))^T\right] \\ &= E\left[x(t)x^T(t)\right] - E\left[\tilde{x}(t)(\hat{x}(t) + \tilde{x}(t)^T\right] \\ &\quad - E\left[(\hat{x}(t) + \tilde{x}(t))\ \tilde{x}^T(t)\right] + E\left[\tilde{x}(t)\tilde{x}^T(t)\right] \end{aligned} \qquad (2\text{-}109)$$

where the relationship $\tilde{x} = x - \hat{x}$ has been used.

If the covariance matrices of the error in estimate, $\tilde{x}(t)$, and the deviation state, $x(t)$ are defined as

$$P(t) = E(\tilde{x}(t)\ \tilde{x}^T(t)) \qquad (2\text{-}110)$$

$$PAR(t) = E(x(t)\ x^T(t)) \qquad (2\text{-}111)$$

and $E\ (\hat{x}\tilde{x}^T) = 0$, then the covariance matrix of the state estimate in (2-109) can be simplified to

$$E(\hat{x}(t)\ \hat{x}^T(t)) = PAR(t) - P(t) \qquad (2\text{-}112)$$

Substitution of (2-112) into (2-108) yields the covariance matrix of the estimated velocity correction

$$E(\hat{\dot{\underline{x}}}_g \hat{\dot{\underline{x}}}_g^T) = G(T;t)\ (PAR(t) - P(t)\ G^T(T;t) \qquad (2\text{-}113)$$

The RMS estimated velocity is given by

$$\text{RMS } \Delta V = \sqrt{\text{Trace } E(\hat{\dot{\underline{x}}}_g \hat{\dot{\underline{x}}}_g^T)} \qquad (2\text{-}114)$$

2.6.2 Definition of a New Nominal

Previous derivations have assumed that the same nominal trajectory would be used throughout the mission and also that errors resulting from the execution of the velocity correction are zero. In general, however, it is desirable to compute a new nominal that will satisfy the end contraints following the correction; also, the execution errors are not zero, and therefore will now be considered.

The deviation of the state from the nominal trajectory following a correction, $x_a(t)$ is given by

$$x_a(t) = \begin{pmatrix} \underline{x}_b(t) \\ \\ \dot{\underline{x}}_b(t) + \hat{\dot{\underline{x}}}_g + \epsilon \end{pmatrix} \qquad (2\text{-}115)$$

where $\underline{x}_b(t)$, $\dot{\underline{x}}_b(t)$ are the position and velocity deviation prior to the correction, and

$$\hat{\dot{\underline{x}}}_g + \epsilon = G(T;t)\ \hat{x}_b(t) + \epsilon(t) = \text{actual correction mode} \qquad (2\text{-}116)$$

$\epsilon(t)$= the error in carrying out the estimated velocity correction

The covariance matrix of the deviation state from the nominal following a correction could be derived; however, this matrix is not very meaningful. At a guidance correction (for either a fixed or a variable time of arrival system), a new nominal trajectory is chosen based on the estimate of the state which satisfies the end constraints (at least in the linear sense).

The new nominal trajectory at time (t) after the correction is

$$\mathfrak{x}_{nom}(t) = \hat{x}_b(t) + \left(G\hat{x}_b(t)\right) \tag{2-117}$$

the deviation of true trajectory from this nominal, using (2-115), (2-116), and (2-117) is

$$x_a(t) - \hat{x}_{nom}(t) = x_{nom}(t) = x_b(t) - \hat{x}_b(t) + \begin{pmatrix} 0 \\ \varepsilon(t) \end{pmatrix}$$

$$x_{nom}(t) = \tilde{x}_b + \begin{pmatrix} 0 \\ \varepsilon(t) \end{pmatrix} \tag{2-118}$$

where $x_{nom}(t)$ = state deviation from the new nominal trajectory and will be called x(t) in the presentation which follows.

The covariance matrix of the state deviation from the new nominal then becomes

$$E(x(t)\ x(t)^T) = PAR_a(t) = E(\tilde{x}_a(t)\ \tilde{x}_a^T(t)) + \begin{bmatrix} 0 & 0 \\ 0 & E(\varepsilon\varepsilon^T) \end{bmatrix} \tag{2-119}$$

or

$$PAR_a(t) = P_b(t) + \begin{bmatrix} 0 & 0 \\ 0 & E(\varepsilon\varepsilon^T) \end{bmatrix} \tag{2-120}$$

where $E(\tilde{x}_b \varepsilon^T)$ and its transpose are assumed to be zero.

$P_b(t)$ = covariance matrix of error in estimate of the state prior to the correction.

The propagation of the covariance matrix of state deviations to the end point PAR(T) is particularly useful when transformed into end-point constraints (C(T)), since it then indicates the constraint deviations after a correction has been made. This covariance matrix PAR(T) in terms of end point constraints is found by the use of (2-31), and is given by

$$E\left\{\begin{bmatrix}\delta B \cdot T\\ \delta B \cdot R\\ \delta V_{INF}\end{bmatrix}\begin{bmatrix}\delta B \cdot T\\ \delta B \cdot R\\ \delta V_{INF}\end{bmatrix}^T\right\} \equiv DEV = C(T)\ \Phi(T;t)PAR_a(t)\Phi^T(T;t)C^T(t), \tag{2-121}$$

where DEV is the 3 x 3 covariance matrix of the end constraint deviations.

The RMS position deviation of the $\vec{B}$ vector is found from the trace of the upper left 2 x 2 in equation (2-121)

$$\sigma_B = \sqrt{DEV_{11} + DEV_{22}} = \text{RMS Position Deviation} \tag{2-122}$$

2.6.3 Midcourse Execution Errors

The final derivation is concerned with the three sources of the midcourse execution errors which have been defined as ϵ in (2-116). The errors considered are the following:

a. Pointing errors resulting from the attitude control system which is commanded to align the body axis of the vehicle along that direction determined by the guidance law.

b. Proportional and resolution errors resulting from the thrust command system which ignites and cuts off the engine to give the velocity magnitude determined by the guidance law.

The problem is to define a mathematical model of the errors introduced by these systems.

The errors caused by the thrust command system are the simplest from which to form a mathematical model, and are considered first. The two error types which can exist are classified as:

a. Proportional Error ($k_2 \hat{\dot{x}}_g$) proportional to the commanded velocity magnitude and in the direction of correction. Such an error could be caused by

   1. Uncertainty in the scale factor of the accelerometer (if the acceleration is nearly constant as it should be for the small midcourse maneuver)

   2. Uncertainty in an accelerometer bias value

b. Resolution Error ($k_2 \frac{\hat{\dot{x}}_g}{|\dot{x}_g|}$ independent of the velocity magnitude, but in the direction of the correction. Such an error could be caused by

   1. Resolution of the integrating accelerometer pick off transducer

   2. Uncertainty in the engine tail-off characteristics following the shutoff command signal.

Pfeiffer (Reference 9) has termed these two error sources as shutoff and resolution, respectively. They will be referred to here as <u>proportional</u> and <u>resolution</u> errors.

Following Reference 9, it will be assumed that these errors are independent and, therefore, the total error resulting from the thrust command system (neglecting second-order effects introduced by the pointing errors considered later) is given by

$$\epsilon_{tc} = k_1 \hat{\dot{\underline{x}}} + k_2 \frac{\hat{\dot{\underline{x}}}_g}{|\hat{\dot{\underline{x}}}_g|} \tag{2-123}$$

and since k_1 and k_2 are independent scalar random variables

$$E\left(\epsilon_{tc}\epsilon_{tc}^T\right) = E(k_1)^2\, E(\hat{\dot{\underline{x}}}_g \hat{\dot{\underline{x}}}_g^T) + E(k_2)^2\, E\left(\frac{\hat{\dot{\underline{x}}}_g}{|\hat{\dot{\underline{x}}}_g|} \frac{\hat{\dot{\underline{x}}}_g}{|\hat{\dot{\underline{x}}}_g|}^T\right) \tag{2-124}$$

Letting $E(\hat{\dot{\underline{x}}}_g \hat{\dot{\underline{x}}}_g^T) = \Lambda_v$ and $E \frac{\hat{\dot{\underline{x}}}_g}{|\hat{\dot{\underline{x}}}_g|} \frac{\hat{\dot{\underline{x}}}_g^T}{|\hat{\dot{\underline{x}}}_g|} = \Gamma_v$ (2-125)

$$E(k_1^2) = \sigma_v^2 \quad \text{proportional error variance} \tag{2-126}$$

$$E(k_2^2) = \sigma_r^2 \quad \text{resolution error variance} \tag{2-127}$$

The covariance matrix of the errors resulting from the thrust system is therefore given by

$$E(\bar{\epsilon}_{tc}\bar{\epsilon}_{tc}^T) = \sigma_v^2 \Lambda_v + \sigma_r^2 \Gamma_v, \tag{2-128}$$

where the quantity Λ_v is given by $E(\dot{x}_g \dot{x}_g^T)$ in (2-108). The method of calculation of Γ_v is described in Appendix A.

A mathematical model of the pointing errors introduced by the attitude control system derived in Reference 9 is somewhat more restrictive than the above. The basic error sources are the result of:

a. The accuracy of the attitude reference from which the maneuvers are made

b. The accuracy of the alignment of the thrust and body axis of the vehicle

c. The accuracy of the system in carrying out the commanded maneuvers.

The model given in Reference 9 applies only to error sources (a) and (b), and is quite approximate in its treatment of these errors. As a result of the mathematical difficulties involved in considering an error source of type (c), an adequate solution has not been found.

If the assumption is made that the attitude errors can be represented by a cone about the commanded velocity vector where the direction is equally likely, then a mathematical model can be readily derived.

The derivation of the pointing error is given in Reference 9, and is as follows:

Let $\sigma_p \bar{u}$ be a random three-dimensional vector with zero mean and equal probability in any direction, σ_p is a scalar and $\bar{u}$ is a unit vector

$\sigma_p \left[\hat{\dot{\bar{x}}}_g \times \bar{u} \right]$ is a vector lying in a plane normal to the commanded velocity direction.

$$E(\sigma_p \left[\hat{\dot{\bar{x}}}_g \times \bar{u} \right] \sigma_p \left[\hat{\dot{\bar{x}}}_g \times u \right]^T = \sigma_p^2 E \left[[\hat{\dot{\bar{x}}}_g \otimes] uu^T [\hat{\dot{\bar{x}}}_g \otimes]^T \right] \quad (2\text{-}129)$$

where

$$[\hat{\dot{x}}_g \otimes] = \text{a matrix} \quad (2\text{-}130)$$

Since $\bar{u}$ is independent of $\hat{\dot{\bar{x}}}_g$

and $$E [uu^T] = I \quad (2\text{-}131)$$

then,

$$\sigma_p^2 E \left[\hat{\dot{\bar{x}}}_g \otimes \right] uu^T \left[\hat{\dot{\bar{x}}}_g \otimes \right]^T = \sigma_p^2 E \left[[\hat{\dot{\bar{x}}}_g \otimes] [\hat{\dot{\bar{x}}}_g \otimes]^T \right] \quad (2\text{-}132)$$

and using the matrix identity

$$[v \otimes] [v \otimes]^T = [v^T v I - v v^T]. \quad (2\text{-}133)$$

The covariance matrix of pointing error Λ_p is then found to be

$$\Lambda_p = \sigma_p^2 \left[\text{Trace of } \Lambda_v)I - \Lambda_v\right] \tag{2-134}$$

If the original density function $\sigma_p u$ is assumed to be gaussian, then the probability density function of the half-cone γ is a Rayleigh density function given by

$$P(\gamma) = \frac{\gamma}{\sigma_p^2} e - \frac{\gamma^2}{2\sigma_p^2} \tag{2-135}$$

and the probability distribution function for γ is

$$P\left(\frac{(\gamma)}{(\sigma_p)}\right) = \int_o^{\frac{\gamma}{\sigma_p}} \frac{\gamma^2}{2\sigma_p^2} = \left[1 - e - \frac{\gamma^2}{2\sigma^2_p}\right] \tag{2-136}$$

This distribution curve is shown in Figure 2-7. If some idea of the attitude control system capability is known, however (e.g., that the half-cone angle would be less than 1^o with a proability of 0.67), then the distribution curve shows that σ_p should be set such that $\frac{1^o}{\sigma_p} = 1.5$ or $\sigma_p = \frac{2^o}{3}$.

SECTION 3

DESCRIPTION OF THE DIGITAL COMPUTER SIMULATION

In order to accomplish the objectives of this study, it has been necessary to build a digital computer program which has the capability of simulating both the navigation and the guidance systems for an interplanetary mission. The program enables the statistical errors resulting from the guidance and the navigation systems to be studied in terms of their effect on the mission requirements by using linear perturbation theory. Some of the important functions that the program must perform are : (1) the computation of transition matrices along a nominal trajectory, (2) the processing of observations from Earth-based or onboard tracking, (3) the estimation of the vehicle state using the Kalman filter theory, (4) the specification of guidance corrections, and (5) the propagation of deviations resulting from guidance errors to the end-point on the trajectory.

The Conic Error Propagation Program (CEPP) has been used for this study. It is a combination of subroutines previously developed at Philco WDL and subroutines that have been developed for this study. In particular, the subroutine for computing transition matrices has been changed in this program as the result of numerical difficulties experienced with the precision program. A flow chart of the various subroutines used in (CEPP) is shown in Figure 3-1. This program has been written so that it may be used in conjunction with the Quick Look Programs (See References 10 and 11).

The Advanced Error Propagation Program (AEPP) now under development at WDL (Reference 12) also has the simulation capability required for a study of this type. It is mentioned here because it has a greater flexibility and capability than the CEPP. With AEPP, it will be possible to consider bias error sources and either solve them directly or determine their effect on the state estimate. In fact, this program has been used to evaluate the station location bias errors which will be discussed in Section 5. In this section the features of the CEPP are described.

3.1 THE NOMINAL TRAJECTORY

It has been found that the nominal trajectory is sensitive to the eighth figure of the starting value of the injection position and velocity. The sensitivity of the end-point position to initial conditions is on the order of 10^5 km/km for position and 10^8 km/km/sec for velocity. Therefore, for injection from Earth park orbit with a radius of 6500 km and a velocity of 15 km/sec, the significance of the eighth figure of position and velocity in terms of position variations at the target is on the order of 10 km and 100 km, respectively. This caused a problem in the integration process used to find a precision nominal trajectory. For example, if the integration is stopped in the middle of the trajectory (such as at a guidance correction), and then restarted, the round-off error results in a different end-point than would have been obtained if the integration had not been stopped. As a result of these difficulties, the CEPP uses a patched conic for the nominal trajectory. This produces better results since the problem can be restarted at various points and the same end-point values obtained (the trajectory was rectified at each patch point); also, this program is faster than integrating the n-body trajectory. The three conic sections from Earth to Mars (Earth-centered, Sun-centered, and Mars-centered) or Mars to Earth are input data which are obtained from the Quick Look Programs. (References 10 and 11).

The inputs for each conic are:

Body center	(Earth, Sun, Mars)
Date	(Year, Month, Day)
Fractional Date	(Hours, Minutes, Seconds)
Time Length of Conic	(Seconds)
Time of Coordinates	(Equator Date, 1950, Ecliptic)
Vehicle State	$(X, Y, Z, \dot{X}, \dot{Y}, \dot{Z})$

The patch distances which were used to obtain the trajectories are the following:

Earth	925,000 KM	Patch Distance
Moon	66,000 KM	Patch Distance
Mars	565,000 KM	Patch Distance

The ephemeris which was used for the planets was the JPL ephemeris tape (Reference 13), which is in Earth equator of 1950 coordinates. The computations, therefore, were carried out in equator of 1950 coordinates using kilometers and kilometers/second.

3.2 THE TRANSITION MATRIX

The subroutine for calculating the transition matrix $\Phi(T,t)$ is one of the important computations used in this study. It is used for propagating estimates of the vehicle state resulting from injection errors and guidance errors, to the end-point for each phase of the mission. It is, however, a computation that has resulted in a number of problems in earlier studies. Methods of computing $\Phi(T,t)$, as well as problems that have been experienced in the use of these methods, are described in the following paragraphs.

The transition matrix $\Phi(T,t)$ is computed in the Interplanetary Error Propagation Program (IEPP) (References 14 and 15) by the following method:

$$\begin{aligned}
\Phi(T, t_1) &= \Phi(T,t_o)\,\Phi^{-1}(t_1,t_o) \\
\Phi(T, t_2) &= \Phi(T,t_1)\,\Phi^{-1}(t_2,t_1) \\
&\vdots \\
\Phi(T,t_m) &= \Phi(T,t_m)\,\Phi^{-1}(t_m,t_{m-1}),
\end{aligned} \tag{3-1}$$

where the times t_1, t_2 ... t_m represent points at which results are printed out or guidance corrections are made. The inverse matrices in (3-1) have

been calculated directly using a single precision inverse subroutine. An alternate method for inverting Φ is given by relationship

$$\Phi = \begin{bmatrix} \Phi_{11} & \Phi_{12} \\ \Phi_{21} & \Phi_{22} \end{bmatrix} \qquad \Phi^{-1} = \begin{bmatrix} \Phi_{22}^T & -\Phi_{12}^T \\ -\Phi_{21}^T & \Phi_{11}^T \end{bmatrix} . \tag{3-2}$$

Numerical difficulties have been experienced in both methods. For long time intervals along the trajectory (10 days), the elements of Φ become large, with the result that inverse matrices become inaccurate.

To improve the numerical problem described above, a transition matrix has been used in the CEPP which is obtained from a closed-form analytic expression (Reference 16). These analytic expressions for the transition matrix are valid under the assumption of a conic trajectory. A comparison of the closed-form transition matrix and one obtained by integrating the variational equations from injection to the end-point along a precision n-body trajectory (no inversions are required and therefore this method is quite accurate), showed that the two matrices agree to within 2 percent. The use of the closed-form expression for the transition matrix allows rapid calculation of the matrix from any time (t) to the end-point time (T), and does not require the inversion shown in 3-1. It has been found that replacing the n-body trajectory integration by a patched conic trajectory and using the closed form transition matrix increases the speed of CEPP over IEPP by a factor of two.

3.2.2 Navigation Capability

The CEPP, which is shown in block diagram form in Figure 3-2, has the capability of simulating onboard navigation, Earth-based navigation, or a combination of both.

The Earth-based tracking capability consists of three tracker stations. Each station can make the following measurements when the vehicle is above the station horizon:

a. Range
b. Range-Rate
c. Azimuth
d. Elevation.

There is a random error associated with each type of observation for each station. The magnitude of these errors are inputs to the program.

The onboard measurement capability consists of the following types:

a. Range (Radar)
b. Range-Rate
c. Theodolite (right ascension and declination)
d. Sextant (Star-Planet Angle)
e. Range (Subtended Angle).

For each of these measurements, there is a random error which is an input to the program. The result of an observation is expressed mathematically by

$$y = H\,x + q, \tag{3-3}$$

where y is the measurement
H is the gradient of the measurement with respect to the state
x is the deviation state
q is the random noise in the measurement

The optical instruments (Theodolite and Sextant) which are described in Section 4 have an error model of the form:

$$\sigma = \sqrt{k_1^2 + 4k_2^2 \left(\mathrm{Sin}^{-1} \frac{RAD}{|r|}\right)^2} \tag{3-4}$$

where σ is the standard deviation of the measurement error q. This error model is discussed, and error curves for the planets of interest in the study are presented in Section 4.

These different navigation measurements may be grouped in any desired combination by the input control. The influence of these measurements is included in the covariance matrix of the error in estimate of the state P(t) at the appropriate times under the assumption that the data are being processed with a Kalman filter. This results in a new covariance matrix, P, which is given by (2-88) and a new estimate of the state x_n given by (2-87).

Between observations, the covariance matrix of the error in estimate is propagated along the nominal trajectory using linear perturbation techniques. This is expressed by

$$P(t_1) = \Phi(t_1,t)\, P(t)\, \Phi^T(t_1,t) \qquad (3\text{-}5)$$

The errors in estimate data are output for the present time (t) and also the end-point time (T). The following quantities are output at each time:

RMS Error in position estimate	(time, t, X, Y, Z)
RMS Error in velocity estimate	(time, t, $\dot{X}$, $\dot{Y}$, $\dot{Z}$)
RMS Error in end position estimate	(time, T, B·T and B·R or XYZ)
Error in end constraint estimate	(time, T, V_∞)

The error in estimates of the terminal constraints is determined by the equation

$$P'(T) = C(T)\ (T,t)\ P\ (t)\ \Phi^T(T;t)\ \ C^T_{(T)} \qquad (3\text{-}6)$$

where P' (T) is a 3 x 3 covariance matrix of the error in estimate of the end constraints

C(T) Point transformation from the state to the end constraints

Φ(T;t) Transition Matrix

P(t) Covariance Matrix of error in estimate of the state at time (t).

3.2.3 Guidance Capability

The CEPP guidance routines are entered after the navigation is completed at a given time point as shown in Figure 3-2. The program is capable of using either of two guidance laws: Fixed Time of Arrival (FTA) or Variable Time of Arrival (VTA), both of which are described in Paragraph 2.2.2.

When the VTA guidance law is being used, the program also computes the minimum velocity correction required to control $\vec{B}\cdot\hat{T}$ and $\vec{B}\cdot\hat{R}$ to their nominal values.

The program is capable of making six corrections along the trajectory. The correction times are input to the program, and are assumed to be step changes in velocity. There is no powered flight simulation.

There are three error sources included in the onboard simulation of the control system and thruster: (1) pointing error, (2) proportional error, and (3) resolution error. These errors may be written as:

$\epsilon_{PROP} = k_1 \dot{x}_g$ — error proportional to velocity correction and in the direction of the correction

$\epsilon_{RES} = k_2 \frac{\dot{x}}{|\dot{x}_g|}$ — error independent of velocity correction but in the direction of correction

$\epsilon_{PT} = k_3 \hat{u} \otimes \dot{x}_g$ — error proportional to velocity correction and in a direction normal to the correction

$\hat{u}$ is a vector. The magnitude of the three constants associated with these errors are input to the program.

The simulation also has the capability of including onboard instrumentation to monitor the corrections. This enters into the

simulation at the times a correction is made. It provides the capability of increasing the error in the estimate of the velocity state by a fraction of the error in execution of the maneuver. The effect of the monitor is determined by the value of α in the equation

$$P_{NEW} = P_{OLD} + \alpha \begin{bmatrix} 0 & 0 \\ 0 & E(\epsilon\epsilon^T) \end{bmatrix} \tag{3-7}$$

where $E(\epsilon\epsilon^T)$ = covariance matrix of guidance system execution errors and

$$0 \leq \alpha \leq 1.0.$$

The quantity, α, is input to the program. The covariance matrix of the expected guidance correction at time (t) is obtained as follows:

$$E(\hat{\underline{x}}_g \hat{\underline{x}}_g^T) = G(T;t) \left[PAR(t)-P(t)\right] G^T(T;t) \tag{3-8}$$

A special guidance routine was designed to permit the parametric study of the three guidance system error sources. The navigation data for a system of interest is input to the program in the form of the covariance matrix of error in estimate of the state at each time a correction is made. The state deviation matrix (guidance data) is then propagated through a maximum of four corrections. The variances on each of the guidance system error sources can be stepped through a range of values at each correction point. The range of values and size of steps are controlled by input. A sample of the data is shown in Paragraph 5.4.4. In this mode of operation, it is possible to make 250 guidance data runs to Mars in five minutes of computer time.

SECTION 4

ONBOARD MEASUREMENT TECHNIQUES

4.1 INTRODUCTION

The overall function of the navigation system, as defined in this study, is to determine the best estimate of the vehicle's position and velocity. An important part of this estimation process is the set of observations of the vehicle state which may include range, range-rate, altitude, the angle from the center of a planet to a star as observed from the vehicle, etc. At each observation the measurement is represented by

$$y = H x + q \tag{4-1}$$

where the two parameters h and q are, respectively, the measurement gradient respect to the state, and the measurement noise. The analysis in this section is concerned with determining the relationships between the measurement parameters h and q and the accuracy of the state estimate. Since these parameters are automatically specified for a given Earth-based tracking system, this section considers only onboard tracking. Measurement accuracy, celestial body selection, navigation instruments, and star selection are considered. Although the analysis applies directly to the outbound leg of the midcourse phase, the techniques that are used are sufficiently general that they apply to onboard measurements for the other phases of this study as well as any other interplanetary mission. The techniques of onboard scheduling in this section are treated in more detail in Reference 17.

4.2 SIGNIFICANCE OF THE MEASUREMENT GRADIENT

The problem of defining an observation schedule for navigation systems that contain an onboard tracking capability is considerably more difficult than for systems that rely on Earth-based tracking. There is a much wider choice of observations that can be made onboard as well as more restrictions on the number of observations that can be taken and processed. Each

observation, in fact, may impose a penalty on the spacecraft system because of: (1) the fuel required to make a maneuver and hold an attitude during an observation, (2) the reliability of the control system, or (3) the measuring instrument itself. It is, therefore, important to establish the effect of a particular observation on the estimation of the state. The change in the state estimate with the inclusion of an observation for the Kalman filter has been derived in Equation (2-87), and is repeated here for convenience;

$$\hat{x}_N = \hat{x}_o + P(HPH^T + Q)^{-1} H^T(y-\hat{y}) \tag{4-2}$$

where

$\hat{x}_N$ is the new state estimate
$\hat{x}_o$ is the old state estimate
y is the measurement
$\hat{y}$ is the estimate of the measurement.

The vector change in the state estimate at an observation, $\Delta\hat{x} = P(HPH^T + Q)^{-1} H^T(y-\hat{y})$, may be divided up into two orthogonal vectors, one in the direction of the gradient vector, H, and one normal to it. Using projection operators on the vector $\Delta\hat{x}$, these two vectors are obtained as follows:

$$(h^T h)\ \Delta\hat{x} = \Delta\hat{x}_H = \left(\frac{(y-\hat{y})}{1 + \frac{Q}{HPH^T}}\right) \frac{h^T}{|H|}\ , \tag{4-3}$$

$$(I - h^T h)\ \Delta\hat{x} = \Delta\hat{x}_{\bar{H}} = \left(\frac{P}{hPh^T} - I\right)\left(\frac{(y-\hat{y})}{1 + \frac{Q}{HPH^T}}\right)\frac{h^T}{|H|}\ , \tag{4-4}$$

where

$\Delta\hat{x}_H$ = change in state estimate along H direction.

$\Delta\hat{x}_{\bar{H}}$ = change in state estimate normal to H direction.

$h = \frac{H}{|H|}$ unit row vector in direction of H.

Equations (4-3) and (4-4) illustrate two characteristics of the H vector. Equation (4-4) shows that if the covariance matrix of errors in estimate, P, is diagonal with equal variances on all states, $P = \sigma^2 I$, the only improvement in the estimate occurs along H. The vector $\Delta\hat{x}_H$ is zero in this instance. In the case of a general covariance matrix, there is, because of the correlation between states, an improvement in the estimate along H and also normal to it. The second characteristic of H which is of interest is the manner in which its orientation affects the magnitude of the vector change in the state estimate in both the H direction and the space normal to H. As shown in (4-3) and (4-4), each vector is scaled by the factor

$$\frac{1}{1 + \frac{Q}{HPH^T}} \tag{4-5}$$

The quantity Q is the variance of the measurement due to the errors in the instrument being used. The quantity, HPH^T, is a scalar which indicates the variance in the measurement due to the uncertainty in the estimate of the state. The following limiting cases are of interest in evaluating this scale factor:

$$Q \gg HPH^T \qquad \frac{1}{1 + \frac{Q}{HPH^T}} \doteq 0 \tag{4-6}$$

$$Q \ll HPH^T \qquad \frac{1}{1 + \frac{Q}{HPH}} \doteq 1 \tag{4-7}$$

The first case corresponds to a very poor instrument or measurement along a direction in the state space which has a very small uncertainty associated with it. This measurement would provide little or no information. The second case illustrates a very fine instrument or measurement along a direction of large undertainty or both. It can be seen, therefore, that for a given

instrument accuracy, Q, it is desirable, if possible, to select the gradient of the measurement (H) so that it will be along a direction of large uncertainity in the six-dimensional state space. An objective of selecting a set of measurements would be to have the gradient vectors corresponding to the measurement set span the total six-dimensional state space. This would then allow estimation of the total state. This is not in general required, however, because correlations between states which occur due to the equations of motion allow a state to be estimated without actual observation of that state (Equation (4-4)). For example, velocity information can be obtained from smoothing position measurements.

The above discussion has been presented because once the type of navigation measurements is selected, the scheduling of the measurements is the only control that can be exercised over the gradient vector H orientations. The gradient vectors for the measurements which were used in the analysis are shown in Table 4-1.* The directions of these vectors can be used as aids in setting up the measurement schedule, and are particularly useful in selecting an onboard observation schedule.

4.3 ONBOARD NAVIGATION INSTRUMENTS

A primary consideration for onboard tracking is the instruments which are used to make the observations. In general, the two categories of onboard instruments that can be used for determining position and velocity are:

a. Radar-type Devices. In their simplest form these devices may provide measurements of altitude and altitude rate. In more complex forms where several devices are coupled with an inertial reference, it is conceivable that one could obtain the following additional quantities:

---

* Derivations of these gradients are presented in Appendix B.

1. Direction of the apparent local vertical in inertial coordinates

2. Velocity relative to the surface and inertial direction of this velocity vector.

b. Optical Type Devices

1. Scanners (Visible or Infrared Region). These devices are generally automatic, and can be arranged such that their optical center remains near the center (or rim) of a celestial body of the solar system. If the device is combined with an inertial reference platform, the inertial direction is obtained. With other modifications the subtended angle can also be obtained.

   Another scanner possibility would combine the instrument with a star tracker. The star tracker will establish an inertial direction, and an appropriately designed and mounted planet tracker could provide the angle from the star to the planet rim or center.

2. Theodolite. This device may be used on manned space vehicles where the man directs the theodolite to the apparent center of the body in the solar system. If the theodolite is mounted on an inertial platform, then the measurements possible are the directions (two angles) of the celestial body (apparent center or landmarks) in a known inertial reference system. Modifications could also allow the measurement of the subtended angle.

3. Sextant. This device is also used on manned vehicles. It has the capability of measuring a single angle. One can measure an inertial angle (e.g., from some star to the apparent center, rim, or a landmark of a body of the solar system) without the need of an inertial reference platform. An appropriately designed sextant can be used for a variety of purposes in addition to the above such as:

(a) Measurement of the subtended angle of the body, or perhaps the angle between two landmarks

(b) The angle between two given bodies of the solar system.

In addition, the instrument may be calibrated onboard by star-to-star measurements.

c. Photograph of the Celestial Body In The Solar System In The Star Background. The reduction of the photograph by the onboard personnel can provide the inertial direction (two angles and perhaps the subtended angle of the body).

Since the radar devices are restricted to use in the immediate vicinity of a celestial body, the measurement schedule developed in this section will assume the use of an optical device. The analysis applies to either: (1) a theodolite which measures the direction of the line of sight (LOS) to a planet or the Sun, or (2) a sextant which measures the angles between a planet and a star.

For the onboard measurement instruments that have been selected, it is possible to develop a measurement schedule that is based on: (1) position measurement accuracy associated with a planetary body, (2) the positions of the planetary bodies, and (3) the selection of stars for use with sextant measurements. The position measurement accuracy specifies the numerical value of the error in a single vehicle position estimate when using a specific body. The selection of planetary bodies and the stars determines the direction of the H vectors associated with the measurements such that a maximum amount of position and velocity information is obtained from each of the six dimensions of the state space. The remainder of this section is devoted to developing a measurement schedule for the midcourse trajectory.

4.4 MEASUREMENT ACCURACY

The purpose of this subsection is to develop the error model for the instrument errors and to show the position measurement accuracy along the nominal trajectory. The angular measurement accuracy which is attainable with an optical device is usually specified in terms of minutes or seconds of arc. The standard derivation of this error has been assumed to be

$$\sigma_\epsilon = \sqrt{k_1^2 + 4k_2^2 \left(\sin^{-1} \frac{RAD}{|R|}\right)^2} \qquad (4\text{-}8)$$

where

k_1^2 = the variance of the angular error when the instrument is used for star-star measurements

k_2^2 = the variance of the angular error when the instrument is used to measure the subtended angle of the body at some low altitude

RAD = radius of the body

R = range to body center

The standard deviation of the measurement noise ((q) in (4-1)) is therefore specified by σ_ϵ in (4-8). The error model given by Equation (4-8) is based on the assumption that, as the body is approached, its size in the field of view increases, which causes a greater error in detecting the apparent center (or rim). It is likely that the magnitude of the total LOS rate should also enter in this error model due to the difficulties of tracking a moving object. The LOS rate effect has been neglected because of a lack of information on how to include it.

Since the measurement error is an angular error, the position uncertainty established with such a device is directly related to the range of the body being observed. The uncertainty in a position measurement ϵ_P as a function of range to the center of the planet of interest is given by

$$\epsilon_P = \sigma_\epsilon |R| \qquad (4\text{-}9)$$

where $|R|$ = Range to planet,

σ_ϵ = Measurement error (standard deviation).

One can, therefore, use (4-9) to calculate the uncertainty in a position measurement when using the celestial bodies of interest along a nominal trajectory. The standard deviation of the measurement error, σ_ϵ, which was used in the study for the 10 arc second device is shown in Figure 4-1. Also, the error in a single position measurement is shown for this instrument.

The main results of this measurement accuracy section are given in Figure 4-2, which shows the error in position estimate (ϵ_p) for a single observation of various planets as calculated by (4-8) and (4-9) along the nominal trajectory. This figure indicates that the Earth and Moon provide the smallest position uncertainty early in the flight. In the middle of the flight, the Earth, Moon, Sun, Venus, and Mars give about the same uncertainty (10,000 km). At the end of the flight, however, Mars has by far the smallest position uncertainty. Also, as seen from the figure, Jupiter is not of importance in selecting a schedule since the measurement error for this body is very large during the entire flight. Thus the results shown in this figure indicate which planets should be selected along the trajectory in order to obtain good measurement accuracies.

4.5 BODY SELECTION

This section is primarily concerned with determining the direction of the measurement gradient H for various planets and the Sun, such that the observations will provide information on all six dimensions of the state space. The results of determining the direction of the H vectors may then be combined with the measurement accuracy data in order to select a measurement schedule. This is illustrated by selecting a measurement schedule for the outbound leg of the midcourse trajectory.

The LOS to a planetary body is important because the plane of the H vector associated with a sextant or theodolite measurement to the body is normal to it. Therefore, this is the plane in which information on the position of the vehicle can be obtained. This is shown analytically in Table 4-1 and graphically in Figure 4-3. From Figure 4-3, it is seen that any two star-planet measurements using a planet along OA result in H vectors that lie in a plane perpendicular to OA. The two orthogonal star measurements shown are identical to one theodolite measurement, i.e., they determine the vehicle position in the plane spanned by H_1 and H_2.

The problem of selecting planetary bodies such that information is obtained on the three position coordinates of the vehicle state can be considerably simplified. For interplanetary trajectories with reasonable launch energies, the trajectory plane and the orbit planes of all the planetary bodies are nearly in the plane of the ecliptic. As a result, the problem of determining the vehicle position can be resolved into: (1) position normal to the ecliptic plane, and (2) the two-dimensional position in the ecliptic plane.

Information on the vehicle position along the coordinate normal to the ecliptic can be obtained by measuring the angle between any planetary body and a background star which has a direction normal to the plane of the ecliptic. This measurement results in an H vector which is perpendicular to the ecliptic plane. For out-of-plane measurements, it is therefore reasonable to use the planetary body that provides the best measurement accuracy.

The problem of determining the two-dimensional position in the trajectory plane is more difficult, since it is necessary to select two bodies whose measurement H vectors span the trajectory plane. The selection of a schedule for inplane measurements is made on the basis of the location of the bodies in the ecliptic plane relative to the vehicle as well as the measurement accuracy data. The location of the bodies in the ecliptic

plane relative to the vehicle can be determined from the RA of each body in the vehicle-centered ecliptic coordinate frame. As shown in Figure 4-4. If the difference between the RA of two bodies is 90°, the H vectors will be orthogonal and will therefore provide the best estimate of the inplane components. The values of RA for the planets of interest are shown in Figure 4-2B with the same abscissa as in Figure 4-1A, and can therefore be used in conjunction with the measurement accuracy.

Figure 4-2A indicates that, for the early part of the trajectory, the Earth provides the best measurement accuracy. The Moon would also provide good navigation data in the early part of the trajectory. Although from Figure 4-2A the Sun appears to provide fairly good measurement data, the use of this body would not be expected to provide any additional information for the first 40 days. This is because the RA of the Earth and the RA of the Sun in the early part of the trajectory are almost 180° apart, and therefore, the position information obtained from these two bodies is almost colinear. Figure 4-5, which shows the propagation of injection errors and includes the effects of Earth and Sun observations made along the trajectory, shows that there is, in fact, no improvement in either the $\vec{B} \cdot \hat{T}$ or $\vec{B} \cdot \hat{R}$ end constraints by combining Earth and Sun observations, rather than using just Earth observations. This figure also indicates no change in the $\vec{B} \cdot \hat{T}$ error and implies, therefore, that this constraint is dependent on the coordinate which is normal to that determined by either the Earth or the Sun.

In order to obtain a good position estimate along the direction normal to the position estimate provided by the Earth, it is necessary to use a body whose RA is about 90° from that of the Earth. This value of RA is defined by A-A on Figure 4-2B. Any body whose RA passed through the cross-hatched area will provide good information on the coordinate normal to A-A for the first 60 days. At 12 hours from injection, the Moon passes through the area as shown by the figure. During this time, it is possible to obtain a good measurement of the coordinate normal to A-A, since the measurement accuracy using the Moon at this time is good as seen in Figure

4-2A. The value of Moon observations at this time is verified by Figure 4-6, which shows a reduction in the $\vec{B} \cdot \hat{T}$ error in estimate starting at about five hours from injection.

An alternate method for obtaining information on the coordinate normal to A-A is to make Sun observations starting at 40 days. At this time, the Sun crosses the region of interest in Figure 4-2B and takes 40 days to cross it. The tracking data shown in Figure 4-7, which uses Sun and Earth observations during the first 100 days, shows that the Sun observations at about 40 days have the same effect as the Moon in reducing $\vec{B} \cdot \hat{T}$ errors in estimate. The improvement is not a great as when the Moon was used. This might have been expected since the measurement accuracy with the Moon is greater than that with the Sun at this time as shown in Figure 4-1A.

During the second half of the trajectory, Mars is in a good position to maintain the position information along the A-A direction. The Earth and Sun are in a position to permit estimation of the vehicle's position normal to A-A, although the quality of the measurements is poor. Over the second half of the trajectory, it is therefore possible to have near orthogonal directional coverage of the trajectory plane by observing Mars and either the Earth or Sun.

As the result of both the measurement accuracy and direction of the measurement gradient, H for each body (Figures 4-2A and 4-2B, respectively), a schedule has been defined for observing planetary bodies, and is presented in Table 4-2. This schedule may be used for measurements with a theodolite on an inertial platform, or it may be used with a sextant in conjunction with a star selection schedule.

An additional body selection schedule has been developed for use with the low energy trajectory. Figures 4-8A and 4-8B give the measurement accuracy and RA data, respectively, for this trajectory. This data indicates a more favorable tracking situation because Earth and Mars provide an average measurement accuracy that is better than that for the nomina

trajectory. The fact that their measurement accuracies are good allows the two bodies to provide position coverage of the ecliptic plane. The bodies differ from being colinear by 10 to 30 degrees. The schedule that has been defined for the low energy trajectory is given in Table 4-3, and again is based on measurement accuracies and the position of the bodies.

The body selection schedules of Tables 4-2 and 4-3 have both been developed without considering the number of observations that should be taken for each body. The numbers of observations is important because each observation requires a certain amount of time and fuel to maneuver the vehicle into the proper attitude. It is therefore, desireable to adopt a schedule where the number of observations is not excessive. One of the main considerations in determining the number of observations is the accuracy of the measurement. During the early part of the midcourse trajectory, the Earth provides accurate measurements, and near the end Mars provides accurate measurements. Also, at these times there is only one body to observe and, therefore, maneuvering is held to a minimum.

The number of observations is also important because there is a tradeoff between instrument accuracy and the number of observations. This is shown in Figure 4-9, where the navigation performance is compared for two sextants with accuracies of 10 arc seconds and 20 arc seconds. Curves (1) and (2) have been obtained with 162 inplane measurements and 32 out-of-plane measurements. The degradation in performance with the 20-arc-second device at 220 days is 100 percent. This is the type of increase that would be expected in a linear system where a parameter is estimated with an instrument having only random errors. The results in curve (3) show that the error in estimate is reduced very nearly by the square root of the number of observations

$$\left(\sigma_{EST} = \frac{\sigma_{INST}}{\sqrt{N}} . \right)$$

Curve (3) represents the results obtained for a 20-arc-second device and four times as many observations as in the other two cases. As seen from the figure, the error in estimate is almost identical to that for the more accurate instrument.

4.6 STAR SELECTION

In this subsection, the equivalence between a theodolite measurement and two sextant measurements is established; the star selection problem is evaluated in terms of obtaining a good estimate of the vehicle velocity; and, finally, a technique is developed for selecting a star schedule based on the body selection as well as the velocity state.

The direction of the LOS can be obtained by using either a theodolite measurement or two star-planet measurements. Either of these measurements will determine the vehicle's position in a plane normal to the direction of the LOS. When the two background stars used with the sextant are perpendicular (Figure 4-10), the accuracy of the direction of the LOS measurement should be equal to that obtained with a theodolite. This equivalence is verified by Figure 4-11 which gives the RMS error in estimate of position miss ($\vec{B}\cdot\hat{T}$ and $\vec{B}\cdot\hat{R}$) at Mars encounter, as a function of time from Earth injection for both sextant and theodolite observations. Two orthogonal sextant measurements were taken for each theodolite measurement. The figure indicates that both schemes are equivalent and provide a miss distance error in estimate of 10 km at Mars. The platform which was used with the theodolite was aligned with the Earth equator and equinox of 1950. The stars which were used had the reference direction shown in Figure 4-10 in the ecliptic plane. This also illustrates the fact that, as long as two orthogonal measurements are made using an instrument with uncorrelated measurement errors, the platform orientation or reference direction is not important.

It is of interest to note the degradation in performance if the measurement conditions with the sextant are not optimum. The data in Figure 4-12 show a comparison of the error in end-point estimates for two cases. The one case used two sextant measurements at each point with star-planet lines which were orthogonal. The second case considered the same measurement pairs, but the star-planet lines were separated by 45 degrees. The degradation in the estimate at the end time under what would be quite unfavorable conditions is from 3.1 km to 3.5 km.

If the sextant is used in such a manner that two measurements are not taken at each point, a number of questions arise:

a. Is the choice of the reference direction in Figure 4-10 important?

b. What is the relative importance of the measurements taken using Star No. 1 and those taken using Star No. 2 once a reference direction is chosen?

Since the principal uncertainties in the estimate of the terminal miss are due to errors in velocity estimate, it is reasonable to now consider the orientation of the reference direction such that maximum information may be obtained on the vehicle's velocity.

To do this, the problem is again reduced to determining velocity components in the orbit plane. It is, therefore, reasonable to select the reference directions in Figure 4-10 so the stars are in the following directions:

1) Star No. 1 is in the direction of maximum rotation rate of LOS due to the vehicle's inertial velocity.

2) Star No. 2 is in the direction of zero rotation rate of the LOS due to the vehicle's inertial velocity.

It is the vehicle's "inertial velocity" that is important because the celestial body ephemeris in the star background is accurately known and, therefore, the clestial body's velocity does not provide information on the estimate of the vehicle's position or velocity.

The direction of the maximum and zero LOS rate are defined by the $\hat{u}$ and $\hat{\ell}$ unit vectors respectively which are

$$\hat{u} = \frac{r \times v}{|r \times v|} \times \frac{r}{|r|} \tag{4-16}$$

and

$$\hat{\ell} = \frac{r \times v}{|r \times v|}, \tag{4-17}$$

where

r = instantaneous vector between the vehicle and the celestial body

v = inertial velocity vector of the vehicle relative to the central body

Also, since the orbit planes, of the celestial bodies and vehicle orbit plane are all essentially in the ecliptic plane, the unit vectors $\hat{u}$ and $\hat{\ell}$ are in the ecliptic plane and normal to the ecliptic plane, respectively. This establishes the ecliptic as the plane of reference ($\delta = 0^{o}$) in Figure 4-10.

The body selection schedule was chosen so that the two bodies selected have a difference in RA as close to 90^{o} as possible. Use of the two bodies in that schedule with stars in the $\hat{u}$ direction, therefore, provides good two dimensional inplane position information, and use of any body with a star in the $\hat{\ell}$ direction provides information on the position coordinate normal to the ecliptic plane. This position information is smoothed to provide the velocity information.

In order to determine the availability of specific stars along the trajectory that can be used in conjunction with the body selection schedule, the right ascension of Earth, Mars, and the Sun in a vehicle-centered 1950 equator of date coordinate system is shown in Figure 4-13A as a function of time from injection. Figure 4-13B shows the celestial sphere as seen from the spacecraft, where the dotted line is the ecliptic plane projected onto the sphere, and some of the first, second, and third magnitude stars near the ecliptic have been included. The feasibility of taking a sextant measurement at a given time can be determined by first selecting a body from the body selection schedule, and then by using Figure 4-13A and Figure 4-13B to determine whether the availability of stars and the position of the Sun will make the observation possible.

In order to illustrate the use of Figure 4-13, an example is now considered. Assuming the body selection data indicates that the observations of the Sun and Earth are desirable at 120 days, Figure 4-13A is entered at this time. As shown by the dotted lines, the right ascensions of these bodies are projected into the ecliptic plane shown on the celestial sphere in Figure 4-13B.

The intersection of the dotted lines and the ecliptic plane represent the positions of the Sun and Earth on the celestial sphere as viewed from the spacecraft at 120 days along the trajectory. Forty by sixty degree sectors about each of these points have been enlarged and are shown in Figure 14. It can be seen in Figure 14B that both bodies are very near the ecliptic plane and that the $\hat{u}$ and $\hat{e}$ measurement directions are tangent (in the plane) and normal to the plane. Overlayed on each sector is a 20-degree-diameter circular window. The overlay could be made to any size and shape which corresponds to the vehicle's observations window constraints. The vehicle windows shown in the figure present the bodies of interest and the background stars available at the specific time.

The upper part of Figure 4-14 shows that the first magnitude star Regulus can be used for a measurement of the position in the $\hat{u}$ direction. The use of the star would be restricted to a slightly earlier or later time since it is directly in the sun at the time shown. The time difference which would be required would depend on the angular separation between a star and the Sun required for making such a measurement when using a specific instrument. Slightly earlier in the flight (three degrees right ascension or about four days), the third magnitude star, ν_{LEO}, in the upper part of the window would be in an ideal position for a position measurement in the $\hat{\ell}$ direction. It is within the vehicle's window for the time shown and not too far from the reference $\hat{\ell}$ direction. The same type of analysis can be performed for the Earth which is shown in the lower portion of Figure 4-14. In this case, the star Spica could be used for a $\hat{\ell}$ measurement, and a few days later it would be positioned for a measurement in the $\hat{u}$ direction.

If these two bodies, Sun and Earth, were to be observed at approximately the same time, Figure 4-13 also indicates that the vehicle must be reoriented 52 degrees in RA and 20 degrees DEC. With a specific control system, these required excursions could be used to generate data on the time and fuel requirements for such a maneuver. The data generated in this manner would likely dictate how often one might want to switch bodies being observed.

The data in Figure 4-13A can also be used to evaluate the position of the Sun relative to a body of interest. This would be done to ensure that the Sun did not "blind" the instrument being used. For example, at the time of 120 days the Earth is 50 degrees away from the Sun. The figure also indicates that this is as close as the Earth gets to the Sun along the whole trajectory.

These data are presented to indicate the manner in which stars might be selected for use with a specific body. It also indicates that, with a star tracker with the capability of tracking a third magnitude star, selection of a star in a specific direction is not difficult.

With the reference direction chosen, it is of interest to determine the relative importance of inplane measurements in the $\hat{u}$ direction) and out-of-plane measurements (in the $\hat{t}$ direction). Although this question is quite complex because it is a function of the particular trajectory as well as the navigation time histories up to the point of interest, it is possible to point out some of the important considerations for a given set of data. Three sets of data with a fixed number of measurements are shown in Figure 4-15 which indicate the relative importance of inplane and out-of-plane measurements for the nominal trajectory*.

Curve (1) has been obtained by taking seven inplane observations for each out-of-plane observation (7:1 ratio). Curve (2) was obtained by reversing the ratio (1:7). Curve (3) has been obtained by using the Curve (1) ratio (7:1) during the first 100 days and a 1:1 ratio during the remainder of the flight. Regions on these curves where measurements are being taken but no reduction in the estimation error occurs indicate measurements which are not useful (90 to 150 days on Curve (1)). Also, points on the curves where a large reduction in the error occurs (70 days on Curve (2)) when the less frequent measurement is taken indicate that the measurement is not being taken often enough. During the first 100 days, a comparison of curves (1) and (2) indicate that the inplane measurement is more important. In particular, curve (1) shows a gradual decrease in error from 40 to 80 days with the large number of inplane measurements. During this same interval on Curve (2), there is very little reduction in the error in estimate while out-of-plane measurements are taken. When an inplane measurement has been taken there is a

*These results have been obtained using System IV navigation system as described in Paragraph 5.3.2.

relatively large decrease in the estimation error (35 to 70 days). During the time from 130 days to the end of the flight, the data in the two curves indicate an importance in both types of measurements. There are regions in which reductions in the error in estimate occurs for both types of measurements.

The third curve has been generated using a 1:1 ratio of measurements from 90 days to the end. During the period from 220 days to 234 days 0 hours, Curve (3) provides a better estimate than Curve (1). This illustrates that replacing some of the inplane measurements with out-of-plane ones from 90 days up to this time produces a better estimate. On the other hand, from 234 days to the end-point, Curve (2), shows the out-of-plane measurements, but provides no information; Curve (1) shows that inplane measurements are extremely important over the last 12 hours.

SECTION 5

EARTH-MARS MIDCOURSE STUDY

5.1 INTRODUCTION

The principal results of this study, which include a statistical error analysis for the navigation and guidance systems, are presented in Sections 5, 6 and 7. The analysis in this section pertains to the midcourse phase of the Earth-Mars mission. It is defined to be the interval of time between injection onto the transfer trajectory from a 185 km altitude Earth park orbit and the point of closest approach to Mars. Since it has been found that the accuracy of the guidance system is highly dependent on the accuracy of the navigation system, the navigation is studied first, and these results are then used to study the guidance system.

The analysis of the navigation system is concerned with determining the accuracy with which the position and velocity of the vehicle can be estimated. Since one of the primary objectives of the study is to compare the capabilities of ground-based and onboard navigation systems, the navigation analysis is carried out for each of the four systems described in Section 1. The overall figure of merit that is used for comparing the navigation systems is the error in estimate of the end-point constraints on the nominal trajectory.

The guidance analysis for the midcourse phase is concerned with determining the number of corrections and times at which they are made, evaluating two different guidance laws, and analyzing the effects of errors resulting from the thrusting maneuvers. The figure of merit used for the guidance system evaluation is the deviations of the end-point constraints. The specific requirements on these deviations are quite mission-dependent. For example, on Mariner IV the primary concern was to fly by the planet with a high probability of not impacting. With the large distance of closest approach which was used, large guidance

deviations could be tolerated. If, instead, an atmospheric braking maneuver were to be executed at Mars, a much smaller tolerance on the deviations is required. In the analysis of the four systems which follows, a basis of comparison which is used is a $\pm$ 3.5 km deviation in the altitude direction. This would provide sufficient accuracy for the terminal maneuver to be performed with atmospheric maneuvering. This deviation error represents approximately a three-sigma confidence level of hitting a 21 km entry corridor at Mars. This corridor width was obtained in a previous study.*

The analysis in this section has been performed for a given nominal trajectory and for assumed numerical values of the statistical errors. Use of the results in this section to specify hardware requirements is, therefore, limited by these assumptions that have been made for the Earth-Mars mission. The techniques that have been developed to analyze the guidance and navigation requirements are not limited, however, and in fact could be applied to any interplanetary mission.

5.2 MIDCOURSE STUDY RESTRICTIONS

In order to keep the scope of the study to a reasonable size, two restrictions have been made on the midcourse phase study. The restrictions concerned: (1) the nominal midcourse trajectory, and (2) the initial injection errors.

5.2.1 Nominal Trajectory

The trajectory that has been considered as a nominal for the midcourse phase is shown in Figure 5-1 and described in Appendix C. It has been selected from a previous mission analysis study (Reference 19), and is based on a 1975 launch date and the fact that the position of Earth and Mars must be favorable for the return to Earth after a short time in a Martian orbit. As a result, the two planets are not in a favorable position at launch from Earth; therefore, an extremely high injection velocity (16 km/sec) is necessary.

*The study parameters and the definition of the corridor bounds are described in Reference 18.

In order to investigate the effects of choosing a particular trajectory, the trajectory shown in Figure 5-2 and described in Appendix C has also been considered. This trajectory has a considerably lower injection velocity (11.8 km/sec) and is more representative of the type that would be used for a Mars flyby (Mariner IV). For a round trip it might be used with a Venus swing-by on the return.

The nominal trajectory has been constrained to pass Mars in the desired manner by using the B vector constraints described in Section 2 and Reference 3. The specific constraints that have been used are $\vec{B}\cdot\hat{T} = |\vec{B}|$ and $\vec{B}\cdot\hat{R} = 0$. The $\hat{T}$ and $\hat{R}$ unit vectors have been selected to be in the Mars orbit plane (x-y plane of the target coordinates)and normal to the Mars orbit plane, respectively. The approach geometry and the nominal values of the $\vec{B}$, $\hat{R}$, $\hat{S}$, and $\hat{T}$ vectors for this trajectory are shown in Figure 5-3. The nominal values of $\vec{B}\cdot\hat{T}$ and $\vec{B}\cdot\hat{R}$ indicate that the trajectory passes on the Sun-lighted side of Mars near the ecliptic plane. Furthermore, these nominal constraint values indicate that deviations in $\vec{B}\cdot\hat{T}$ are associated with deviations in the $\vec{B}$ vector magnitude or the radius of closest approach and deviations in $\vec{B}\cdot\hat{R}$ are associated with deviations in the inclination of the approach trajectory relative to Mars.

Figure 5-4 shows the relationship between the $\vec{B}$ vector magnitude and the radius of closest approach for both the nominal and low-energy trajectories. These curves have been computed from equations given by Battin (Reference 4). Since the slope of these curves is 0.95, there is approximately a 1:1 correspondence between deviations in the $\vec{B}$ vector magnitude and deviations in the radius of closest approach. As a result, it is possible to perform the analysis of the navigation and guidance systems in terms of $\vec{B}$ vector deviations and interpret the results in terms of the deviations in the radius of closest approach.

5.2.2 Injection Errors

Since neither the powered flight nor the Earth park-orbit phases are considered in this report, the errors from these phases become initial

errors at injection onto the midcourse trajectory and, therefore, affect the results of this section.

Numerical values of typical injection errors have been supplied by MSFC (Reference 20). The standard deviations of position and velocity for these errors are shown in Figure 5-5 as a function of time in park-orbit. The nominal trajectory used in this analysis has a 30-minute park time. The complete covariance matrix of injection errors for this park time is shown in Figure 5-6. Propagation of this covariance matrix along the nominal trajectory to the end point yields one-sigma deviations in the end constraints, $\vec{B} \cdot \hat{T}$ and $\vec{B} \cdot \hat{R}$, of $2.01 \cdot 10^4$ km and $8.40 \cdot 10^4$km, respectively.

The second launch opportunity on 10 February 1975, has a park time of 85 minutes. Due to the longer park time, this trajectory has larger injection errors and, therefore, has been used to generate data illustrating the effects of larger injection errors.

5.3 NAVIGATION ANALYSIS

The analysis in this section consists of studying the ensemble statistical behavior of the four navigation systems defined in Section 1. This is accomplished by propagating the covariance matrix (P) of errors in estimate of the vehicle state ($\tilde{x}$) along the nominal trajectory, using the linear perturbation techniques and Kalman filtering theory discussed in Paragraph 2.5.1. The navigation systems as defined in this study perform the following functions:

a. Make measurements of observable quantities such as range, range rate, azimuth, elevation, angles of celestial bodies, etc.

b. Obtain a best estimate of the vehicle position and velocity by filtering the data taken at each observation.

c. Predict future states and compute the end constraints.

The general problem of estimating the vehicle state which includes the times at which the observations are made as well as which quantities are observed, is considered in the following subsections.

5.3.1 Measurement Schedule

This subsection presents a description of the measurement schedules which are used with the four system configurations as well as a description of the characteristics of the measurements which are used.

System I uses only Earth-based tracking for its navigation data. The types of measurements available when using Earth-based tracking are largely determined by the available tracking facilities. The use of the DSIF (Deep Space Instrumentation Facility) has been assumed in this study with the tracking stations at Johannesburg, Goldstone, and Woomera. The measurements taken at these stations are range-rate, elevation, and azimuth. Table 4-1 gives the gradient of each of these measurements with respect to the vehicle state. The results in the table show that, with this combination of measurements, it is possible to obtain information on the vehicle position in a plane normal to the line-of-sight (LOS) from the tracker to the vehicle, and information on the vehicle velocity along the LOS direction. The position information degrades as $\frac{1}{R}$, where R is the radius from the tracker to the vehicle. The velocity information from the range-rate data is independent of range.

The time at which observations are made for Earth-based tracking does not require selection. It is likely that observations would be made whenever the vehicle is in view of the stations being used. The schedule used in this study with the DSIF is given by Table 5-1.

Although the computational facilities of an Earth-based navigation system could process nearly all the observed data, thus making schedule selection an unimportant consideration, it is possible that one particular trajectory may be selected because it provides a more favorable schedule.

The influence of the trajectory itself on the navigation capability of a fixed-navigation system such as the DSIF is shown by comparing the tracking data in Figures 5-7 and 5-8 obtained for the nominal trajectory and the low-energy trajectory. The two important factors of a trajectory which influence the tracking capability of an Earth-based navigation system are: (1) the time which is spent at small ranges because the position data degenerates as $\frac{1}{|R|}$, and (2) the inertial angle swept out by the tracker-vehicle line-of-sight over the trajectory.

The nominal values of the measurement errors which have been used in the analysis of System I are shown in Table 5-2.

Systems II and III represent navigation systems which are combinations of Earth-based tracking and onboard observations. The selection of a schedule for these systems was made by utilizing the information in Section 4 as a guide to the onboard schedule selection. The schedules which were used with these systems are shown in Tables 5-3 and 5-4. The difference in the schedules for the two systems during the approach phase reflects the navigation data restrictions which were imposed in the vicinity of a guidance correction.

These restrictions were made to allow time for the guidance commands to be computed and transmitted to the vehicle as well as time for the maneuvers themselves to take place. These periods are shown in Figure 5-9.

Although the duration of these periods varies somewhat for each navigation system, they may be classified in general as: (1) a period during which the guidance maneuver is computed based on the last estimate of the state, (2) a period to send the guidance corrections to the spacecraft and verify that this command has been received, (3) a period during which the spacecraft's attitude is changed in preparation for the actual thrusting maneuver, and finally (4) the time at which the impulse is applied (the Δv correction).

The schedule selection for System IV is described in Subsection 4-5. The complete schedule which has been used in the analysis in shown in Table 5-5. This again reflects the restrictions shown in Figure 5-9.

5.3.2 Navigation Systems Comparison

In this subsection, the navigation performance is measured by the error in $\vec{B} \cdot \hat{T}$ and $\vec{B} \cdot \hat{R}$ end-point estimates for each of the four systems defined in Section 1. Although bias errors* clearly affect the error in estimate of the state, with the exception of station-location bias errors, only unbiased statistical measurement errors are considered.

Although it is clear that the guidance corrections depend on how well the navigation system can estimate the state, the converse is also true; i.e., the uncertainty in the guidance execution errors becomes part of the overall error in estimate of the state P after the guidance maneuver. As a result, a realistic evaluation of a navigation system should include the effects of guidance errors. For the four navigation systems studied in this section, the effect of nominal guidance errors is included by defining a P after a correction which includes a percentage of the velocity uncertainty due to the execution errors,

$$P_{after} = P_{before} + \alpha \begin{bmatrix} 0 & 0 \\ 0 & E(\varepsilon\varepsilon^T) \end{bmatrix} , \qquad (5\text{-}1)$$

where α is the result of an onboard monitor which reduces the uncertainty in the estimate of the execution errors, ε. A value of 0.01 has been used for α in the analysis. The nominal guidance system whose parameters will be studied in the Guidance Analysis Section is assumed to have the following execution errors: (1) a resolution error of 0.1 meter/sec, (σ_r) (2) a proportional error of 1 percent, (σ_v) and (3) a pointing error of 0.5 degrees (σ_p). The times at which the midcourse guidance corrections are made with

* Described in Subsection 2.5.3

each of the four systems are derived in the Guidance Analysis Section and shown in Table 5-6.

One parameter that determines the capability of the combined navigation and guidance systems to satisfy the mission constraints is the end-point deviations of the miss vector $\vec{B}$. For each of the four navigation systems, the errors in estimate which are studied parametrically are used at each of the guidance correction times to compute the end-point deviations in $\vec{B} \cdot \hat{T}$ and $\vec{B} \cdot \hat{R}$. Figure 5-10 illustrates this process of combining navigation and guidance data to obtain the end-point deviations.

From the results of this section, it is possible to determine the types of missions each of the four systems would be capable of accomplishing. Furthermore, the data shows the instrument accuracies required by each system to satisfy specific requirements under the assumptions of this study.

5.3.2.1 System I. This system as defined in Section 1 is the least complex onboard system of the four systems to be considered since it relies entirely on Earth-based tracking. The purpose of studying this system is to compare its performance with the more complex onboard systems, as well as to determine the penalty paid when a manned mission is forced to rely totally on onboard equipment due to a communication failure.

The navigation data using the DSIF tracking network are shown in Figure 5-11. The measurement errors which were used are shown in Table 5-2. The schedule of observations is shown in Table 5-1.

The error in estimate, P(t), of both position and velocity that resulted from these measurement errors is shown in Figure 5-11. The initial value of P is the covariance matrix of the injection errors that are shown in Figure 5-6. These errors in estimate were also propagated to the end point, Equation (2-62), and transformed into errors in the estimate of the miss vector $\vec{B} \cdot \hat{T}$ and $\vec{B} \cdot \hat{R}$, by using the transformation $C(T)$ in (2-31). These results show the decrease in the error in estimate

of the end constraints as more tracking data are included. The final error in estimates of $\vec{B} \cdot \hat{T}$ and $\vec{B} \cdot \hat{R}$ with this system are 110 km and 8 km, respectively. The nominal guidance system performance has been evaluated using the errors in estimate given in Figure 5-11. The state deviation covariance matrix, PAR(t), following a correction is defined in (2-120). This matrix is particularly useful when projected to the end-point because it then gives a measure of the system's overall performance. The end-point state deviations PAR(t) for System I were transformed into constraint deviations, and are listed in Table 5-7. Deviations are shown after each of the two guidance corrections. The final results, one-sigma deviations in $\vec{B} \cdot \hat{T}$ and $\vec{B} \cdot \hat{R}$ of 28.1 km and 119 km, respectively, are 128 percent and 5.3 percent larger than the estimation errors. This difference is due to the nominal guidance system execution errors.

In order to relate these end-point deviations in terms of in-plane ($\vec{B} \cdot \hat{T}$) and out-of-plane ($\vec{B} \cdot \hat{R}$) components to the capability of the DSIF navigation system, the error in estimate, P(t), at 200 days was transformed into NVW coordinates.* These results are shown in Figure 5-12. This covariance matrix in NVW coordinates has been normalized by dividing each P_{ii} component by P_{ii} and each P_{ij} component by $\sqrt{P_{ii}}\sqrt{P_{jj}}$. As seen from the figure, the position and velocity estimation errors normal to the trajectory plane (σ_W and $\sigma_{\dot{W}}$) are each approximately four times larger than the next smaller corresponding coordinate uncertainty. Since the largest correlation factor between W or $\dot{W}$ and the other states is 0.067, these states are essentially uncorrelated with the other states. Therefore, these states normal to the trajectory cannot be estimated except by observing them directly.

The range-rate data from the DSIF is quite accurate but is limited to in-plane velocity measurements. This is because the measurement gradient, H, is along the tracker-vehicle LOS, which is nearly in the trajectory plane. Although the angular measurements from the DSIF do provide information

* This coordinate system has been defined in Subsection 2.2.2.

on the out-of-plane coordinate (See Table 4-1), these H vectors are dependent on $\frac{1}{R}$, where R is the range from the tracker to the vehicle, and therefore do not provide accurate measurements when the vehicle is near Mars. The net result is that the DSIF does not provide a good estimate of the out-of-plane state. This is indicated by the large error in estimate of $\vec{B} \cdot \hat{R}$ in Figure 5-11 and the large values of σ_W and $\sigma_{\dot{W}}$ in Figure 5-12.

The results in Figure 5-11 may be somewhat optimistic at this time because the analysis did not include the effects of bias error sources. These would include station location errors, constants in the equations of motion, and measurement biases.

These results, for example, have been computed with the Earth as a reference. If they were to be transformed to a Mars-centered coordinate frame, the errors in the physical model would increase the error in estimate of the state. The uncertainty in the AU may vary from 200 km to 500 km (Reference 21). It should, however, be noted that, as the physical constants are estimated to a higher degree of accuracy as the result of current space missions (References 22 and 23), the results that have been obtained will be more realistic.

The theory of treating bias errors has been given in Subsections 2.5.2 and 2.5.3. As shown in those subsections, it is possible to either estimate these errors as part of an expanded state vector or to determine their effect on the state estimate without solving for them.

A source of bias errors that has been considered is the station-location errors. This analysis has been performed with the Advanced Error Propagation (AEPP) (Reference 12).

The effects of the station location errors are shown in Figure 5-7 for three cases. The cases shown are: (1) no station location errors, (2) station location errors included but not solved for, and (3) station

location errors included and solved for. The results shown are the RMS error in estimate of the end-point $\vec{B}$ vector constraints as a function of time. As seen from this figure, there is a degradation in the navigation system performance from 110 km, with no bias errors considered, to 250 km, with the errors included but not solved for. When these bias errors are solved for, however, the degradation in performance is considerably less. The RMS error in estimate of the end-point constraints is 125 km.

The reduction in the error in estimate of the station locations is shown in Figure 5-13 for each of the three stations as the navigation data are processed. These errors result from the inability to define the position of the tracker stations on the Earth's surface, and are presented in terms of errors in the northerly direction and errors in the easterly direction. On this trajectory, the error in estimate of the tracker positions is reduced from 100 meters to approximately 10 meters.

To investigate the degree to which the data which have been generated are trajectory-dependent, the same quantities have been computed for the low-energy trajectory. The RMS error in estimate of the end-point deviations is shown in Figure 5-8 for the three treatments of station location bias errors. A comparison of Figures 5-7 and 5-8 show that the results obtained for the low-energy trajectory are considerably better. This improvement is primarily due to the reduction in the $\vec{B} \cdot \hat{R}$ estimation error. For the case where no bias errors were included, it was reduced from 110 km on the high-energy trajectory to 25 km on the low-energy trajectory. The reason for this improvement is that the distance from the Earth to the vehicle is significantly smaller for a longer period of time as shown in Figure 5-14. As a result, the angular measurements which depend on $\frac{1}{R}$ provide better out-of-plane ($\vec{B} \cdot \hat{R}$) estimates of the vehicle state. The better orbit determination accuracy also improves the bias error estimates when they are included in the complete state vector and solved for. The reduction in the error in estimate of the station locations is shown in Figure 5-15, where the easting and northing estimate errors are plotted as a function of time. A comparison of Figure 5-13

and 5-15 shows that, in some cases, the error in estimate of the station location was reduced more on the low-energy trajectory. In other cases the reverse was true. It should be noted that the significance of a particular bias error source depends on the trajectory itself. For example, it is doubtful that much information on the mass of Mars could be obtained by estimating it along a lunar trajectory. On the other hand, estimation of the Earth's mass or oblateness might yield valuable information along this same trajectory.

5.3.2.2 System II. The System II configuration differs from System I in that it provides the capability of making onboard navigational measurements. As will be shown in this section, the onboard navigation capability allows the approach trajectory relative to Mars to be determined to a greater accuracy; therefore, System II could be used for a close fly-by mission or for a Mars orbiter. It does not have the capability of onboard navigation computation.

The onboard instrument assumed in this section is a theodolite. The observation schedule which is used is shown in Table 5-3. The onboard measurements are made using the planet Mars during the approach phase (200 to 235 days). The reason for restricting onboard measurements to the approach phase is that, prior to this time, the measurement using Mars is much poorer than the error in estimate of the state from the DSIF tracking. Figure 5-11 shows that, during the first five days on the trajectory, the DSIF tracking has determined the vehicle's position to approximately 20 km. Observations of Mars using a theodolite with a 10-arc-second accuracy yield position measurement errors which vary from 15,000 km initially to 700 km at 200 days (Figure 4-2). It is clear, therefore, that prior to 200 days, there is no point in making observations of Mars. The normalized covariance matrix of the error in estimate of the state after 200 days of DSIF tracking is shown in Figure 5-12. This matrix indicates that the largest uncertainties in both position and velocity are in the out-of-plane coordinates W and $\dot{W}$. As discussed in the preceding subsection, these out-of-plane measurements with the DSIF

angle become worse as Mars is approached. The position measurement accuracy of a 10-arc-second onboard instrument improves during the approach phase to 10 km at the point of closest approach. The onboard observations will, therefore, provide good out-of-plane information. Although the use of a theodolite has been assumed in this subsection, two sextant measurements would also give the same information, as discussed in the subsection concerning Star Selection. No attempt has been made to study the manner in which the onboard navigation data should be combined with the Earth-referenced DSIF data. The state estimate which was obtained after 200 days of DSIF tracking was used directly at the time when the onboard observations were started.

The navigation performance of System II as a function of onboard instrument accuracy is shown in Figure 5-16. The error in estimate of $\vec{B} \cdot \hat{T}$ and $\vec{B} \cdot \hat{R}$ is plotted as a function of time for each instrument. An evaluation of the nominal guidance system with these navigation systems is shown in Table 5-8. End-point deviations in $\vec{B} \cdot \hat{T}$ and $\vec{B} \cdot \hat{R}$ are shown following the second and third correction for each navigation system (instrument accuracy). As noted previously, the deviation in $\vec{B} \cdot \hat{T}$ is in the orbit plane and corresponds to deviations in the miss-vector magnitude $|\vec{B}|$. The one-sigma deviation in this coordinate, therefore, defines the mission capabilities of the navigation and guidance system in terms of closest approach control. One of the objectives of this study is to determine whether a system is capable of performing an atmospheric braking maneuver. To accomplish this, the one-sigma deviation in altitude $(\vec{B} \cdot \hat{T})$ must be less than ± 3.5 km. The results in Table 5-8 show that the nominal guidance system with a System II navigation system composed of DSIF and and onboard theodolite having an accuracy of approximately 12-arc-seconds can accomplish such a mission. The results also show that System II with an onboard instrument with an accuracy of 60-arc-seconds has sufficient accuracy to carry out a close approach flyby mission or one that requires a thrusting maneuver into a Martian orbit. The deviation in $\vec{B} \cdot \hat{T}$ for a 60-second instrument accuracy is ± 9.13 km.

The significance of the $\vec{B} \cdot \hat{R}$ deviations in Table 5-8 is that they indicate an uncertainty in the cross range or inclination of the approach trajectory relative to Mars.

5.3.2.3 System III (DSIF and Onboard, Onboard Computation) The only difference between System II and System III which is studied in this section is that System III has the capability of onboard computation. This capability eliminates the need for the two-hour period (shown in Figure 5-9) during which Earth-based guidance commands are sent to the spacecraft and verified. As a result, during this period additional observations can be made which provide a better estimate of the vehicle state at the time the guidance corrections are made. This navigation system is representative of the system that would likely be used for normal operation on a manned mission. Ground tracking data is combined with onboard observations, but in the event of a communication failure, a total onboard navigation capability is available.

The navigation system performance is identical to that of System II for the first 200 days where DSIF tracking occurs. The navigation performance of System III for the onboard tracking phase (200-235 days) is shown in Figure 5-17, where the errors in estimate of $\vec{B} \cdot \hat{T}$ and $\vec{B} \cdot \hat{R}$ are plotted as a function of time for different onboard instrument accuracies. A comparison of the RMS error in estimate of $\vec{B} \cdot \hat{T}$ and $\vec{B} \cdot \hat{R}$ at the time of the last midcourse maneuver and the time of the retro maneuver is shown in Table 5-9 for Systems II and III. These results show an improvement in the estimate on the order of 10-30 percent for System III over System II due to the increased time of observation. Each of the System III navigation systems shown in Figure 5-17 was used to evaluate the nominal guidance system. The resulting end-point deviations for each system are shown in Table 5-10. A comparison of the guidance data in Table 5-8 for System II and 5-10 for System III shows that the decrease in end-point deviations with System III is about 15-25 percent. A comparison of the Δv requirements in these tables for the third correction shows that a 40-50 percent larger Δv is necessary for

System III. Since the Δv requirement for the third correction is only 10-15 percent of the total Δv requirements, this Δv penalty is minor. The reason for this larger Δv third correction requirement is that the correction is made two hours later with System III. The results in Table 5-10 also indicate that, to accomplish a mission with an atmospheric braking maneuver ($\pm$3.5 km guidance accuracy in $\vec{B} \cdot T$), an instrument with an 18-arc-second error accuracy is required. This is a 50 percent increase in the 12-arc-second allowable onboard instrumentation error required by System II.

System III has also been evaluated on the low-energy trajectory with a theodolite having an accuracy of 10-arc-seconds. The end-point navigation estimates and guidance deviations for both the nominal and low-energy trajectories are shown in Table 5-11. These results show a slight improvement with the low-energy trajectory.

Also shown in Table 5-11 are the results for the case where the covariance matrix of error in estimate P has been perturbed at 200 days by adding a 400 km uncertainty to each position coordinate. This has been done to account for the DSIF tracking being less accurate than is indicated in Figure 5-11 due to bias errors such as the AU and mass of Mars which have not been considered. This causes a significant degradation in guidance control of the $\vec{B} \cdot \hat{T}$ constraint. This result indicates that, for a close approach mission such as an entry into the atmosphere, the effects of uncertainties in the physical constant should be evaluated in detail.

A final investigation for System III has been made to determine the effect of adding subtended angle range measurements to the theodolite schedule. The errors in estimates of $\vec{B} \cdot \hat{T}$ and $\vec{B} \cdot \hat{R}$ for this case are shown in Figure 5-18. These results indicate that there is little value to these measurements prior to the time of the last midcourse maneuver.

5.3.2.4 System IV (Onboard Measurements Only, Onboard Computations). The last of the four navigation systems considered assumes only onboard observations and computations; therefore, this system is completely independent of Earth-based support. It is important to determine whether this system satisfies the midcourse constraints, since it is likely that a system of this type would be used as a backup for the primary system on a manned mission.

The onboard measurements for this system are made using a theodolite with the measurement schedule given by Table 5-5*. The data-taking restrictions given by Figure 5-9 also apply to this system at the time of each midcourse maneuver. The navigation performance of System IV is shown in Figures 5-19A and 5-19B. The error in estimate of the $\vec{B} \cdot \hat{T}$ and $\vec{B} \cdot \hat{R}$ end-point constraints is shown in the figure as a function of time for different instrument accuracies. The guidance performance of this system has been obtained by evaluating the nominal guidance system for each of the navigation systems used in Figure 5-19. The results are tabulated in Table 5-12 for each of the four corrections used. These results indicate that the navigation for System IV will satisfy the requirements of an atmospheric entry mission ($\pm$3.5 km deviation in $\vec{B} \cdot \hat{T}$) with a 4-arc-second instrument.

These results also show that an instrument with 60-arc-second accuracy provides a terminal accuracy in $\vec{B} \cdot \hat{T}$ of 36 km, which is probably sufficient if the mission specifies a thrusting retro maneuver into a Mars orbit or a close approach flyby (200-300 km altitude).

A second study has been made for this system with a 10-arc-second instrument to determine the effects of the addition of subtended angle range measurements to the schedule during the last day. The error in estimates of $\vec{B} \cdot \hat{T}$ and $\vec{B} \cdot \hat{R}$ for this case are shown in Figure 5-20.

* This table has been defined based on the considerations discussed in the Body Selection Section of Subsection 4.5.

As shown in the figure, the error in estimate of $\vec{B} \cdot \hat{T}$ at the time of the last maneuver is reduced from 6.4 km to 2.5 km with the subtended angle measurements. The value of the $\vec{B} \cdot \hat{T}$ guidance deviation which has been computed with the 2.5 km error in estimate is 2.8 km compared to 6.5 km deviation with no subtended angle measurements. These numbers indicate that the subtended angle measurements are of value with System IV as the vehicle approaches Mars, since it would enable a 10-arc-second instrument to be used for an entry mission compared to the 4-arc-second instrument required without subtended angle measurements.

Two additional studies have been made with this system for: (1) an onboard schedule using the Moon early in the flight to replace the Sun, and (2) the low-energy trajectory in place of the nominal trajectory. The observation schedule for these cases are given in Tables 5-13 and 5-14, and the navigation performance is shown in Figure 5-21.

The navigation performance of System IV using the moon schedule is very nearly the same as with the Sun schedule at the time of closest approach, as shown by curve (2) in Figure 5-21. The only significant difference between the Moon schedule results and the Sun schedule results is that during the first day the Moon schedule reduces the RMS error in estimate of the $\vec{B}$ vector constraints to 900 km prior to the first correction (1 day) as compared to 10,000 km with the Sun. This difference in the error in estimate of the constraints at this time has a considerable effect on the guidance Δv requirements. The constraint deviation after the first correction is much smaller when the moon schedule is used in place of the sun schedule. This makes the following three corrections smaller. The total Δv required for the entire trajectory using the Sun schedule is 23.3 meters/sec; this requirement is reduced to 15.8 meters/sec if the Moon schedule is used.

The navigation performance using the low-energy trajectory, Curve (3) in Figure 5-21, shows that the RMS error in estimate of the end-point

position, $\sigma_{\vec{B}} = (\vec{B} \cdot \hat{T}^2 + \vec{B} \cdot \hat{R}^2)^{1/2}$, is 4.6 km as compared to 6.4 km for the nominal trajectory case.

5.3.3 Navigation Systems Performance Summary

The navigation and guidance performances that have been determined for the four navigation systems in the preceding subsystems are compared in this subsection, in order to determine which systems will satisfy different types of mission requirements and what onboard instrument accuracy is required.

The principal results of the navigation analysis are summarized in Figures 5-22A and 5-22B, where the error in estimates of $\vec{B} \cdot \hat{T}$ and $\vec{B} \cdot \hat{R}$, respectively, are plotted as a function of instrument accuracy for Systems II, III, and IV. These data are the errors in estimate at the time of the last midcourse maneuver. System I is represented by a point on each of these curves, since this system has not been studied with the DSIF measurement errors as parameters. As noted before, the overall figure of merit for the combined navigation and guidance systems is the end-point deviation in $\vec{B} \cdot \hat{T}$ and $\vec{B} \cdot \hat{R}$. Since it is the navigation system parameters that are of interest in this section, the end-point deviations are evaluated with the nominal guidance system for each navigation system. The results are presented in Figures 5-23A and 5-23B as a function of instrument accuracies. System I is again represented by a point on each curve. The 3.5 km $\vec{B} \cdot \hat{T}$ deviation requirement for an entry mission is shown by the solid line in Figure 5-23A. From this figure, the mission capabilities of the four systems can be determined in terms of closest approach ability.

Figure 5-23B shows the magnitude of $\vec{B} \cdot \hat{R}$ deviations for each system as a function of instrument accuracy. The $\vec{B} \cdot \hat{R}$ deviations indicate cross-range or inclination deviations. System IV results in the smallest $\vec{B} \cdot \hat{R}$ deviations, since its onboard measurements provide a better out-of-plane estimate than the DSIF tracking used in System I, II and III for the first 200 days. The DSIF cannot determine this coordinate at large ranges.

System I does not have the performance accuracy which is required for an entry mission. It does, however, show that a flyby mission or a thrusting retro into a Martian orbit is possible. The large deviation in $\vec{B} \cdot \hat{R}$ and the additional fact that no navigation data were obtained relative to Mars with this system means that the Martian orbit might be poorly defined.

Systems II, III, and IV all show a good ability to establish an approach trajectory relative to Mars which would satisfy most mission objectives. In particular, each of these three systems could accomplish a mission with an atmospheric entry maneuver at Mars as a requirement. The onboard instrument accuracy which would be required with Systems II, III, and IV for this type mission is 12, 18, and 4-arc-seconds, respectively. The results for these systems indicate they could control the trajectory for a close approach flyby or a thrusting retro mission with instrument errors as large as 60-arc-seconds.

Figure 5-23A also shows the total Δv guidance requirements for each of the systems as a function of the onboard instrumentation accuracy.

The value of adding subtended angle range measurements to System IV is shown in Figure 5-23A. The $\vec{B} \cdot \hat{T}$ deviation in this figure reduces from 6.5 km without subtended angle measurements to 2.8 km with these measurements added. The $\vec{B} \cdot \hat{R}$ deviations, however, do not change for this case as seen from Figure 5-23B.

The effect of using System IV with the low-energy trajectory is also shown in Figures 5-23A and 5-23B. Figure 5-23A shows a decrease in the $\vec{B} \cdot \hat{T}$ deviation from 6.5 km to 4.1 km; however, in Figure 5-23B, the low-energy trajectory shows an increase in the $\vec{B} \cdot \hat{R}$ deviations from 2 km to 2.7 km. The difference in the Δv requirements for these two trajectories is small (Figure 5-23A).

5.4 GUIDANCE ANALYSIS

As noted previously, the navigation system performance is somewhat dependent on the guidance system, since the guidance execution errors at each correction add to the uncertainty in the state estimate, equation (5-1), and observations are restricted at the time of each maneuver (Figure 5-9). In order to compare the performance of the four navigation systems in the previous section, a guidance system was assumed that consisted of a nominal set of execution errors and a time schedule for making midcourse maneuvers. This enabled the end-point deviation to be computed; therefore, it was possible to evaluate the overall performance of the four systems as a function of the navigation system parameters. In this section, however, it is the guidance system which is studied parametrically.

The time schedule for making midcourse maneuvers, based on end-point deviations and velocity requirements for each of the four navigation systems, is derived. In addition, the performance of the guidance system is evaluated as a function of injection errors, guidance execution errors, and the type of guidance law that is used.

The function of the guidance system as defined in this study is to apply midcourse velocity corrections such that the estimated end-point deviations in the constraints are corrected. The corrections are assumed to be step changes in velocity.

5.4.1 Midcourse Guidance Times

In this section, the midcourse maneuver times are derived for the nominal guidance system with a Variable Time of Arrival (VTA) guidance law. The end-point constraints which are used with this law are $\vec{B} \cdot \hat{T}$, $\vec{B} \cdot \hat{R}$, and $V_{inf.}$ Although the guidance times can be optimized, the derivation in this section is based on: (1) the velocity requirements

for the maneuver, and (2) the deviations in the end constraints after the correction. There are a number of parameters which affect these two criteria, including the guidance execution errors, the injection errors, the sensitivities of the end constraints to velocity changes at time (t), and the accuracy of the deviation estimate as determined by the navigation system. In fact, since the error in estimate at a given time may be different for each of the four navigation systems, it may be necessary to select separate guidance times for Systems I, II, III and IV.

At the time of injection from the Earth park orbit, the error in the estimate of the state and error in the state are assumed to be the same, that is,

$$P(0) = PAR\ (0)$$

As observations are made, the error in estimate of the end constraints decreases. The state deviations grow as the initial errors are progated in time. This relationship is shown pictorially in Figure 5-10. It is the estimate of the deviation state that is used in computing the guidance corrections.

The first correction guidance data for System I are shown in Figure 5-24. The RMS error in the estimate of the end-point position constraints (σ_B) shown in the figure represents the performance of the navigation system being used. The curve of the RMS Δv required is the square root of the trace of the covariance matrix of the expected velocity correction (Δv) in (2-33). The correction Δv is computed for the VTA guidance law. The curve of the RMS end-point position deviation after a correction indicates the end-point constraint deviation which would occur if a correction were made at any of the times shown. It

has been computed by propagating PAR, the state deviation covariance matrix, following a correction (Equation 2-120) to the end point, and transforming it into target constraints $\vec{B} \cdot \hat{T}$ and $\vec{B} \cdot \hat{R}$. The large values of the deviations after the correction in comparison to the error in estimate that are shown are due to the guidance execution errors. The fourth curve in Figure 5-24, minimum Δ v, is also an RMS value of Δ v required similar to the first Δ v curve except that the V_{inf} constraint is not controlled, but instead has now been selected such that the maneuver Δ v is minimized as given by (2-39). This Δv represents the minimum value required to control the end position constraints, $\vec{B} \cdot \hat{T}$ and $\vec{B} \cdot \hat{R}$. The difference between this curve and the other Δv curve is the penalty which is paid to control V_{INF}.

The time at which the first guidance correction should be made can be determined from the data in Figure 5-24. As previously mentioned, an important criteria for selecting a guidance time is the Δv required and the deviations after the correction. These two curves in Figure 5-24 indicate that at two days, the position deviation after a correction is at a minimum; also, the required Δv is low (10.6 m/sec). This first correction primarily compensates for the injection errors. The cause for the magnitude of the end position deviation (1720 km) being considerably larger than the RMS error in estimate (405 km) is the guidance system execution errors. The required Δv at two days is approximately 10 m/sec which produces a 0.1 m/sec proportional error (1 percent). The resolution error with the nominal guidance system is also 0.1 m/sec. The sensitivity coefficients relating the end position constraints and velocity changes at this time (shown in Figure 5-25 and 5-26) have a magnitude of approximately 10^4 km/m/sec. Therefore, propagation of the 0.1 m/sec execution errors to the end-point will produce deviations on the order of 1000 km.

The results in Figure 5-24 show that it would be very undesirable to make a correction at 60 days because of the large Δv requirements. The reason for this large requirement is that part of the matrix that relates changes in the velocity requirements to changes in the end-point constraints,

D_2 in (2.28), becomes almost singular. This near singularity occurs at the time when the true anomaly to the target on the Sun-centered conic is 180° (Figure 5-1). (This type of singularity is discussed in Reference 24). The elements of the 3 x 3 transition matrix, D_2 in (2-32), are plotted in Figures 5-25, 5-26, and 5-27, where the three velocity components are expressed in the NVW coordinate system. These data show that at 60 days the relationship between changes in the constraints and changes in the velocity requirements is given by

$$\begin{bmatrix} \Delta \vec{B} \cdot \hat{T} \\ \Delta \vec{B} \cdot \hat{R} \\ \Delta V_{inf} \end{bmatrix} = \begin{bmatrix} d_{11} & d_{12} & 0 \\ d_{21} & d_{22} & 0 \\ d_{31} & d_{32} & d_{33} \end{bmatrix} \begin{bmatrix} \Delta \dot{N} \\ \Delta \dot{V} \\ \Delta \dot{W} \end{bmatrix} \qquad 5\text{-}2$$

Since the d_{13} and d_{23} components are zero at this time, the $B \cdot \hat{T}$ and $B \cdot \hat{R}$ constraint deviations completely determine the $\Delta \dot{N}$ and $\Delta \dot{V}$ velocity components. Therefore, V_{INF} must be controlled by the $\Delta \dot{W}$ component of the correction. Since d_{33} is 0.07, an extremely large increment is required in the $\Delta \dot{W}$ component.

The solution for v, which is the vector sum of $\Delta \dot{N}$, $\Delta \dot{V}$, and $\Delta \dot{W}$, can be illustrated graphically by reducing the three-dimensional guidance problems to two dimensions. This is shown in Figure 5-28 where Δv is found by solving 5-2 for $\Delta \dot{V}$ and $\Delta \dot{W}$ at both one day and 60 days. The numerical values of the coefficients in 5-2 are obtained from Figures 5-25, 5-26, and 5-27. The magnitude of the ΔV_{INF} and $\Delta B \cdot \hat{R}$ constraints in Figure 5-28 corresponds to the RMS values due to the injection errors. At one day, the ΔV_{INF} constraint can be controlled by the $\dot{V}$ coordinate, since the $\dot{W}$ increment at this time is able to control B. R. The Δv resulting from these two increments is 19.3 m/sec, which is about equal to the three dimensional Δv shown in Figure 5-24 at one day. At 60 days, the $\Delta \dot{V}$ component controls only

$\vec{B}.\hat{R}$; therefore, V_{inf} must be controlled by the small 0.07 sensitivity in the $\dot{W}$ direction. As a result, a very large $\dot{W}$ component is required to control ΔV_{INF}. therefore, the total Δv is large (533 m/sec). It should be noted that, if ΔV_{inf} were not a constraint but were selected to minimize the velocity correction as described in Subsection 2.3.3, the Δv required would be in a direction normal to the $\vec{B}.\hat{R}$ constraint. The required Δv is then 15 m/sec in the $\dot{V}$ direction. This is the same type of difference which occurs at 60 days in Figure 5-24 for the Δv requirements, using VTA and Δv minimum.

The data used to select the second guidance time are shown in Figure 5-29. The curves shown are similar to those of Figure 5-24, except they have been computed on the assumption that a first correction has been made at two days. The Δv curve is the velocity correction required to correct the constraint deviations which are now caused by the execution errors of the first correction. Figure 5-29 shows that the estimate of the end-constraint (RMS error in estimate curve) is much less than the deviation in the constraints (RMS position deviations) until late in the trajectory. This is the effect of the resolution error (0.1 m/sec) in the guidance system projected to the end-point. The proportional errors are quite small since the RMS Δv required is less than 1 m/sec. The sensitivity coefficients (Figures 5-25, 5-26, and 5-27), however, are quite large until near the end of the trajectory; therefore, the resolution error causes large end-point deviations. After 100 days, the RMS position deviations after a correction decrease rapidly. Although the Δv requirements increase from 100 days to 235 days, these Δv values are still small for the increased guidance accuracy that results. The second correction time for System I is, therefore, chosen to be at 231 days. The Δv at this time is 5 m/sec. The end-point deviation after the correction at this time is 120 km, which is only 7 percent larger than the error in estimate at this time. Since the navigation system is not improving the estimate of the state at this time, there is no need for additional corrections. The nominal guidance system used with System I will control the trajectory to within 7 percent of the capability of the navigation system to estimate the

end constraints. The total Δv requirements for the two corrections is 15.5 m/sec.

The criteria for selecting guidance times for Systems II and III are shown in Figures 5-30 and 5-31. Since both of these systems use DSIF tracking initially, the first correction time is identical to that of System I. However, since the DSIF combined with the onboard tracker continues to improve the estimate of the vehicle state as Mars is approached, it is advantageous to make two more corrections with these systems. Figure 5-30 shows that there is a limit to the accuracy which can be obtained with only one more correction. During the last day (234-235 days) the error in estimate is reduced by a factor of 5 (15 km to 2.8 km), but the errors in executing the maneuver limit the guidance accuracy to 23 km. This is the result of the increasing velocity requirements which cause large proportional errors. However, if two additional corrections are made-- one at 232 days 12 hours, and the second at 234 days 18 hours (Figure 5-31) -- the terminal deviations are reduced to 4.7 km and the total Δv for the last two corrections is 10 m/sec. Therefore, these times are used for System II. For System III, two additional hours of tracking are possible, since the guidance commands are computed onboard as has been shown by the schedule in Figure 5-9. The final maneuver for System III therefore is at 234 days 20 hours.

The data that apply to the selection of guidance times for System IV are shown in Figures 5-32 through 5-35. These data show a different character because the error in estimate of the terminal constraints is reduced much more slowly with the System IV navigational system. The first and second correction data (Figures 5-32 and 5-33) show that the guidance performance is limited by the estimation error (deviations after a correction are approximately equal to the estimation error). The first correction (10.6 meters/second) was made at one day, which reduced the terminal miss from 86,500 km (due to injection errors) to 10,700 km. The second correction data (Figure 5-33) shows an accuracy limit of 150 km is reached near the end point. At this time the estimate has an error of 10 km. Therefore, in order to improve the guidance performance below

150 km, a third correction is required. With a second correction of 8.2 meters/second at 220 days, the data for the third correction are shown in Figure 5-34. The third correction provides the capability of a terminal guidance accuracy of 8 km, which is within 20 percent of the error in estimate. The third correction Δv is 20 meters/second.

The guidance accuracy which can be attained with three corrections is quite good, but there are two advantages to dividing the third correction into two corrections. The data shown in Figure 5-35 is for a fourth corrections, assuming the third correction of 3.6 meters/second was made at 234 days. These data show that a final correction at 234 days 20 hours requires a Δv of 0.92 meters/second. This combination of two corrections requires a total Δv of 4.5 meters/second, which is a 75 percent reduction in the 20 meters/second required for a single third correction. The position deviation after the fourth correction is 6.8 km, which is within 2 percent of the navigation accuracy. The two corrections, therefore, yield a significant reduction in the total Δv and an increase in the accuracy attainable.

The guidance times which have been used for the system studies are summarized in Table 5-6.

5.4.2 Injection Errors

The injection errors used in the navigation and guidance analyses are the injection conditions after a 30-minute park-orbit. The numerical values of these errors have been given in Figure 5-6. In this section, however, the performance of the guidance system is evaluated for a different set of injection errors. These errors result from the 85 minute park orbit which is associated with the second launch opportunity on February 10, 1975. As shown in Figure 5-5, the RMS errors for the 85-minute park orbit are almost twice as large as the 30-minute park orbit errors. The velocity requirements at each correction for the two sets of injection errors are shown in Table 5-15. The analysis has been made for System IV with the

nominal guidance system. The required Δv's at each time have been determined, and again are RMS values. These results show that the Δv required at the first correction is approximately twice as large for the 85-minute park orbit injection errors, but the remaining Δv corrections are very nearly the same. Since the injection velocity deviations are twice as large for the 85-minute case, it may be concluded that the injection errors influence the magnitude of the first correction, but have little effect on further corrections.

The extent to which the velocity injection errors influence the magnitude of the first correction is shown in Figure 5-36 for the nominal injection errors. The fact that the RMS Δv correction curves and the RMS velocity deviation curves are very nearly the same indicates that the injection velocity errors primarily determine the magnitude of the first correction Δv requirement. Actually, the velocity requirements shown in this figure are slightly larger because the correction must also compensate for the position deviations.

5.4.3 Guidance Laws

The previous analysis of the guidance system has assumed a Variable Time of Arrival (VTA) guidance law. In this subsection, the performance of the guidance system is compared for the three different guidance laws discussed in Subsection 2.3.1. They are: (1) the VTA guidance law with $\vec{B} \cdot \hat{T}$, $\vec{B} \cdot \hat{R}$ and V_{INF} as constraints, (2) the Variable Time of Arrival Guidance Law with minimum Δv, and (3) the Fixed Time of Arrival Guidance Law (FTA) where the constraints are the position of the nominal trajectory at the nominal time of closest approach. These laws are illustrated in Figure 2-5.

The velocity correction requirements are shown in Figure 5-37 for the FTA, VTA and Δv minimum guidance laws. In Figure 5-38, the deviation of the end-point constraints immediately following a correction is shown.

The Δv requirements for all three guidance laws assume a perfect navigation system. The RMS position deviations shown in the figure are the result of projecting the covariance matrix of execution errors to the end point, since P = 0 for a perfect navigation system in the definition of PAR after a correction, Equation (2-120). The values of the RMS deviations for the FTA have been separated into components along the velocity vector and normal to the velocity vector at the time of closest approach. This miss component normal to the velocity vector is the RMS position deviation in the altitude and cross-range plane. The deviation along the velocity vector is associated with the error in arrival time.

During the first 50 days, the VTA and FTA guidance laws exhibit very nearly the same performance after a correction as seen by comparing the RMS $\vec{B}$ vector deviations in Figure 5-38 with the deviation normal to the velocity vector. The deviation curve for the Δv minimum law has not been computed. The Δv requirements for FTA and VTA are essentially identical (10.6 meters/second at one day). The minimum Δv correction is approximately two meters/second less than other two requirements. Between 50 and 70 days, the FTA and VTA guidance laws require excessive correction velocities. This is the part of the trajectory when the true anomaly to the target at arrival is 180 degrees. Through this region, the minimum Δv requirement increases slightly but does not become excessive. During the time from 70 days to the end point, the difference between the FTA and VTA guidance laws begins to show. For example, at 180 days the VTA velocity requirement is 20 meters/second, which results in a terminal position miss of 1350 km. At the same time, the FTA velocity requirement is 100 meters/second, and the miss normal to V is 5100 km. The larger velocity requirements for FTA are the penalty which is paid to control the arrival time.

The data for a second correction for each of these guidance laws is shown in Figures 5-39 and 5-40. The first correction in each case was made at one day. These data exhibit the same general characteristics as the first correction data. The differences in Δv and accuracy begin to grow during the last 150 days.

The effects of the guidance laws on performance can be summarized as follows. Early in the flight there are only small differences between the three guidance laws. Near the singularity, the only reasonable guidanee law which could be used is the one which minimizes the maneuver. Near the end of the trajectory, the FTA guidance law which controls the arrival time does this at the expense of the Δv requirement. It is of interest to note that the Δv required when using the VTA guidance law controlling V_{INF} is within 20 percent of the minimum correction required. This is exclusive of the period near the singularity.

The three guidance laws have been compared on the basis of correction requirements and deviations after a correction, assuming a perfect navigation system. The VTA and FTA guidance laws are now each compared using System IV navigation for: (1) the nominal trajectory, (2) the nominal trajectory with subtended angle range measurements, and (3) the low-energy trajectory. The results are shown in Table 5-16. In the first two cases, the Sun tracking schedule in Table 5-5 with a 10-arc-second theodolite, and the guidance times shown in Table 5-6 have been used.

The data for these two cases show an increase in the Δv requirements, when using FTA, by a factor of nearly three. This is the penalty associated with controlling the arrival time. The standard deviation of the arrival time with VTA guidance is approximately 0.64 hours. For FTA guidance, the first case has an arrival time deviation of 0.32 minutes. The second case, which has range measurements to aid in determining the position along the trajectory, has an arrival time deviation of 0.17 minutes. This improvement in arrival time is directly related to the reduced position deviations along the velocity vector. The deviation with FTA was 270 km for case one and 74.3 km for case two. The arrival time improvement with FTA case two is accomplished at the expense of a 5.5 meters/second increase in the total Δv required over that which is required with FTA case one.

The data for case three were generated using a 10-arc-second theodolite on the low-energy trajectory with the schedule shown in Table 5-13. This trajectory shows a larger sensitivity to time deviations than the nominal with VTA. The VTA guidance law has an arrival time deviation of approximately 1.3 hours. The FTA guidance law has a time deviation of 0.49 minutes, which is 21 percent smaller than case one. The Δv requirements on the low-energy trajectory for FTA are approximately 15 percent larger than FTA case one.

The results in Table 5-16 indicate that the value of a particular guidance law depends upon the mission for which it is to be used. The Variable Time-of-Arrival law VTA requires less Δv for maneuvers; however, the Fixed Time of Arrival law (FTA) results in time deviations that are much smaller than the VTA law.

The results show that an increased Δv is required by the FTA guidance law to control the deviations along the velocity vector. The deviations in the components normal to the velocity vector with FTA are comparable to the B vector deviations with the VTA guidance law.

5.4.4. Analysis of the Guidance Execution Errors

The performance of the guidance system as measured by the RMS deviations in the end-point constraints is studied in this subsection, with the execution errors as parameters. The navigation performance of System IV -- with subtended angle measurements during the approach phase, and correction times shown in Table 5-6 -- has been used for this analysis. The three error parameters considered are: (1) the resolution error (σ_r in (2-127), (2) the proportional error (σ_v in (2-126), the pointing error (σ_p in (2-129).

The effect of the execution errors on the RMS deviation of $\vec{B} \cdot \hat{T}$ and $\vec{B} \cdot \hat{R}$ is shown in Figure 5-41A and 5-41B after each of the four corrections. Contours of constant deviations resulting from different combin-

ations of the error parameters are shown in the figure. The curves indicate that the deviations following each of the first two corrections are dependent on both the resolution and proportional errors. Also, a comparison of the curves for pointing errors of 0.5 degrees and 2 degrees indicates that the deviations are also dependent on the pointing error in the first two corrections. For example, with the nominal guidance system which has a 0.5 degree pointing error, a 1 percent proportional error, and a 0.1 m/sec resolution error, the position deviation after the second correction is approximately 310 km. With the same resolution and proportional errors, but a 2-degree pointing error, the deviation increases to 500 km. The Δv for the first correction, which depends on the injection errors, is 10.6 m/sec for all the cases shown.

The lines of constant deviation after the third correction Figure 5-41B are nearly horizontal. This indicates that the deviations at this time are still dependent on the resolution errors, but less dependent on the proportional errors. A comparison of the results for the two pointing errors again shows the deviations are dependent on the pointing errors.

The deviations after a fourth correction Figure 5-41B indicate that the guidance accuracy is only limited by the resolution errors and essentially independent of both the pointing and proportional errors. Since the number of corrections has not been limited, the final correction requires only a small Δv to correct the small remaining deviations. The proportional and pointing errors are therefore both small due to the small Δv. The resolution error, which is independent of the magnitude of Δv, therefore limits the guidance accuracy in this case.

Although there appears to be no difference between the most accurate system (0.RES, 0.PROP, 0.5^{o} PT) and the poorest system (2.m/sec RES, 2.percent PROP, $2.^{o}$ PT) shown in Figure 5-41B after the fourth correction, the penalty which is paid for maintaining a fixed accuracy with the poorer system is a larger Δv. The most accurate system (3.2km) requires a Δv for

the four corrections of 22.4 m/sec, while the poorest system shown (4.4 km) requires a Δv of 28.4 m/sec. These velocity requirements indicate that the Δv penalty associated with a less accurate guidance system is small.

If the number of guidance corrections is limited (e.g., the one correction for the Mariner IV mission), then the effect of each of the error sources is more important. This is illustrated by the data in Figures 5-42A and 5-42B, where a single correction is made at 180 days based on a perfect navigation system. In this case, it is possible to see the trade-offs that might well exist between the three error sources. For example, if the mission objectives require a maximum standard deviation in the end position of 2000 km following the correction, data such as those shown in Figure 5-42 can be used to define the limits on the guidance system errors. If the pointing error is fixed at 0.75 degrees, the dotted lines in Figure 5-42Bshow two possible limits for the resolution and proportional errors. In one case, if the resolution error is 0.05 m/sec, the proportional error is restricted to be less than 1.62 percent. In the second case, the resolution error increases to 0.2 m/sec, but the proportional error is now limited to 1.25 percent.

The data in Figure 5-42A for the case of zero resolution error shows maximum allowable errors of 1.05 degrees and 3.0 percent (extrapolated) for the pointing and proportional error sources in order to satisfy a deviation of 2000 km. Attitude control and rocket motor subsystems with larger error magnitudes than these could not be considered for the mission which was defined above.

The time of the correction is another parameter which was not varied, but would change the figures shown and, therefore, the relationships between the error sources and the error limits.

5.4.5 Guidance Analysis Summary

In addition to defining the midcourse guidance times for the four navigation systems, the preceding analysis has indicated the differences between the three guidance laws and has also shown the effect of the guidance errors.

The primary difference between the VTA and FTA guidance laws is the Δv requirements during the second half of the trajectory. During the first part of the trajectory, the requirements as well as the performance of all three guidance laws are approximately the same. Both the VTA and FTA guidance laws, however, exhibited near singularities when the true anomoly to the target was 180 degrees. The minimum energy guidance law did not have a near singular point at this time. Also, at times other than where the singular point occurred, the VTA guidance law had Δv requirements that were 20 percent larger than those for the minimum correction guidance law.

The analysis of the effects of guidance execution errors has shown that, as long as the number of corrections is not restricted, the guidance system will perform to an accuracy which is limited only by the navigation estimation error and the guidance resolution error. The effect of the resolution error can be reduced by making the final correction as late as possible along the trajectory. If the number of corrections is limited, however, the guidance performance may be restricted by all of the execution errors. The type of data that have been presented for this case to show the tradeoffs between the guidance errors would be useful in specifying hardware requirements to accomplish a specific mission.

SECTION 6

MARS-EARTH MIDCOURSE STUDY

6.1 INTRODUCTION

The statistical error analyses of the navigation and guidance systems for the midcourse phase of the Mars-Earth return trajectory are presented in this section. The return trajectory of the mission starts at injection onto the transfer trajectory following a 40-day period in a 500 km altitude park orbit at Mars, and terminates at the time of virtual perigee at Earth. Although the Martian park orbit phase follows the out-bound phase for the Earth-Mars round-trip mission, the return trajectory analysis is presented first for two reasons.

First, it is assumed that the major sources of errors for both the orbital phase and the return leg are the burning maneuvers into and out of a Martian orbit, respectively. Therefore, the injection error covariance matrix for both of these phases is to a large extent due to the burning maneuvers, and as a result, the orbital phase can be studied independently of the outbound leg, and the return leg can be studied independently of the orbital phase.

The second reason for presenting the return trajectory analysis next is that the analyses for both midcourse phases are very similar. In fact, the purpose of this section is again to determine the capability of the navigation systems to satisfy a given mission. In this case, the mission requirement was selected to be an atmospheric braking maneuver at Earth. This, then, defines the maximum allowable deviation in the entrance corridor at Earth. Since only Systems III and IV are reasonable choices for a manned Mars mission, it is these two systems that are discussed in Section 6.

6.2 STUDY RESTRICTIONS

The restrictions applied to the study of the Earth-Mars midcourse phase are described in the following paragraphs, and include: (1) the nominal trajectory and the target constraints, (2) the injection errors, and (3) the error sources.

6.2.1 Nominal Trajectory

The nominal trajectory that has been assumed for the Mars-Earth return leg is shown in Figure 6-1 and described in Appendix C. It has been obtained from a mission analysis study (Reference 19). The trajectory leaves Mars 40 days after the arrival of the out-bound trajectory; it departs a 500 km altitude park orbit, has a flight time of 296 days 18 hours, and a virtual perigee of 75 km altitude at 223.1° longitude and 60.0° latitude.

In addition to the trajectory described above, a second trajectory is considered which is a Venus swingby on the return to Earth. This trajectory is shown in Figure 6-2 This type of return could be combined with a low-energy outbound for a round trip trajectory.

For the return trajectory, the target constraints are expressed N V W coordinates* at perigee. At perigee, these coordinates are equivalent to altitude, down-range, and cross-range, respectively. The altitude coordinate N is of particular interest on the return trajectory since deviations in this direction indicate the feasibility of hitting an entry corridor at Earth. The reason for defining the target constraints for the return leg in N V W coordinates is that, in general, the navigation analysis in Subsection 6.3 will assume a Fixed Time-of-Arrival (FTA) guidance law. With this guidance law, it is convenient to express the six-dimensional position and velocity state in this coordinate system. When a Variable Time-of-Arrival (VTA) law is use, however, the deviations will again be expressed in terms of the $\vec{B}$ vector.** For the return leg, the orientation of $\hat{R}$ and $\hat{T}$ vectors is defined so that $\vec{B} \cdot \hat{T}$ deviations indicate deviations in altitude as shown in Figure 6-3.

---

* Described in Subsection 2.2.2.

** These coordinates are defined in Subsection 2.2.3.

The altitude deviations are equal to 0.92 times the B·T deviations. This reduction is due to the "focusing" on the trajectory as perigee is approached.

6.2.2 Injection Errors

As previously noted, the intial errors in estimate of the state for the return leg are the result of : (1) the error in estimate of the state at the end of the orbital phase, and (2) the rocket motor and inertial guidance system used to burn out of park orbit. The RMS value of the velocity has been assumed to be about 1 percent of the RMS ΔV for the injection maneuver (3.3 km/sec). Although this choice is somewhat arbitrary, it represents a pessimistic value in terms of the rocket motor accuracies that can be obtained with present day hardware. The covariance matrix of injection errors which is used for both the deviation state (PAR(0)) and the error in estimate of the state (P(0)) are shown in Figure 6-4 to be a diagonal matrix with RMS position and velocity equal to 30 km and 30 m/sec, respectively. The value of the position deviations resulting from propagating PAR(0) to the end point (perigee) are

$$\sigma_{ALT} = 1.49 \times 10^6 \text{ km} \quad \sigma_{DR} = 1.96 \times 10^6 \text{ km} \quad \sigma_{CR} = .872 \times 10^6 \text{ km}$$

6.2.3 Error Sources

The error sources that are considered in this analysis are identical to those discussed in Section 5, and include the instrument measurement errors for the navigation systems and the execution errors for the guidance system. These errors have again been assumed to be random, i.e., bias errors are not considered. Also, the guidance errors are again based on the assumption of step changes in velocity.

6.3 NAVIGATION ANALYSIS

Although the type of navigation analysis presented in this section for the return leg is identical to that of Section 5 for the outbound leg, the objective as well as the scope of this analysis are more limited.

Since the return leg would obviously exist only for a manned mission, the objective of this section is to determine the capability of the navigation systems to achieve an atmospheric entry maneuver at perigee. The data shown in Reference 18 indicates that a 21 km entry corridor* is required at Earth for a vehicle with a L/D ratio of one and a speed of 18 km/sec. A one-sigma limit of $\pm$ 3.5 km guidance accuracy is therefore defined in order to obtain a three-sigma confidence of hitting such an atmospheric entry corridor at Earth.

The scope of this analysis is also limited by the mission itself. Since only Systems III and IV are reasonable choices for a round-trip mission to Mars, it is these systems which are considered in Section 6. System III could represent the primary navigation system, and uses the Earth-based tracking network as well as a complete onboard navigation system. The performance of System IV is also important, however, since it could be used in the event of a ground communication failure.

The navigation systems discussed in this Subsection again assume the nominal guidance system with the execution errors defined in Section 5. However, a Fixed Time-of-Arrival (FTA) nominal guidance law is now assumed for most of the analysis since it is likely the return would be to a preselected Earth-fixed landing site. Some additional data has been obtained using a Variable Time-of-Arrival (VTA) guidance law to illustrate the dependence of the results on a particular guidance law.

6.3.1 Measurement Schedule

The measurement schedule used with System III is shown in Table 6-1. The DSIF stations which have been used and their measurement accuracies are shown in Table 4-5. The onboard instrument is assumed to be a theodolite.

*The corridor limits are defined in the reference.

The measurement schedule that has been used for System IV (onboard only) was obtained with the aid of the data shown in Figure 6-5. This is similar to the body selection data which are described in Subsection 4.5 for the out-bound trajectory. These data for the return trajectory show a much more favorable measurement coverage of the vehicle's three position coordinates early in the flight than was available on the out-bound trajectory. During the first part of the trajectory, Mars is the primary body since it results the smallest measurement error (Figure 6-5A). On this basis the Earth is the secondary body. It is also in a position nearly orthogonal to Mars. Therefore, Mars and the Earth provide good orthogonal measurement coverage of the vehicle's position state which is to be estimated. The value of using either the Earth or the Sun with Mars early in the flight is shown by the data in Figure 6-6 where the $\vec{B}\cdot\hat{T}$ and $\vec{B}\cdot\hat{R}$ error in estimates of the end-point constraints are plotted as a function of time. Each of the three sets of curves was generated with 70 observations. Curves number one show that, after one day, the continued use of Mars provides no significant improvement in the terminal estimate. At about 10 days, the use of either the Earth or Sun as a secondary body becomes important. The use of Earth (curves 2) as a secondary body is the more important, as would be expected from the accuracy of measurement data (Figure 6-5A). The Earth measurement has an accuracy of approximately 4000 km, while the Sun measurement has an accuracy of 10000 km.

A practical problem associated with the use of the Earth for observations at about 30 days is shown by the data in Figure 6-5B. The Earth will occult the Sun as observed from the vehicle, and an optical instrument observing the Earth would be "blinded".

During the second half of the trajectory, the Earth is the primary body to be observed from the accuracy consideration. The Sun during this time is the secondary body of interest, and it is in a position relative to the Earth to provide good positional measurement coverage when used as a secondary body.

Parametric data were generated which showed that the use of Sun was not required during the second half of the schedule. The complete schedule that has been used with System IV is shown in Table 6-2.

6.3.2 Navigation Systems Comparison

6.3.2.1 System III

The navigation performance of System III is shown in Figure 6-7, where the RMS error in estimate of the end-point position constraints is shown as a function of time. One curve shows the state obtained using DSIF tracking alone, while the second curve has assumed the use of a 10-arc-sec theodolite. Both curves represent the vector sum of the N, V, and W position components. Also, the individual components of the error in estimates are shown from 290 days to the end of the trajectory. The increase in the error in estimate at 50 days that is shown is due to error in monitoring the first guidance correction. From the data shown in the figure, it is seen that the addition of the onboard tracker produces only a very small improvement in the estimate of the state at perigee. Also, it is clear that the DSIF alone is capable of providing a navigation accuracy sufficient for an atmospheric entry maneuver (3.5 km guidance accuracy), since the error in estimate of the altitude coordinate is 1.96 km at the time of the last midcourse maneuver (296 days 14 hours). Therefore, the navigation performance of System III has not been studied as a function of the onboard instrument errors.

The deviations in the end-point constraints, resulting from guidance corrections at the four times given in Table 6-3 and a FTA guidance law, are given in Table 6-4 for System III, with and without onboard observations. The deviations following the final correction are 10-15 percent larger than the error in estimate. This indicates that the guidance system with four corrections can control the trajectory to approximately the same accuracy as it can be estimated with the navigation system. System III without the aid of the onboard data has a guidance accuracy in the altitude direction at perigee of 2.17 km, which is well within the 3.5 km corridor which is allowed.

The ΔV requirements for both cases shown are approximately 70 meters/second.

6.3.2.2 System IV

Since this system is assumed to be a back-up for System III, it is essential to determine the onboard instrument accuracy required to satisfy specific mission objectives. The RMS errors in estimate of the perigee position are shown in Figure 6-8 for System IV. The data is shown for a theodolite with various accuracies, and has been obtained using the observation schedule in Table 6-2. The data which is shown as a function of time in Figure 6-8 is summarized in Figure 6-9, where the errors in estimate at perigee for each of the position coordinates are shown as a function of the instrument accuracy. The error in estimate of the RMS velocity is also shown in this figure. These errors result from the propagation of the errors in estimate of the state at 296 days 16 hours to the end-point, 296 days 18 hours, and would be the estimates used for computing the retro maneuver.

The nominal guidance system performance data for System IV are shown in Figure 6-10 as a function of instrument accuracy. In Figures 6-10A, 6-10B, and 6-10C, both the error in estimate of the state at the time of the last correction and the end-point deviations are shown for the N, V, and W components, respectively. These figures show that the deviations are not significantly different from the error in estimates; therefore, it may be concluded that the nominal guidance system is capable of controlling the trajectory to an accuracy which is approximately equal to that of the navigation system. The main result of this data is the fact that an atmospheric entry at perigee could be achieved with a 4-arc second instrument, as shown in Fugure 6-10A. The ΔV requirements and time deviations in arrival are shown in Figure 6-10D. The ΔV which is required with the 4-arc-second instrument is 85 meters/second.

An additional study has been made to determine the effect of Moon observations on the System IV performance. For this case, 40 observations

of the Moon were added to the nominal observations schedule during the final two days. The results of this study are shown in Figure 6-11, where the errors in estimate of the ALT, DR, CR positions at perigee are compared with those obtained using the same onboard system but without using Moon observations. The improvement resulting from Moon observations is quite apparent. The error in estimate of the altitude at perigee is reduced from 4.90 km to 2.52 km. There is also a large reduction in the DR error in estimate. The guidance performance data for System IV with both the nominal schedule and the schedule that includes Moon observations are shown in Table 6-5. The data shown refer to the errors in estimate of the constraints at the time of the last correction (296 days and 14 hours) and deviations following the correction. The use of the Moon observations produces a large performance improvement in all of the coordinates. The reduction in the altitude deviation from 6.80 km to 3.75 km would nearly permit the use of a 10-arc-second instrument to satisfy the entry corridor limits, whereas this system without Moon observations requires a 4-arc-second instrument, as shown in Figure 6-10A. There is also a 20 meter/second reduction in the velocity requirement, which is primarily the result of the improved estimate at the time of the third correction (Figure 6-11 at 295 days 18 hours).

6.3.3 Venus Swingby Mission

The use of Venus swingby on the return trajectory from Mars to Earth has been described in two references (References 18 and 25). Its primary value is in reducing the entry velocity at Earth. This type of trajectory also shows promise in providing 500-600 day round trip Mars trajectories, which are low-energy in both directions. Because of these important aspects of such a trajectory, preliminary data have been generated for such a trajectory. The nominal trajectory which was used is shown in Figure 6-2, and is characterized by: (1) a total flight time of 360 days, (2) a first leg to Venus having a flight time of 200 days with a radius of closest approach to Venus of 7478 km (1428 km altitude), (3) a flight time from Venus to Earth of 160 days, (4) a virtual perigee

altitude of 24 km at - 16.2 degrees latitude and 270 degrees longitude, and (5) a velocity at perigee of 12.1 km/sec, as compared with 15.2 km/sec on the direct return trajectory which was used.

This trajectory has been considered using System IV with a 10-arc-second theodolite, and the "nominal" guidance system and an observation schedule as shown in Table 6-6. The navigation data are shown in Figure 6-12A and 6-12B. The data in Figure 6-12A are the errors in the predicted estimates of the X, Y, and Z components of position in target coordinates at the time of closest approach to Venus as a function of time. The data in 6-12B are the corresponding error data for the Venus to Earth part of the trajectory. They are errors in predicted estimates of the altitude, cross-range and down-range positions at perigee.

The guidance data for both parts of the trajectory are shown in Table 6-7, and include times of corrections, error in estimate of contraints at time of correction, velocity requirements, and constraint deviations after the corrections. Table 6-8 presents the total deviation state at the time of closest approach to Venus and at perigee. The coordinates are altitude, cross-range and down-range. These data indicate that the trajectory can be estimated and controlled to same degree of accuracy as the direct return. With the 10-arc-second accuracy theodolite and the nominal guidance system, this swingby trajectory was controlled to the entry corridor at perigee (altitude coordinate) with an accuracy of 4.38 km. The same guidance and navigation system controlled the altitude coordinate on direct return trajectory to 6.8 km. In table 6-7, the close approach to Venus data shows that the passage distance and altitude was controlled to 10.2 km.

The penalty which is paid when using the swingby trajectory is in the mid-course ΔV required. The ΔV on the direct return is 110.34 meters/second while on the Venus flyby return trajectory the ΔV requirement is 255.21 meter/second. A more detailed study of the guidance aspects on this type of a trajectory could possibly reduce the

difference. In particular, the use of a combination of guidance laws should be considered. In the case shown, a fixed time of arrival guidance law was used for all corrections. Therefore, the position state at the time of closest approach to Venus was the only constant being controlled. By considering the continuing trajectory to Earth, it is apparent that the velocity state of the time of Venus passage is also important. With the fixed time-of-arrival guidance law, the position state at Venus passage was controlled quite well, but the velocity had an RMS deviation of 360 meters/second (Table 6-8). The large velocity deviation contributes significantly to the large velocity corrections on the Venus-Earth part of the trajectory. Therefore, a study which included consideration of various guidance laws and possible combinations of them would very likely produce a more favorable guidance logic for such a mission.

The results of the preliminary analysis of the Venus flyby mission indicate: (1) the navigation system does not present any unique problems, and (2) the guidance system should be studied in more detail in order to attempt to reduce the midcourse velocity requirements which were considerably larger than those required for the direct trajectory to Earth.

6.4 GUIDANCE ANALYSIS

The performance of the guidance system for the return trajectory has not been studied as a function of the execution errors, since the navigation analysis in the preceeding section has shown that, if four corrections are made, the nominal guidance system can control the trajectory an accuracy within 10-15 percent of the accuracy of the constraint estimates. A detailed study of the guidance times has been made for this phase; however, since the results are very similar to the data in Subsection 5.4.1, it has not been included. The schedule of guidance times based on this data (the ΔV requirements and end-point deviation tradeoffs) is shown in Table 6-3. The two aspects of the guidance analysis which have been considered and are discussed in this section are: (1) the affect of the particular guidance law that is used on the velocity requirements, and (2) the importance of the injection error covariance matrix on the guidance performance.

6.4.1 Guidance Laws

The velocity requirements for the first and second corrections have been determined for three different guidance laws, with the injection error covariance matrix shown in Figure 6-3, for the assumption of a perfect navigation system (P(0) = 0). These ΔV requirements are shown in Figures 6-13 and 6-14 for the FTA, VTA, and Minimum ΔV guidance laws. The difference between the ΔV requirements at zero time (for all guidance laws) for the outbound trajectory and return trajectories 12 m/sec and 30 m/sec, as shown by Figures 4-60 and 6-13, is primarily due to the different RMS velocity deviations at injection which have been used. During the early phase of a trajectory, the ΔV required is very nearly equal to the velocity deviation. This is due to the large sensitivities of the end constraints to velocity changes at this time.

The curves for the required velocity in Figures 6-13 and 6-14 are similiar in form to those of the outbound leg (Figures 4-60 and 4-61). The singularity at 170 days is again due to the true anomaly to the end-point being 180 degrees (Figure 6-1). A comparison of the return ΔV curves (Figure 6-13) with the outbound curves (Figure 4-60) indicates two significant differences in the return trajectory velocity requirements. The first difference is that at 110 days the VTA law exhibits a second singularity which has a wide time period of large ΔV requirements about it. The result is that, during the first 170 days, the VTA ΔV requirement is significantly larger than FTA. The singularity is the result of controlling V_∞ with the VTA law along with $\vec{B}\cdot\hat{T}$ and $\vec{B}\cdot\hat{R}$ as constraints. If V_∞ is not controlled and ΔV is minimized, the curve for ΔV minimum shows a considerable reduction in the ΔV required during this period. In fact these curves, in general, indicate that the selection of the guidance law during the early part of the return trajectory is quite important, since the ΔV requirements, unlike those for the outbound trajectory (Figure 4-60), are quite dependent on the particular guidance law that is used.

The second significant difference between the data for the return and outbound trajectories is the rate of increase in the velocity requirements with time (neglecting the singular regions). The first correction velocity requirements on the return trajectory grow from 30 meters/second at the start to approximately 150 meters/second during the first 150 days (Figure 6-13) for all three guidance laws. On the out-bound trajectory (Figure 4-60) the first correction ΔV with a VTAV guidance law increases from 10 meters second at injection to 15 meters/second at 150 days. The corresponding increase for the FTA law is from 10 meters/second to 65 meters/second. These rates of increase in the requirements on the out-bound are significantly lower than those on the return. The result of this is that on the out-bound trajectory there is a much smaller penalty in ΔV as more time is taken to allow the navigation system to obtain a good estimate on which to base the guidance corrections. This rapid growth in the velocity requirements on the return trajectory is due primarily to the diagonal injection covariance matrix (Figure 6-4) which was used in the analysis. Figure 6-15 shows the first correction ΔV requirements for the injection covariance matrix which was used on the out-bound trajectory (Figure 5-6). This matrix shows a significantly slower growth during the early part of the trajectory for all the guidance laws. The midcourse ΔV requirements for these different injection matrices are presented in the next Subsection.

In addition to determining the ΔV requirements for various guidance laws, the effect of a VTA guidance law on the end-point deviations has also been determined. This effect is of interest because the navigation systems in Section 6 have assumed the use of a FTA guidance law. Table 6-9 shows a VTA guidance law reduces the altitude deviation from 6.8 km to 6.4 km and the ΔV requirement by 10 m/sec. A significant disadvantage of the VTA law, however, is that the standard deviation of the arrival time varies from 25 seconds for the FTA to 4 hours 17 minutes for the VTA. If an Earth-fixed landing site were to be used, this time deviation might prohibit the use of a VTA guidance law.

6.4.2 Injection Errors

The covariance matrix of injection errors used in the analysis is shown in Figure 6-3. This matrix was used for both the error in estimate of the state and the state deviations. In this Subsection, some additional guidance data are presented to show the influence of these injection conditions on the guidance results. The deviations resulting from different injection conditions (shown in Table 6-10) indicate that the guidance performance at perigee is relatively independent of the injection conditions. In particular, the variation in the altitude constraints, which control the corridor, was 10 percent with the various injection conditions shown in Table 6-10. The velocity requirements as shown, however, are dependent on the injection conditions, with the major differences occurring in the first correction.

The first two cases in the table show the influence of a better initial estimate of the state on the performance. The error in estimate of the initial velocity state was reduced from 30 m/sec. to 3m/sec. There is a 1 percent decrease in the velocity requirements and a 5 percent decrease in the perigee position deviations. The third case represents a reduction in both the error in estimate of the velocity and the velocity deviation from 30 m/sec. to 3m/sec. The primary effect of this change is to reduce the first correction by 27 meters/second. This is essentially the same as the reduction in the initial velocity deviation. The other three corrections were also slightly reduced.

The total ΔV of 110.34 m/sec. required for case one shown in Table 6-10 represents nearly twice the 56.8 m/sec. ΔV required on the out-bound for the corresponding navigation system. This difference is due primarily to the manner in which the ΔV requirements grow on the return trajectory (Figure 6-13) with the diagonal matrix. The data in Table 6-11 shows a comparison of the ΔV requirements on the out-bound and return using System IV with a 10-second theodalite and a FTA quidance law. The injection error covariance matrix used for both cases is the one shown in Figure 4-6 , which was used on the out-bound trajectory. The data indicates

that, with the same injection errors, the velocity requirements on both trajectories are very nearly the same.

6.5 SUMMARY

The navigation analysis of System III indicated that the DSIF tracking system alone was capable of an accuracy which would permit an atmospheric maneuver at perigee. System IV, the on-board system, requires a 4-arc-second instrument to provide the accuracy required to achieve a 3.5 km corridor deviation.

The midcourse ΔV requirements are larger on the return trajectory than on the out-bound for a VTA Guidance Law.

The Venus swingby trajectory for the return shows no navigation system difficulties, but does indicate the guidance logic should be analyzed in an attempt to reduce the ΔV requirements. The ΔV required on the swingby mission is approximately twice the ΔV as the direct-return trajectory.

SECTION 7

MARS ORBITAL ANALYSIS

7.1 INTRODUCTION

The Mars orbital phase starts immediately after the retro maneuver and continues for 40 days. As previously stated, this phase has been assumed to be independent of both the outbound and return phases of the mission. The uncertainties that resulted from the outbound midcourse phase, as well as the retro maneuver into orbit, have not been used as injection errors for the orbital phase. This is because the values of these errors, as discussed in Section 5, are quite small. Since it is desired to evaluate the capability of the navigation systems under adverse conditions, injection errors that are several orders of magnitude larger than might normally be obtained are defined for the orbital phase. It has been assumed that the required ΔV for the departure maneuver would be computed by using the current best estimate of the trajectory as the nominal park orbit. It is also assumed that the guidance errors resulting from the burn maneuver would be about 1 per cent of the ΔV maneuver requirements. With this assumption, the uncertainties in estimating the orbit are orders of magnitude less than the uncertainties from the guidance errors, and therefore the return phase does not depend on the results of the orbital phase.

No guidance corrections are considered for this phase and no specific mission requirements have been defined. The purpose of this section, therefore, is to investigate the orbit determination capabilities of the DSIF and onboard navigation systems. The results are interpreted in terms of the orbital elements, as well as the state vector of position and velocity in the NVW coordinate system, for various orientations of the orbit.

7.2 STUDY RESTRICTIONS

A number of the restrictions discussed in previous sections also apply to the analysis of the orbital phase. In particular, the error sources considered are again of a random nature and result from either Earth-based or onboard tracking devices. The filtering theory and error propagation methods discussed in Section 2 also apply to this phase of the analysis. The restrictions that differ for this phase, however, pertain to the park orbit used and the injection errors. Only errors in the basic measurement instruments are considered. These errors are tabulated in the RMS position and velocity plots for each instrument.

7.2.1 Nominal Orbit Plane

The park orbit configurations considered in this phase are described in terms of the orbital elements shown in Figure 7-1. Numerical values of the orbital elements and the injection conditions are shown in Table 7-1 for the nominal trajectory.* The eccentricity of the orbit, however, has been changed from 0 to 0.0199. This change has been made to enable the error in estimates of the orbital elements to be computed. As shown in Appendix D, the gradient of some of the orbital elements with respect to position and velocity state contain $\frac{1}{e}$ terms which prevent the analysis of circular orbits in terms of the orbital elements (i.e., not all elements are defined for circular orbits). The orbit and planetary body configurations for the nominal trajectory at injection are shown in Figure 7-2. It has also been assumed that the central body of attraction (Mars) is spherical with homogeneous mass distribution and, therefore, no variations in the orbital elements due to oblateness exist.

Since the DSIF tracking capability is highly dependent upon the orientation of the park orbit with respect to the tracker line-of-sight, some additional trajectories have been considered. These trajectories have the same conic sections (a, e, and q) as the nominal, but different orientation parameters.

* This park orbit was supplied by Marshall Space Flight Center.

The orbital parameters and injection conditions for $\hat{R}.\hat{W} = 0$ and $\hat{R}.\hat{W} = -1$ orbits, which represent the limiting cases, are given in Tables 7-2 and 7-3, respectively, in both 1950 equatorial coordinates and ecliptic coordinates. The x-y-z coordinate system used to define these special orbits is shown in Figure 7-3. The $\hat{R}.\hat{W} = 0$ and $\hat{R}.\hat{W} = -1$ orbits, in terms of x-y-z coordinates, are shown in Figure 7-4.

7.2.2 Injection Errors

Injection errors for each position and velocity component of 1000 km and 1 km/sec, respectively, are considered except where otherwise noted. These errors are much larger than the errors that have been found to exist at the end of the midcourse phase.

7.3 NAVIGATION ANALYSIS

In the analysis that follows, the performance of Systems I, III, and IV is evaluated on the nominal Martian orbit. System I is also evaluated for various orientations of the park orbit with respect to the Earth-Mars line. In the analysis of Systems III and IV, a number of different measurements as well as combinations of certain measurements are considered.

7.3.1 System I

The results of studying the navigation capabilities of DSIF tracking are presented in this sub section. The measurement errors (q) of the three tracker stations have been given in Section 5. The measurements taken are azimuth, elevation, and range-rate. Gradient vectors (H) for these measurements are given in Appendix B. These gradients are of particular interest because they indicate that: (1) both azimuth and elevation measurements are not very useful as the magnitude of the H vector is reduced by $\frac{1}{R}$ (R is the

magnitude of the LOS vector), and (2) the range rate gradient provides only information on the velocity components of the state that are along the LOS direction $\vec{R}$. It is clear then that the performance of DSIF tracking is highly dependent on the orientation of the park orbit plane with respect to the tracker LOS, $(\vec{R})$. A number of park orbits are therefore considered in this subsection where the angle between the $\hat{R}$ vector and $\hat{W}$ vector (perpendicular to the orbit plane in the NVW coordinate system) is varied. The effects of vehicle occulation, different injection errors P(0), the transition matrix of the orbital equations, and the frequency of observations are also considered in this subsection.

The first orbit plane analyzed using DSIF tracking, is oriented such that R.W=0. This orbit is defined in Table 7-3. Tracking is initiated with a diagonal P(0) matrix consisting of a 1000 km uncertainity for each position coordinate and a 1 km/sec uncertainty for each velocity coordinate. Observations have been made at the rate of 1/min. All tracking was initiated at the point of closest approach to the planet.

The results of this study are presented in Figures 7-5 through 7-7. The RMS errors in estimate of position and velocity $\sigma_{\tilde{\underline{x}}}$ and $\sigma_{\dot{\tilde{\underline{x}}}}$ respectively, are shown in Figure 7.5. These tracking data indicate that, after three days of continuous tracking, a reduction of about one order of magnitude in both the position and velocity uncertainties occurs. The reason for these uncertainties not being reduced by a greater amount is that the tracker LOS is in the orbit plane for this park orbit, therefore, no information is obtained on the out-of-plane (W) components of position and velocity. This particular $\hat{R}.\hat{W}$ orbit plane was defined initially to lie in the Earth-Mars plane. As a result, the tracker Line-of-Sight still lies in the orbit plane after three days of continuous tracking. It is the W components of position and velocity that are the major part of the uncertainties for this orbit as shown in Table 7-4. These same results are also expressed in terms of the orbital element a, e and q, and i, Ω, ω, in Figures 5-6 and 5-7, respectively.

The effects of considering the vehicle occulation by Mars is shown in Figure 7-5 to increase the uncertainty in position and velocity by 40 km and 0.45 km/sec, respectively, after three days of tracking. These figures represent a 30 per cent increase in the position uncertainty and a 25 per cent increase in velocity uncertainty. The period of occulation for this orbit is nearly equal to that shown in Figure 7-8. This figure also contains the observation schedule. Since the $\hat{R}\cdot\hat{W} = 0$ orbit results in the maximum occulation of the vehicle, it may be concluded that the effects of occulation do not present a serious limitation for DSIF tracking. The period of occulation decreases with increasing altitude and as a result is less significant for orbits of increasing radius. The projection of the positions of Earth and Mars onto the ecliptic plane, shown in Figure 7-9, indicates the heliocentric motion of the two planets during the 40-day orbit period.

The effect of a small initial covariance matrix P(0), is shown in Figure 7-10. The initial position and velocity component uncertainties are 3 km and 0.095 km/sec, respectively. Two features of the error in estimate curves are considerably different from the curves in Figure 7-5 where the initial P matrix is larger. First, the initial RMS position uncertainty in Figure 7-10 represents a greater accuracy than the DSIF instrumentation is capable of maintaining and, therefore, the $\sigma_{\tilde{x}}$ curve increases from the initial value. The second feature that may be noted for both the position and velocity uncertainty curves, is that the curves themselves are oscillatory, unlike those in Figure 7-5. These oscillations reflect the dynamics of the orbital equations (and, in particular, the dynamics normal to the nominal orbit plane). Whereas the dynamics of the midcourse trajectories can essentially be represented by straight line segments, the park orbits are nearly circular and the transition matrix contain periodic as well as secular terms. As the errors in estimate in Figure 7-10 consist mainly of errors along the W component, the curves in this figure represent the effect of propagating the error in estimate ($\Phi P \Phi^T$) of the W component along the trajectory. The equations for the variances of W and $\dot{W}$, are respectively:

$$\sigma^2_{\omega}(t) = \sigma^2_{\omega}(t)\cos^2\left[\omega(t-t_o)\right] + \left(\frac{1}{\omega^2}\right)\sigma^2_{\dot{\omega}}\sin^2\left[\omega(t-t_o)\right] \quad 7\text{-}1$$

and

$$\sigma^2_{\dot{\omega}}(t) = \sigma^2_{\omega}(t_o)\,\omega^2\sin^2\left[\omega(t-t_o)\right] + \sigma^2_{\dot{\omega}}(t_o)\cos^2\left[\omega(t-t_o)\right] \quad 7\text{-}2$$

Solving these equations at true anomaly angles of 90^o, 270^o, 0^o, 180^o yields the maximum errors in estimate shown in Figure 7-10, which are 67 km and 0.055 km/sec.

An additional study has been made to determine whether increasing the observation frequency would decrease the errors in estimate shown in Figure 7-10. By doubling the observation frequency from one per minute to one every 30 seconds, it has been found that there exists no improvement in the position or velocity uncertainties. The curves in Figure 7-10 represent the highest degree of accuracy that can be obtained with DSIF tracking for this particular orbit.

Two additional variations in the R.W=0 orbit have been made. First, the park orbit plane was rotated 90 degrees about the LOS so that it is perpendicular to the Earth-Mars orbit plane at injection. The second change consisted of the 90 degree rotation about the LOS as well as a 90 degree rotation of the true anomaly of the park orbit. The results of studying these orbits about the angular momentum vector (for positive rotation) are shown in Figures 7-11 and 7-12. It may be seen that the magnitude of the uncertainties in these figures is slightly less than that of the uncertainties in Figure 7-5. This is because the tracker LOS is not always perpendicular to the $\hat{W}$ unit vector for these orbits (i.e., at the end of three days $\measuredangle\hat{R}.\hat{W} \approx 89$ degrees), and, therefore, a slightly better estimate of this component is obtained. It may also be seen from Figures 7-11 and 7-12 that a shift in the true anomaly by 90 degrees relative to the tracker LOS does not change the position or velocity uncertainties, moreover, the only difference in these curves is the shift in the peak error of 90 degrees which, of course, is a direct result of the shift in the orbit true anomaly.

7.3.1.1 Nominal Park Orbit

The nominal park orbit has approximately the same orbital elements a, e, and q as the $\hat{R}.\hat{W}$ =0 orbit; however, the angle between the tracker LOS and the orbital plane for the nominal orbit is 6 degrees, $\sphericalangle \hat{R}.\hat{W}$ = 96 degrees. The DSIF tracking data for this orbit is shown in Figures 7-13 through 7-15. A comparison of the position and velocity uncertainties for this orbit with the R.W = 0 orbit of Figure 7-5 shows that both $\sigma_{\tilde{x}}$ and $\sigma_{\dot{\tilde{x}}}$ uncertainties have reduced considerably as the result of the 6 degree rotation of the orbit plane. The maximum uncertainties which occur near the end of the three day tracking period are 2 km and 0.025 km/sec.

7.3.1.2 Addition Park Orbit Inclinations. A typical case where information is obtained on both in-plane (N and V) and out-of-plane (W) components is where $\sphericalangle \hat{R}.\hat{W}$ = 130 degrees. The DSIF tracking data for this case is shown in Figures 7-16 and 7-18. The peak RMS position and velocity uncertainties near the end of the tracking period, as shown in Figure 7-14, are 160 km and 0.4 km/sec., respectively. The components of the uncertainties in position and velocity, shown in Figures 17 and 18, indicate that, in addition to large uncertainties in the W position and velocity components, the V position uncertainty and the N velocity uncertainty are also large.

The DSIF tracking data for the park orbit whose plane is perpendicular to the LOS is shown in Figures 7-19 through 7-21. This orbit represents another extreme case where it would be expected that very good estimates might be obtained for the W components of position and velocity, and poor estimates for the in-plane components. The RMS position and velocity uncertainties shown in Figure 7-19 indicate that actually this orbit results in the smallest uncertainties of any of the orbits considered. These uncertainties have been reduced by three orders of magnitude to 10 km and 8 m/sec at the end of three days of tracking. The uncertainties of the orbital elements for the last three hours of tracking are shown in Figures 7-20 and 7-21. These figures indicate that the Ω, and i parameter uncertainties,

which are a function of the out-of-plane uncertainty, are very small for this orbit.

The effect of making only range-rate observations is shown in Figure 7-22.

An additional study has been made using this orbit to show the effect of a very large covariance matrix P(0). These results are shown in Figure 7-23.

7.3.1.3 Summary of $\hat{R}.\hat{W}$ Orientation. A summary of the results of varying the tracker LOS-orbit plane angle ($\measuredangle \hat{R}.\hat{W}$) between 90 degrees and 180 degrees is given in Tables 7-4 and 7-5. After 8 hours 5 minutes of tracking, these results verify the fact that the range-rate measurement produces the best estimate on the component of position and velocity that lie along the tracker LOS. In general, the V component of position uncertainty is larger than the N components because of the secular term in the V element of the transition matrix. For the velocity uncertainties, however, it is the N component that is the larger of the two in-plane components N and V. This is also the result of a secular term in the element of the transition matrix that affects $\dot{N}$. The optimum orientation angle, as shown in Figure 7-24, is $\measuredangle \hat{R}.\hat{W}$ = 180 degrees or 0 degrees, as this results in the smallest uncertainties for both RMS position and velocity.

7.3.2 System III (DSIF-Sextant, DSIF-Radar)

The navigation analysis of this system consists of studying the performance of DSIF tracking combined with onboard radar and sextant measurements. The nominal park orbit has been used, and observations are made at the rate of one per minute.

The results of the DSIF-radar measurements are shown in Figures 7-25 through 7-27. A comparision of the uncertainties in position and velocity is shown in these figures; with the same quantities using only DSIF, Figure 7-13 indicates that the addition of onboard radar measurements adds nothing to the orbit determination capabilities of DSIF. It should be noted, however, that the value of onboard radar measurements depends on the orientation of the park orbit. For example, if the park orbit were inclined such that R.W = -1, then the radar could result in improvements for estimating the components of position and velocity in the orbit plane. The uncertainties in the orbital elements for this system are shown in Figures 7-26 and 7-27.

The combination of DSIF and sextant observations provides very good navigation information, as shown in Figures 7-28 through 7-30. These results have been obtained by assuming two simultaneous sextant observations, with one measurement in the nominal orbit plane and the other at a declination of 45 degrees to the orbit plane. A 10-arc-sec instrument has been assumed. As a result of these particular sextant measurements, the out-of-plane components can be estimated quite well. In fact, for this system the uncertainties in position and velocity after three days tracking were respectively 0.015 km and 0.2 m/sec. These estimates are significantly better than any of the other systems evaluated for the nominal park orbit.

7.3.3 System IV

The performance of this system has been studied for the following onboard measurements: (1) sextant, (2) onboard radar, (3) subtended angle, and (4) a combination of sextant and subtended angle.

The same sextant measurements have been assumed that were discussed in the previous section. The results of these measurements with 432 in-plane observations and 432 observations at a 45 degree angle to the orbit plane, are shown in Figures 7-31 through 7-33. The RMS uncertainties in

position and velocity for these measurements at the end of 72 hours of tracking are 750 m and 0.5 m/sec., respectively.

The onboard radar system measures both range and range-rate, which are essentially altitude and altitude-rate. The measurement gradient, H, lies in the orbit plane. Therefore, the performance of this system, shown in Figures 7-34 through 7-36, is limited by the W components of position and velocity, since these components can not be reduced directly by radar measurements. The measurement accuracies are tabulated in Figure 7-34. The final uncertainties for this system are about 1.4 km and 1.1 km/sec.

The capability of a planet tracker (subtended angle measurements) for determining the vehicle's orbit is indicated by the data in Figures 7-37 through 7-39. These observations result in range information and, therefore, again provide good estimates of the in-plane components of position and velocity. The final uncertainties for this system are essentially the same as those obtained using onboard radar.

The results of combining subtended angle and sextant measurements are shown in Figures 7-40 through 7-42. The RMS position and velocity uncertainties shown in these figures are identical to those resulting from sextant measurements alone (Figure 7-31), at the end of three days of tracking. In fact, the only difference between the combined measurements and the sextant alone is that the uncertainties decrease faster during the first orbit with combined measurements (as can be seen by comparing Figures 7-31 and 7-40 for the first two hours of tracking).

7.4 COMPARISON OF SYSTEMS PERFORMANCE

The performances of the seven navigation systems studied for the orbital phase are summarized in this section. The data is presented in terms of both position and velocity component uncertainties, as well as orbital element uncertainties.

7.4.1 NVW Component Summary

The results of studying the DSIF tracking for various orbit inclinations (Figure 7-22) have shown that the most accurate tracking is obtained when the park orbit is inclined ± 90 degrees to the Earth-Mars line. Also, it has been found that the worst case of tracker occulation by Mars increases the position and velocity uncertainties over the case where no occulation occurs by 30 percent and 25 percent respectively. As seen in Table 7-4, for almost any R.W angle, the V components of position and the N components of velocity are the largest of the in-plane component errors, as these components contain secular terms in the transition matrix elements.

A summary of the results of evaluating the seven navigation systems for the nominal trajectory is given in Table 7-6. These systems would be part of Systems I, III, and IV as defined in Section 1. The results in Table 7-6 show that System III with DSIF and sextant observations is the most accurate, with uncertainties of 0.2 km and 0.17 m/sec after three days of tracking.* System IV with sextant or sextant and subtended angle observations is the second most accurate with uncertainties of 0.75 km and 0.6 m/sec. These two systems possess good capabilities of determining the park orbit. This is true because, with sextant observations, it is possible to obtain estimates of the out-of-plane components of position and velocity.

System I (DSIF tracking only), System III with DSIF and onboard radar measurements, and System IV with either onboard radar or subtended angle measurements possess significantly poorer performance

*These values represent the time averages where oscillations occur in the uncertainty curves.

than the systems that contain sextant or sextant and DSIF tracking. This is also shown in Table 7-6, and is the result of very little out-of-plane information. These results are presented in a different form in Table 7-7. Here a fixed accuracy of 1 km and 1 m/sec has been established as a minimum acceptable level for the RMS position and velocity uncertainties. Again, the only systems capable of achieving this level are those containing sextant observations; i.e., sextant alone, sextant-DSIF, and sextant subtense measurements. The times required for these systems to attain this level of accuracy, as well as the minimum level of the uncertainties obtained with the other systems, are shown in the table.

7.4.2 Orbital Element Summary

A composite summary of the navigation capabilities of the seven systems for determining the six orbital elements is given in Table 7-8 for the nominal trajectory. Also included in this table are the results of two special orbits (R.W = 0 and R.W = 1) and the results of making only range-rate measurements. Three figures are listed for each case; the standard deviation of the error in estimate of the orbital element, the ratio of the particular standard deviation to the standard deviation for the DSIF-sextant system, and the order of magnitude by which the DSIF-sextant is superior. The DSIF-sextant system has been considered as a basis for comparison, since this system produced the most accurate estimates.

The second most accurate system is again the sextant subtense system, and the capability of this system for determining the conic section parameters is approximately one order of magnitude poorer than that of the DSIF-sextant. The capability of this system to determine the orbit orientation parameters i, w, and Ω, however, is just as good as that of the DSIF sextant system. This is an important result because it indicates that the degradation of the navigation performance of an onboard system (System IV) is not significant compared to the most accurate system (System III

with DSIF-sextant). The data in Table 7-8 for the orbital elements display many of the same results that have been found in Table 7-6. In particular, the three DSIF cases for different orbits and range-rate measurement show that the R.W = -1 orbit is again the orientation that can be the most accurately determined and also the DSIF tracking with azimuth, elevation, and range-rate measurements is not any better than that with only range-rate measurements.

The results of the seven system comparisons for the nominal trajectory can be interpreted to a large extent by the type of measurement information that is obtained. The DSIF-onboard radar system for example, is not better than the DSIF alone. It also may be noted from Table 7-8 that in-plane measurements may be capable of determining the conic section parameters, but in general, out-of-plane-measurements (e.g. sextant) are also required to accurately estimate the orientation parameters i, ω, and Ω. The numerical data that is given in Table 7-8 is also presented in Table 7-9 in bar-chart form. In Table 7-10 the orbit determination capabilities of the seven systems are summarized by plotting the vector sum of the six components (a, e, q, i, Ω, and ω), the sum of the three orientation parameters (i, Ω, and ω), and the sum of the three conic section parameters (a.q.e).

In Table 7-11, the performance of System III with both DSIF-Sextant and DSIF radar measurements is compared to DSIF tracking. Table 7-12 shows a comparison of the four different onboard systems: radar, subtended angle, subtended angle-sextant, and sextant. The most accurate of these systems is the one with sextant observations; therefore, this system is the basis for comparison in the table.

SECTION 8

RECOMMENDATIONS

Additional study areas which would extend the scope of the present study, and which are considered to be important for defining the navigation and guidance requirements of an interplanetary mission, are the following:

a. Precision Trajectory. The results which are obtained in this study with a patched conic trajectory should be verified with the use of a precision trajectory.

b. Bias Errors. The influence of bias error sources which are neglected in this study should be evaluated. These errors include uncertainities in the physical constants, (mass of the sun, oblateness of Mars, mass of Mars, etc.), measurement instrument biases, onboard clock bias, and tracker station location errors.

c. Filtering Technique. The study has assumed the use of a Kalman filter in the data processing. The various other filtering techniques should be evaluated and, in particular, consideration should be given to their onboard implementation.

d. Beacons. The importance of having beacons on Mars should be evaluated for the approach phase of the mission, terminal maneuvering phase and the orbital phase.

e. Terminal Maneuvers. The guidance system inertial equipment requirements should be determined for the retro maneuver (powered and/or atmospheric) and the powered flight out of the Mars orbit. A retro analysis is also required at perigee on the return.

f. Onboard Computer. The design of the onboard computer should be studied to determine means of trading off speed for reliability (500 to 600-day missions). Also, techniques for simplifying calculations for estimating and predicting the state should be investigated. This investigation should include the effects of truncation errors in the computer.

g. Mars Orbit. The navigation requirements in orbit should be determined in terms of specific mission objectives. The influence of the oblateness of Mars on these requirements should be evaluated.

The errors resulting from park orbit navigation and the burning maneuver out of orbit should be evaluated in terms of their effect on the return trajectory computations and performance.

h. Venus Swingby. The Venus swingby mission should be studied in detail because of its apparent importance in a round-trip Mars mission.

DERIVATION OF THE COVARIANCE MATRIX Γ_v

The covariance matrix

$$\Gamma_v = E\left(\frac{v}{|v|}\,\frac{v^T}{|v|}\right)$$

will be derived under the assumption that

$\Lambda_v = E(vv^T)$ is known.

Since Γ_v deals only with the direction of the velocity correction which can be specified by two quantities and it is a 3 x 3 matrix, Γ_v is obviously singular. The error ellipsoid of Γ_v in 3 dimensions will only in very special cases bare an exact resemblance to the error ellipsoid Λ_v.

Let $v = T\,\omega$ where T is the orthogonal transformation which diagonalizes Λ_v, i.e., $E(\omega\omega^T)$ is a diagonal matrix.

Then,

$$\frac{v}{|v|} = T\,\frac{\omega}{|\omega|}$$

and

$$E\left(\frac{v}{|v|}\,\frac{v}{|v|}^T\right) = T\,E\left(\frac{\omega}{|\omega|}\,\frac{\omega}{|\omega|}\right)T^T \qquad \text{(A-1)}$$

Let

$$\omega = \begin{pmatrix} x \\ y \\ x \end{pmatrix}$$

Then, it is desired to determine

$$A = E\left(\frac{x^2}{x^2 + y^2 + z^2}\right) \quad B = E\left(\frac{y^2}{x^2 + y^2 + z^2}\right) \quad \text{and} \quad C = E\left(\frac{z^2}{x^2 + y^2 + z^2}\right)$$

where x, y, and z are independent normal random variables with zero mean and variances σ_x^2, σ_y^2, and σ_z^2. It will be assumed here that the eigenvectors of T are so chosen such that

$$\sigma_x^2 \geq \sigma_y^2 \geq \sigma_z^2$$

The joint density function of x, y, and z is

$$p(x,y,z) = \frac{1}{(2\pi)^{3/2}\left[\sigma_x\ \sigma_y\ \sigma_z\right]}\ e^{-\frac{1}{2}\left(\frac{x^2}{\sigma_x^2} + \frac{y^2}{\sigma_y^2} + \frac{z^2}{\sigma_z^2}\right)}$$

By introducing spherical coordinates

$$\frac{x}{\sigma_x} = r\cos\phi\sin\theta$$

$$\frac{y}{\sigma_y} = r\sin\phi\sin\theta$$

$$\frac{z}{\sigma_z} = r\cos\theta$$

the Jacobian

$$J = \begin{vmatrix} \frac{\partial x}{\partial r} & \frac{\partial y}{\partial r} & \frac{\partial z}{\partial r} \\ \frac{\partial x}{\partial \theta} & \frac{\partial y}{\partial \theta} & \frac{\partial z}{\partial \theta} \\ \frac{\partial x}{\partial \phi} & \frac{\partial y}{\partial \phi} & \frac{\partial z}{\partial \phi} \end{vmatrix} = (\sigma_x\ \sigma_y\ \sigma_z)\ r^2\sin\theta$$

So the joint density function in spherical coordinates is

$$p(r,\theta,\phi) = (2\pi)^{-3/2} \; r^2 \sin\theta \; e^{-\frac{1}{2}(r^2)}$$

Let

$$E\left(\frac{x^2}{x^2+y^2+z^2}\right) = A$$

then in rectangular coordinates

$$A = \int_{-\infty}^{+\infty}\int_{-\infty}^{+\infty}\int_{-\infty}^{+\infty} \frac{x^2}{x^2+y^2+z^2}\, p(x,y,z)\, dxdydz$$

and in spherical coordinates

$$A = (2\pi)^{-3/2} \int_0^{2\pi}\int_0^{\pi}\int_0^{\infty} \frac{\sigma_x^2 \cos^2\phi \sin^2\theta \sin\theta \; r^2 e^{-\frac{1}{2}r^2}}{\sigma_x^2 \cos^2\phi\sin^2\theta + \sigma_y^2 \sin^2\phi\sin^2\theta + \sigma_z^2\cos^2\theta}$$

The r integral which is from 0 to ∞ is readily integrated to give a value of $\sqrt{\pi/2}$ thus

$$A = \frac{1}{4\pi} \int_0^{2\pi}\int_0^{\pi} \frac{\sigma_x^2\cos^2\phi\sin^3\theta \; d\phi d\theta}{\sigma_x^2\cos^2\phi\sin^2\theta + \sigma_y^2\sin^2\phi\sin^2\theta + \sigma_z^2\cos^2\theta} \qquad \text{(A-2)}$$

Next consider the ϕ integral. Dividing by σ_x^2 and arranging

$$A = \frac{1}{4\pi} \int_0^{\pi} \sin^3\theta d\theta \int_0^{2\pi} \frac{\cos^2\phi d\phi}{\cos^2\phi\sin^2\theta + \frac{\sigma_y^2}{\sigma_x^2}\sin^2\phi\sin^2\theta + \frac{\sigma_z^2}{\sigma_x^2}\cos^2\theta}$$

Let

$$\gamma = \frac{\sigma_y^2}{\sigma_x^2} \leq 1$$

$$\rho = \frac{\sigma_z^2}{\sigma_x^2} \leq 1$$

$$\sin^2\phi = 1-\cos^2\phi$$

Also the ϕ integral limits may be changed to $\pi/2$ and the resultant integral multiplied by 4

$$A = \frac{1}{\pi}\int_0^{\pi}\sin^3\theta d\theta \int_0^{\pi/2}\frac{\cos^2\phi d\theta}{\cos^2\phi\,\sin^2\theta(1-\alpha) + \alpha\sin^2\theta + \beta\cos^2\theta} \tag{A-3}$$

Consider the special case $\alpha = 1$

Then

$$A = \int_0^{\pi}\frac{\sin^3\theta\ d\theta}{\sin^2\theta + \beta\cos^2\theta}\ \frac{1}{\pi}\left[\frac{\phi}{2} + \frac{\sin(2\phi)}{4}\right]_0^{\pi/2}$$

$$= \frac{1}{4}\int_0^{\pi}\frac{\sin^3\theta\ d\theta}{\cos^2\theta(\beta - 1) + 1} \tag{A-4}$$

In the very special case for $\alpha = \beta = 1$, then

$$A = \frac{1}{4}\int_0^{\pi}\sin^3\theta d\theta = \frac{1}{4}\left[\frac{\cos^3 x}{3} - \cos x\right]_0^{\pi} = \underline{1/3}$$

For $\beta < 1$ introduce $\sin^2\theta = 1-\cos^2\theta$ in equation (A-4)

$$A = \frac{-1}{4}\int_0^{\pi}\frac{(\cos^2\theta-1)\sin\theta d\theta}{\cos^2\theta(\beta-1) + 1}$$

$$= \frac{-1}{4}\int_0^{\pi}\left(\frac{1}{\beta-1} - \frac{\left(\frac{\beta}{\beta-1}\right)}{(\beta-1)\cos^2\theta + 1}\right)\sin\theta d\theta$$

$$= -\frac{1}{4}\left[\frac{-\cos\theta}{(\beta-1)}\right]_0^{\pi} - \frac{\frac{\beta}{\beta-1}}{4}\int_0^{\pi}\frac{-\sin\theta d\theta}{1 - (1-\beta)\cos^2\theta} \tag{A-5}$$

Letting $x = \cos\theta$ the integral of equation (A-5) is of the form

$$\frac{dx}{1-(1-\beta)x^2}$$

$$A = \frac{+1}{2(1-\beta)} + \frac{\beta}{4(1-\beta)} \left[\frac{1}{2\sqrt{1-\beta}} \ell n \left| \frac{1+\sqrt{1-\beta}\cos\theta}{1-\sqrt{1-\beta}\cos\theta} \right| \right]_0^{\pi}$$

$$= \frac{1}{2(1-\beta)} - \frac{\beta}{4(1-\beta)^{3/2}} \left[\ell n \left| \frac{1+\sqrt{1-\beta}}{1-\sqrt{1-\beta}} \right| \right] \qquad \text{(A-6)}$$

Return now to the general case of equation (A-3)

Let $b^2 = \sin^2\theta(1-\alpha)$

$a^2 = \alpha \sin^2\theta + \beta\cos^2\theta$

then

$$A = \frac{1}{\pi} \int_0^{\pi} \sin^3\theta d\theta \int_0^{\pi/2} \frac{\cos^2\phi \, d\phi}{b^2\cos^2\phi + a^2}$$

$$= \frac{1}{\pi} \int_0^{\pi} \sin^3\theta d\theta \int_0^{\pi/2} \left[\frac{1}{b^2} - \frac{a^2/b^2}{b^2\cos^2\phi + a^2} \right] d\phi$$

$$A = \frac{1}{\pi} \int_0^{\pi} \sin^3\theta d\theta \frac{1}{b^2} \left[\phi - \frac{a}{\sqrt{a^2+b^2}} \tan^{-1} \frac{2\tan\phi}{\sqrt{a^2+b^2}} \right]_0^{\pi/2}$$

$$A = \frac{1}{\pi} \int_0^{\pi} \sin^3\theta d\theta \frac{1}{b^2} \left[\frac{\pi}{2} - \frac{a\pi/2}{\sqrt{a^2+b^2}} \right]$$

Expressing the variables a and b as functions of θ gives

$$A = \tfrac{1}{2} \int_0^{\pi} \frac{\sin\theta}{(1-\alpha)} \left[1 - \frac{\sqrt{\alpha \sin^2\theta + \beta \cos^2\theta}}{\sqrt{\sin^2\theta + \beta \cos^2\theta}} \right] d\theta$$

$$A = \frac{1}{1-\alpha} - \frac{1}{2(1-\alpha)} \int_0^{\pi} \frac{\sqrt{\alpha \sin^2\theta + \beta\cos^2\theta}}{\sqrt{\sin^2\theta + \beta \cos^2\theta}} \sin\theta d\theta$$

let $\sin^2\theta = 1-\cos^2\theta$

$$A = \frac{1}{1-\alpha} - \frac{\sqrt{\alpha}}{2(1-\alpha)} \int_0^{\pi} \frac{\sqrt{1 - \frac{(\alpha-\beta)}{\alpha}\cos^2\theta}}{\sqrt{1 - (1-\beta)\cos^2\theta}} \sin\theta d\theta \qquad \text{(A-7)}$$

Consider the special case of $\beta = \alpha$

then

$$A = \frac{1}{1-\alpha} - \frac{\sqrt{\alpha}}{2(1-\alpha)} \int_0^{\pi} \frac{\sin\theta d\theta}{\sqrt{1 - (1-\alpha)\cos^2\theta}}$$

$$= \frac{1}{1-\alpha} + \frac{\sqrt{\alpha}}{2(1-\alpha)^{3/2}} \int_0^{\pi} \frac{-\sqrt{1-\alpha}\sin\theta d\theta}{\sqrt{1 - (1-\alpha)\cos^2\theta}}$$

$$= \frac{1}{1-\alpha} + \frac{\sqrt{\alpha}}{2(1-\alpha)^{3/2}} \left[\sin^{-1}\left(\sqrt{1-\alpha}\cos\theta\right) \right]_0^{\pi}$$

$$= \frac{1}{1-\alpha} - \frac{\sqrt{\alpha}}{(1-\alpha)^{3/2}} \left[\sin^{-1}\sqrt{1-\alpha} \right]$$

$$= \frac{1}{1-\alpha} - \frac{\sqrt{\alpha}}{(1-\alpha)^{3/2}} \tan^{-1}\sqrt{\frac{1-\alpha}{\alpha}}$$

The general solution of equation (A-7) is readily put in the form of an incomplete elliptic integral of the second kind by letting

$$x = \sqrt{1-\beta}\cos\theta \qquad dx = -\sqrt{1-\beta}\sin\theta d\theta$$

$$A = \left(\frac{1}{1-\alpha}\right) + \left(\frac{\sqrt{\alpha}}{2\sqrt{1-\beta}\,(1-\alpha)}\right) \int_{\sqrt{1-\beta}}^{-\sqrt{1-\beta}} \frac{\sqrt{1 - \frac{(\alpha-\beta)}{\alpha(1-\beta)}x^2}}{\sqrt{1-x^2}} dx$$

Since the kernel is symmetric about x = 0 the limits can be changed to go from 0 to $\sqrt{1-\beta}$ and the sign changed and result doubled.

With $k = \sqrt{\frac{\alpha-\beta}{2(1-\beta)}}$ then the result is

$$A = \left(\frac{1}{1-\alpha}\right) - \left(\sqrt{\frac{\alpha}{1-\beta}}\right)\frac{1}{(1-\gamma)}\ E\left(\cos^{-1}\sqrt{\beta}\ ,\ \sqrt{\frac{\alpha-\beta}{\alpha(1-\beta)}}\right) \tag{A-8}$$

Consider the general solution

$$E\left(\frac{y^2}{x^2+y^2+z^2}\right) = B$$

then we wish to evaluate

$$B = \frac{1}{\pi}\int_0^{\pi}\int_0^{\pi/2} \frac{\sigma_y^2 \sin^2\phi \sin^3\phi \ d\phi d\theta}{\sigma_x^2\cos^2\phi\sin^2\theta + \sigma_y^2\sin^2\phi\sin^2\theta + \sigma_z^2\cos^2\theta}$$

Letting $\sin^2\phi = 1 - \cos^2\phi$, $\alpha = \frac{\sigma_y^2}{\sigma_x^2}$, $\beta = \frac{\sigma_z^2}{\sigma_x^2}$

$$= \frac{\alpha}{\pi}\int_0^{\pi}\sin^3\theta\, d\theta \int_0^{\pi/2} \frac{(1-\cos^2\phi)\, d\phi}{\cos^2\phi\sin^2\theta(1-\alpha) + \alpha\sin^2\theta + \beta\cos^2\theta}$$

Let $a^2 = \alpha\sin^2\theta + \beta\cos^2\theta$

$b^2 = \sin^2\theta(1-\alpha)$

$$B = -\frac{\alpha}{\pi}\int_0^{\pi}\sin^3\theta d\theta \int_0^{\pi/2}\frac{(\cos^2\phi - 1)\,d\phi}{b^2\cos^2\phi + a^2}$$

$$= -\frac{\alpha}{\pi}\int_0^{\pi}\sin^3\theta d\theta \int_0^{\pi/2}\left(\frac{1}{b^2} - \frac{\left(1 + \frac{a^2}{b^2}\right)}{b^2\cos^2\phi + a^2}\right)d\phi$$

$$= -\frac{\alpha}{\pi}\int_0^{\pi}\sin^3\theta d\theta \int_0^{\pi/2}\frac{1}{b^2}\left(1 - \frac{a^2 + b^2}{b^2\cos^2\phi + a^2}\right)d\phi$$

$$= -\frac{\alpha}{\pi}\int_0^{\pi}\sin^3\theta d\theta \frac{1}{b^2}\left[\phi - \frac{(a^2 + b^2)}{a\sqrt{a^2 + b^2}}\tan^{-1}\left(\frac{a\tan\phi}{\sqrt{a^2 + b^2}}\right)\right]_0^{\pi/2}$$

$$B = -\frac{\alpha}{2}\int_0^{\pi}\frac{\sin^3\theta}{b^2}\left[1 - \frac{a^2 + b^2}{a}\right]d\theta$$

$$= -\frac{\alpha}{2}\int_0^{\pi}\frac{\sin\theta d\theta}{(1-\alpha)} + \frac{\alpha}{2(1-\alpha)}\int_0^{\pi}\frac{\sqrt{\sin^2\theta + \beta\cos^2\theta}\,\sin\theta d\theta}{\sqrt{\alpha\sin^2\theta + \beta\cos^2\theta}}$$

letting $\sin^2\theta = 1 - \cos^2\theta$, integrating first term and re-arranging

$$= \frac{-\alpha}{1-\alpha} + \frac{\sqrt{\alpha}}{2(1-\alpha)}\int_0^{\pi}\frac{\sqrt{1 - (1-\beta)\cos^2\theta}}{\sqrt{1 - \frac{(\alpha-\beta)}{\alpha}\cos^2\theta}}\sin\theta d\theta$$

let $x = \sqrt{1-\beta}\cos\theta$ $\qquad dx = -\sqrt{1-\beta}\sin\theta d\theta$

$$B = \frac{-\alpha}{1-\alpha} - \frac{-\sqrt{\alpha}}{2(1-\alpha)\sqrt{1-\beta}}\int_{\sqrt{1-\beta}}^{-\sqrt{1-\beta}}\frac{\sqrt{1 - x^2}}{\sqrt{1 - \frac{(\alpha-\beta)}{\alpha(1-\beta)}x^2}}dx$$

Multiply numerator and denominator of integrand by $\sqrt{1-x^2}$ change limits and multiply by 2

$$B = \frac{-\alpha}{1-\alpha} + \frac{\sqrt{\alpha}}{(1-\alpha)\sqrt{1-\beta}} \int_0^{\sqrt{1-\beta}} \frac{(1-x^2)}{\sqrt{1-k^2x^2}\ \sqrt{1-x^2}}\, dx$$

Let numerator $= 1 + \frac{1}{k^2}\left(1 - k^2x^2\right) - \frac{1}{k^2}$

where $k^2 = \left(\frac{\alpha-\beta}{\alpha(1-\beta)}\right)$

then

$$B = -\frac{\alpha}{1-\alpha} + \frac{\sqrt{\alpha}}{(1-\alpha)\sqrt{1-\beta}} \int_0^{\sqrt{1-\beta}} \left(\frac{\left(\frac{k^2-1}{k^2}\right)}{\sqrt{1-k^2x^2}\sqrt{1-x^2}} + \frac{1}{k^2} \frac{\sqrt{1-k^2x^2}}{\sqrt{1-x^2}} \right) dx$$

$$= -\frac{\alpha}{1-\alpha} + \frac{\sqrt{\alpha}}{(1-\alpha)\sqrt{1-\beta}} \frac{\beta(\alpha-1)}{(\alpha-\beta)} F\left(\cos^{-1}\sqrt{\beta}, \sqrt{\frac{\alpha-\beta}{\alpha(1-\beta)}}\right)$$

$$+ \frac{\sqrt{\alpha}}{(1-\alpha)\sqrt{1-\beta}} \frac{\alpha(1-\beta)}{(\alpha-\beta)} E\left(\cos^{-1}\sqrt{\beta}, \frac{\alpha-\beta}{\alpha(1-\beta)}\right)$$

$$= -\frac{\alpha}{1-\alpha} - \frac{\beta\sqrt{\alpha}}{\sqrt{1-\beta}(\alpha-\beta)} F\left(\cos^{-1}\sqrt{\beta}, \sqrt{\frac{\alpha-\beta}{\alpha(1-\beta)}}\right) + \frac{\alpha^{3/2}\sqrt{1-\beta}}{(1-\alpha)(\alpha-\beta)} E\left(\cos^{-1}\sqrt{\beta}, \sqrt{\frac{\alpha-\beta}{\alpha(1-\beta)}}\right)$$

Consider the general solution for

$$C = E\left(\frac{z^2}{x^2 + y^2 + z^2}\right)$$

We must evaluate an expression similar to that of the previous case

$$C = \frac{\beta}{\pi} \int_0^{\pi} \int_0^{\pi/2} \frac{\cos^2\theta \sin\theta d\theta \; d\phi}{\cos^2\phi \sin^2\theta(1-\alpha) + \alpha\sin^2\theta + \beta\cos^2\theta}$$

Let

$$a^2 = \alpha \sin^2\theta + \beta^2\cos^2\theta$$

$$b^2 = \sin^2\theta(1-\alpha)$$

then the ϕ integral may be directly integrated giving

$$C = \frac{\beta}{\pi} \int_0^{\pi} \cos^2\theta\sin\theta d\theta \left[\frac{1}{a\sqrt{a^2 + b^2}} \tan^{-1}\left(\frac{a \tan \phi}{\sqrt{a^2 + b^2}} \right) \right]_0^{\pi/2}$$

$$= \frac{\beta}{2} \int_0^{\pi} \frac{\cos^2\theta \sin\theta d\theta}{\sqrt{\alpha\sin^2\theta + \beta\cos^2\theta}\sqrt{\sin^2\theta + \beta\cos^2\theta}}$$

$$= \frac{\beta}{2} \int_0^{\pi} \frac{\cos^2\theta \sin\theta d\theta}{\sqrt{\alpha - (\alpha-\beta)\cos^2\theta}\sqrt{1 - (1-\beta)\cos^2\theta}}$$

$$\frac{-\beta}{2\sqrt{1-\beta}\sqrt{\alpha}} \int_0^{\pi} \frac{\cos^2\theta \left(-\sqrt{1-\beta}\sin\theta d\theta\right)}{\sqrt{1 - \left(\frac{\alpha-\beta}{\alpha}\right)\cos^2\theta}\sqrt{1 - (1-\beta)\cos^2\theta}}$$

let $x = \sqrt{(1-\beta)}\cos\theta \qquad dx = -\sqrt{1-\beta}\sin\theta d\theta$

then

$$C = \frac{-\beta}{2\sqrt{1-\beta}\sqrt{\alpha}} \int_{\sqrt{1-\beta}}^{-\sqrt{1-\beta}} \frac{\frac{x^2}{(1-\beta)} \; dx}{\sqrt{1 - \left(\frac{\alpha-\beta}{\alpha(1-\beta)}\right)x^2}\sqrt{1 - x^2}}$$

let $k^2 = \left(\frac{\alpha-\beta}{\alpha(1-\beta)}\right)$

Changing limits as before and writing numerator in a different form

$$C = \frac{-\beta}{\sqrt{\alpha}\sqrt{1-\beta}} \left(\frac{\alpha}{\alpha-\beta}\right) \int_0^{\sqrt{1-\beta}} \frac{(1 - k^2x^2 - 1)\, dx}{\sqrt{1 - k^2x^2}\sqrt{1 - x^2}}$$

$$= \frac{-\beta}{\sqrt{1-\beta}} \frac{\sqrt{\alpha}}{(\alpha-\beta)} \int_0^{\sqrt{1-\beta}} \left(\frac{\sqrt{1 - k^2x^2}}{\sqrt{1 - x^2}} - \frac{1}{\sqrt{1 - k^2x^2}\sqrt{1 - x^2}} \right) dx$$

$$= \frac{-\beta}{\sqrt{1-\beta}} \frac{\sqrt{\alpha}}{(\alpha-\beta)} \left[E\left(\cos^{-1}\sqrt{\beta},\ \sqrt{\frac{\alpha-\beta}{\alpha(1-\beta)}}\right) - F\left(\cos^{-1}\sqrt{\beta}\ \sqrt{\frac{\alpha-\beta}{\alpha(1-\beta)}}\right) \right]$$

The quantities B and C for the two special cases of $\alpha = 1$, and $\alpha = \beta$ are all that remains to be evaluated.

From the previous derivations

$$B = \frac{\alpha}{\pi} \int_0^{\pi} \int_0^{\pi/2} \frac{(\sin^2\phi)(\sin^3\theta)d\theta d\phi}{\cos^2\phi \sin^2\theta(1-\alpha) + \alpha(\sin^2\theta + \beta\cos^2\theta}$$

and

$$C = \frac{\beta}{\pi} \int_0^{\pi} \int_0^{\pi/2} \frac{\cos^2\theta\sin\theta d\theta d\phi}{\cos^2\phi \sin^2\theta(1-\alpha) + \alpha\sin^2\theta + \beta\cos^2\theta}$$

Consider B for $\alpha = 1$

$$B = \frac{1}{\pi} \int_0^{\pi} \int_0^{\pi/2} \frac{\sin^2\phi \sin^3\theta \, d\theta d\phi}{\sin^2\theta + \beta\cos^2\theta}$$

$$= \frac{1}{\pi} \int_0^{\pi} \frac{\sin^3\theta d\theta}{\sin^2\theta + \beta\cos^2\theta} \left[\frac{\phi}{2} - \frac{\sin 2x}{4} \right]_0^{\pi/2}$$

$$= \frac{1}{4} \int_0^{\pi} \frac{\sin^3\theta d\theta}{\sin^2\theta + \beta\cos^2\theta} = \frac{1}{4} \int_0^{\pi} \frac{\sin^3\theta d\theta}{\cos^2\theta(\beta-1) + 1}$$

This has been previously solved (see material following equation (A-4)) to give

$$B = \frac{1}{2(1-\beta)} - \frac{\beta}{4(1-\beta)^{3/2}} \ln\left(\frac{1+\sqrt{1-\beta}}{1-\sqrt{1-\beta}}\right)$$

Consider B for $\alpha = \beta$

then

$$B = \frac{\alpha}{\pi} \int_0^{\pi} \int_0^{\pi/2} \frac{\sin^2\phi \sin^3\theta \, d\phi d\theta}{\cos^2\phi \sin^2\theta(1-\alpha) + \alpha}$$

$$= -\frac{1}{\pi} \int_0^{\pi} \sin^3\theta d\theta \int_0^{\pi/2} \frac{(\cos^2\phi - 1) \, d\phi}{\cos^2\phi \sin^2\theta\left(\frac{1-\alpha}{\alpha}\right) + 1}$$

let $b^2 = \sin^2\theta\left(\frac{1-\alpha}{\alpha}\right)$

$$B = -\frac{1}{\pi}\int_0^{\pi}\sin^3\theta d\theta \int_0^{\pi/2}\left[\frac{1}{b^2}\right]\left[1 - \frac{(b^2+1)}{\cos^2\phi\, b^2 + 1}\right] d\phi$$

$$= -\frac{1}{\pi}\int_0^{\pi}\frac{\sin\theta d\theta}{\left(\frac{1-\alpha}{\alpha}\right)}\left[\phi - \frac{b^2+1}{\sqrt{b^2+1}}\tan^{-1}\left(\frac{\tan\phi}{\sqrt{b^2+1}}\right)\right]_0^{\pi/2}$$

$$= -\frac{1}{2}\left(\frac{\alpha}{1-\alpha}\right)\int_0^{\pi}\sin\theta d\theta\left[1 - \sqrt{\sin^2\theta\left(\frac{1-\alpha}{\alpha}\right) + 1}\right]$$

$$= \frac{\alpha}{2(1-\alpha)}\left[\cos\theta\right]_0^{\pi} - \frac{\alpha}{2(1-\alpha)}\int_0^{\pi}\sqrt{\frac{1}{\alpha} - \left(\frac{1-\alpha}{\alpha}\right)\cos^2\theta}\,(-\sin\theta d\theta)$$

letting $x = \sqrt{1-\alpha}\cos\theta$

$$= \frac{-\alpha}{1-\alpha} - \frac{\sqrt{\alpha}}{2(1-\alpha)^{3/2}}\int_{\sqrt{1-\alpha}}^{-\sqrt{1-\alpha}}\sqrt{1-x^2}\,dx$$

$$= \frac{-\alpha}{1-\alpha} - \frac{\sqrt{\alpha}}{2(1-\alpha)^{3/2}}\left[\frac{x}{2}\sqrt{1-x^2} + \frac{1}{2}\sin^{-1}x\right]_{\sqrt{1-\alpha}}^{\sqrt{1-\alpha}}$$

$$= -\frac{\alpha}{1-\alpha} + \frac{\sqrt{\alpha}}{2(1-\alpha)^{3/2}}\left[\sqrt{1-\alpha}\sqrt{\alpha} + \sin^{-1}\sqrt{1-\alpha}\right]$$

$$= -\frac{\alpha}{2(1-\alpha)} + \frac{\sqrt{\alpha}}{2(1-\alpha)^{3/2}}\tan^{-1}\left(\sqrt{\frac{1-\alpha}{\alpha}}\right)$$

Consider the solution for C when $\alpha = 1$

$$C = \frac{\beta}{2} \int_0^{\pi} \frac{\cos^2\theta \sin\theta d\theta}{\sin^2\theta + \beta\cos^2\theta} = \frac{\beta}{2} \int_0^{\pi} \frac{\cos^2\theta \sin\theta d\theta}{(1-\beta)\cos^2\theta - 1}$$

$$= \frac{-\beta}{2(1-\beta)} \int_0^{\pi} \left(1 + \frac{1}{(1-\beta)\cos^2\theta - 1}\right) \sin\theta d\theta$$

letting $x = \sqrt{1-\beta}\cos\theta$ and integrating out the first term

$$= \frac{-\beta}{(1-\beta)} - \frac{\beta}{2(1-\beta)^{3/2}} \int_{\sqrt{1-\beta}}^{\sqrt{1-\beta}} \frac{dx}{1-x^2}$$

$$= \frac{-\beta}{1-\beta} - \frac{\beta}{2(1-\beta)^{3/2}} \left[\frac{1}{2} \ln \left| \frac{1+x}{1-x} \right| \right]_{\sqrt{1-\beta}}^{-\sqrt{1-\beta}}$$

$$= \frac{-\beta}{1-\beta} + \frac{\beta}{2(1-\beta)^{3/2}} \ln \left(\frac{1+\sqrt{1-\beta}}{1-\sqrt{1-\beta}} \right)$$

Consider solution for C when $\beta = \alpha$

then

$$C = \frac{\alpha}{\pi} \int_0^{\pi} \int_0^{\pi/2} \frac{\cos^2\theta \sin\theta d\theta \, d\phi}{\cos^2\phi \sin^2\theta(1-\alpha) + \alpha}$$

$a^2 = \alpha$

$b^2 = \sin^2\theta(1-\alpha)$

$$C = \frac{\alpha}{\pi} \int_0^{\pi} \cos^2\theta \sin\theta d\theta \int_0^{\pi/2} \frac{d\phi}{\cos^2\phi(b^2) + a^2}$$

$$= \frac{\alpha}{\pi} \int_0^{\pi} \cos^2\theta \sin\theta d\theta \left[\frac{1}{a\sqrt{a^2 + b^2}} \tan^{-1}\left(\frac{a \tan \phi}{\sqrt{a^2 + b^2}} \right) \right]_0^{\pi/2}$$

$$= \frac{\sqrt{\alpha}}{2} \int_0^{\pi} \frac{\cos^2\theta \sin\theta \, d\theta}{\sqrt{\alpha + \sin^2\theta(1-\alpha)}}$$

$$= \frac{\sqrt{\alpha}}{2} \int_0^{\pi} \frac{\cos^2\theta \sin\theta \, d\theta}{\sqrt{1 - \cos^2\theta(1-\alpha)}}$$

let $x = \sqrt{1-\alpha}\cos\theta \quad dx = -\sqrt{1-\alpha} \sin\theta \, d\theta$

$$C = -\frac{\sqrt{\alpha}}{2(1-\alpha)^{3/2}} \int_{\sqrt{1-\alpha}}^{-\sqrt{1-\alpha}} \frac{x^2 \, dx}{\sqrt{1 - x^2}}$$

$$= \frac{\sqrt{\alpha}}{2(1-\alpha)^{3/2}} \left[-\frac{x\sqrt{1 - x^2}}{2} + \frac{1}{2} \sin^{-1} x \right]_{\sqrt{1-\alpha}}^{\sqrt{1-\alpha}}$$

$$= \frac{\sqrt{\alpha}}{2(1-\alpha)^{3/2}} \left[\sqrt{1-\alpha}\sqrt{\alpha} - \sin^{-1}\sqrt{1-\alpha} \right]$$

$$= \frac{-\alpha}{2(1-\alpha)} + \frac{\sqrt{\alpha}}{2(1-\alpha)^{3/2}} \tan^{-1}\left(\frac{\sqrt{1-\alpha}}{\sqrt{\alpha}} \right)$$

SUMMARY OF SOLUTIONS

$$\left(\frac{\sigma_y}{\sigma_x}\right)^2 = d, \qquad \left(\frac{\sigma_z}{\sigma_x}\right)^2 = \beta$$

$$A = E\left(\frac{x^2}{x^2 + y^2 + z^2}\right) \qquad B = E\left(\frac{y^2}{x^2 + y^2 + z^2}\right) \qquad C = E\left(\frac{z^2}{x^2 + y^2 + z^2}\right)$$

Case 1 $\alpha = \beta = 1$

Solution $A = B = C = {}^1/_3$

Case 2 $\alpha = 1, \quad \beta < 1$

$$A = B = \frac{1}{2(1-\beta)} - \frac{\beta}{4\,(1-\beta)^{3/2}} \ln\left(\frac{1 + \sqrt{1-\beta}}{1 - \sqrt{1-\beta}}\right)$$

$$C = -\frac{\beta}{(1-\beta)} + \frac{\beta}{2(1-\beta)^{3/2}} \ln\left(\frac{1 + \sqrt{1-\beta}}{1 - \sqrt{1-\beta}}\right)$$

$$= 1 - 2A$$

Case 3 $\alpha = \beta < 1$

$$A = \frac{1}{1-\alpha} - \frac{\sqrt{\alpha}}{(1-\alpha)^{3/2}} \tan^{-1}\sqrt{\frac{1-\alpha}{\alpha}}$$

$$B = C = \frac{-\alpha}{2(1-\alpha)} + \frac{\sqrt{\alpha}}{2(1-\alpha)^{3/2}} \tan^{-1}\sqrt{\frac{1-\alpha}{\alpha}}$$

$$= \frac{1-A}{2}$$

Case 4 $\quad 1 > \alpha > \beta$

with $x = \cos^{-1}\sqrt{\beta}$, $k = \sqrt{\frac{\alpha-\beta}{\alpha(1-\beta)}}$

$$A = \frac{1}{1-\alpha} - \left(\sqrt{\frac{\alpha}{1-\beta}}\right)\left(\frac{1}{1-\alpha}\right)E\left(x,k\right)$$

$$B = \frac{-\alpha}{1-\alpha} - \frac{\beta\sqrt{\alpha}}{\sqrt{1-\beta}(\alpha-\beta)}F(x.k) + \frac{\alpha^{3/2}\sqrt{1-\beta}}{(1-\alpha)(\alpha-\beta)}E(x,k)$$

$$C = \frac{-\beta}{\sqrt{1-\beta}} \frac{\sqrt{\alpha}}{\alpha-\beta}\left[E(x,k) - F(x,k)\right]$$

$$C = 1 - A - B$$

One should note that

$$A + B + C = E\left(\frac{x^2}{x^2+y^2+z^2}\right) + E\left(\frac{y^2}{x^2+y^2+z^2}\right) + E\left(\frac{z^2}{x^2+y^2+z^2}\right)$$

$$= \int_{-\infty}^{+\infty}\int_{-\infty}^{+\infty}\int_{-\infty}^{+\infty} p(x,y,z)\, dxdydz$$

$$= 1 \quad \text{by definition}$$

Thus one may reduce the number of functions which must be evaluated to compute $\lceil \rceil_v$

APPENDIX B

MEASUREMENT GRADIENT

This appendix presents derivations of the gradient of the measurements, H, with respect to the vehicle state. The measurements which are considered are those which were used in the study. They include range, range-rate, azimuth, elevation, theodolite, sextant and subtended angle.

B.1 RANGE MEASUREMENT (FIGURE B-1)

$$\text{RANGE} = |R| = r = (R.R)^{1/2} = (R^T R)^{1/2} \tag{B-1}$$

The gradient is: $H_r = (\nabla_x r;\ \nabla_{\dot{x}} r)$ (B-2)

$$\nabla_x r = \nabla_x (R^T R)^{1/2} = \frac{R^T \nabla_x R}{|R|} \tag{B-3}$$

Since $\nabla_x R = I$ $\quad \nabla_x r = \hat{R}^T$ (B-4)

$$\nabla_{\dot{x}} r = \frac{R^T \nabla_{\dot{x}} R}{|R|} \tag{B-5}$$

Since $\nabla_{\dot{x}} R = 0$ $\quad \nabla_{\dot{x}} r = 0$ (B-6)

Therefore $H_r = (\hat{R}^T\ ;\ 0)$ (B-7)

B.2 RANGE-RATE MEASUREMENT (FIGURE B-1)

$$\text{RANGE RATE} = \dot{r} = \hat{R} \cdot \dot{x} = \hat{R}^T \dot{x} \tag{B-8}$$

The gradient is: $H_{\dot{r}} = (\nabla_x \dot{r}\ ;\ \nabla_{\dot{x}} \dot{r})$ (B-9)

$$\nabla_x \dot{r} = \nabla_x (\hat{R}^T \dot{x}) = \hat{R}^T \nabla_x \dot{x} + \dot{x}^T \nabla_x \hat{R} \tag{B-10}$$

Since $\nabla_x \dot{x} = 0$ and $\nabla_x \hat{R} = \frac{1}{|R|}(I - \hat{R}\hat{R}^T)$ (B-11)

$$\nabla_x \dot{r} = \frac{\dot{x}^T}{|R|}(I - \hat{R}\hat{R}^T) \quad \text{(B-12)}$$

$$\nabla_{\dot{x}} r = \hat{R}^T \nabla_{\dot{x}} \dot{x} + \dot{x}^T \nabla_{\dot{x}} \hat{R} \quad \text{(B-13)}$$

Since $\nabla_{\dot{x}} \dot{x} = I$ and $\nabla_{\dot{x}} \hat{R} = 0$ (B-14)

$$\nabla_{\dot{x}} \dot{r} = \hat{R}^T \quad \text{(B-15)}$$

Therefore $H_{\dot{r}} = \left(\frac{\dot{x}^T}{|R|}(I - \hat{R}\hat{R}^T) \; ; \; \hat{R}^T \right)$ (B-16)

B.3 SEXTANT STAR-PLANET ANGLE MEASUREMENT (FIGURE B-2)

$$\cos\alpha = \hat{S}\cdot\hat{P} = \hat{S}^T\hat{P} \quad \text{(B-17)}$$

The gradient is $H_\alpha = (\nabla_x \alpha \; ; \; \nabla_{\dot{x}} \alpha)$ (B-18)

$$\nabla_x \cos\alpha = \nabla_x (\hat{S}^T\hat{P}) \quad \text{(B-19)}$$

$$-\sin\alpha \, \nabla_x \alpha = \hat{S}^T \nabla_x \hat{P} + \hat{P}^T \nabla_x \hat{S} \quad \text{(B-20)}$$

Since $\nabla_x \hat{P} = \frac{1}{|P|}\left[I - \hat{P}\hat{P}^T\right]$ and $\nabla_x \hat{S} = 0$ (B-21)

$$\nabla_x \alpha = -\frac{\hat{S}^T}{|P|\sin\alpha}\left[I - \hat{P}\hat{P}^T\right] = -\frac{1}{|P|}\left[\frac{\hat{P}\otimes\hat{S}}{|\hat{P}\otimes\hat{S}|}\otimes\hat{P}\right] \quad \text{(B-22)}$$

$$\nabla_{\dot{x}} \alpha = 0 \quad \text{(B-23)}$$

Therefore $H_\alpha = \left[-\frac{1}{|P|}\left(\frac{\hat{P}\otimes\hat{S}}{|\hat{P}\otimes\hat{S}|}\otimes\hat{P}\right) \; ; \; 0 \right]$ (B-24)

This result is of interest because it can be extended to represent any angular measurement with the proper definition of the P and $\hat{S}$ vectors.

B.4 AZIMUTH MEASUREMENT (FIGURE B-3)

Making the substitution of the vectors shown in figure B-3 into Equation (B-24) yields:

$$H_{AZ} = \left[-\frac{1}{|R'|} \left(\frac{\hat{R}' \otimes \hat{N}}{|\hat{R} \otimes \hat{N}|} \right) \otimes \hat{R}' \quad ; \quad 0 \right] \tag{B-25}$$

B.5 ELEVATION MEASUREMENT (FIGURE B-3)

Making the vector substitutions in (B-24) yields:

$$H_{EL} = \left[-\frac{1}{|R|} \left(\frac{\hat{R} \otimes \hat{R}'}{|\hat{R} \otimes \hat{R}'|} \otimes \hat{R} \right) ; \quad 0 \right] \tag{B-26}$$

The RA and DEC measurements with a theodolite have the same form of gradient as (B-25) and (B-26) with the north reference direction and the local horizontal plane (Figure B-3) replaced by an inertial reference direction and the platform reference plane.

B.6 SUBTENDED ANGLE RANGE MEASUREMENT (FIGURE B-4)

$$\sin \frac{\beta}{2} = \frac{RAD}{(R^T R)^{1/2}} \tag{B-27}$$

The gradient is $H_\beta = (\nabla_x \beta ; \nabla_{\dot{x}} \beta)$

$$\nabla_x \sin \frac{\beta}{2} = \nabla_x \frac{RAD}{(R^T R)^{1/2}} \tag{B-28}$$

$$1/2 \cos \frac{\beta}{2} \nabla_x \beta = \frac{RAD \hat{R}^T}{|R|^2} \quad \text{(B-29)}$$

$$\nabla_x \beta = \frac{2 \operatorname{Tan} \beta/2}{|R|} \hat{R}^T \quad \text{(B-30)}$$

$$\nabla_{\dot{x}} \beta = 0 \quad \text{(B-31)}$$

Therefore

$$H_\beta = \left[\frac{2 \operatorname{Tan} \beta/2}{|R|} \hat{R}^T \quad 0 \right] \quad \text{(B-32)}$$

Figure B-1 Tracker-Vehicle Geometry

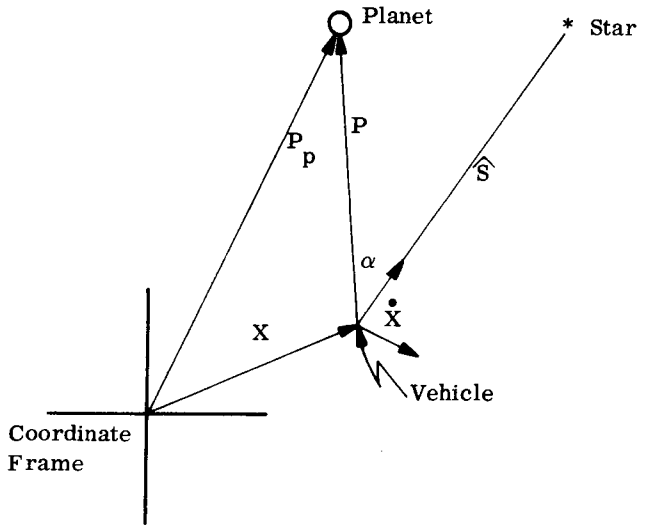

$P_p = X + P$

$P = P_p - X$

$\hat{S}$ = Unit Vector in Direction of Star

P = Vector from Vehicle to Planet

P_p = Position of Planet

X = Vehicle Position

$\dot{X}$ = Vehicle Velocity

Figure B-2 Sextant Measurement Geometry

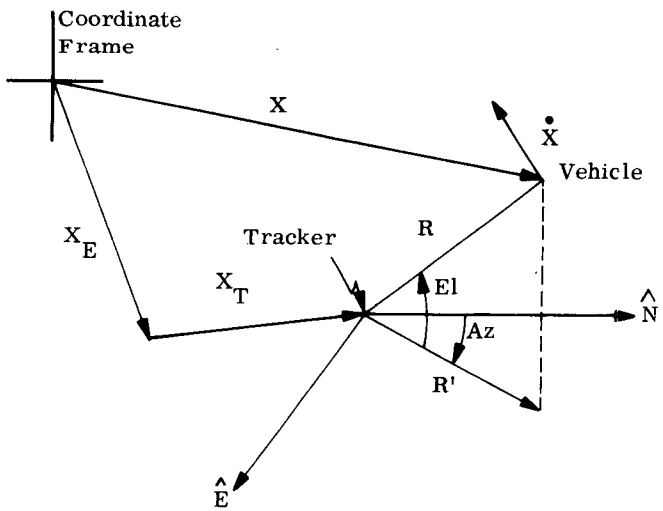

$X = X_E + X_T + R$

$R = X - X_E - X_T$

$\hat{N}$ = Unit North Vector at Tracker

$\hat{E}$ = Unit East Vector at Tracker

X = Vehicle Position

$\dot{X}$ = Vehicle Velocity

X_E = Position of Earth

X_T = Position of Tracker

R = Position of Vehicle WRT Tracker

R' = Projection of R into Tracker Horizonal Plane

Figure B-3 AZ-EL Measurement Geometry

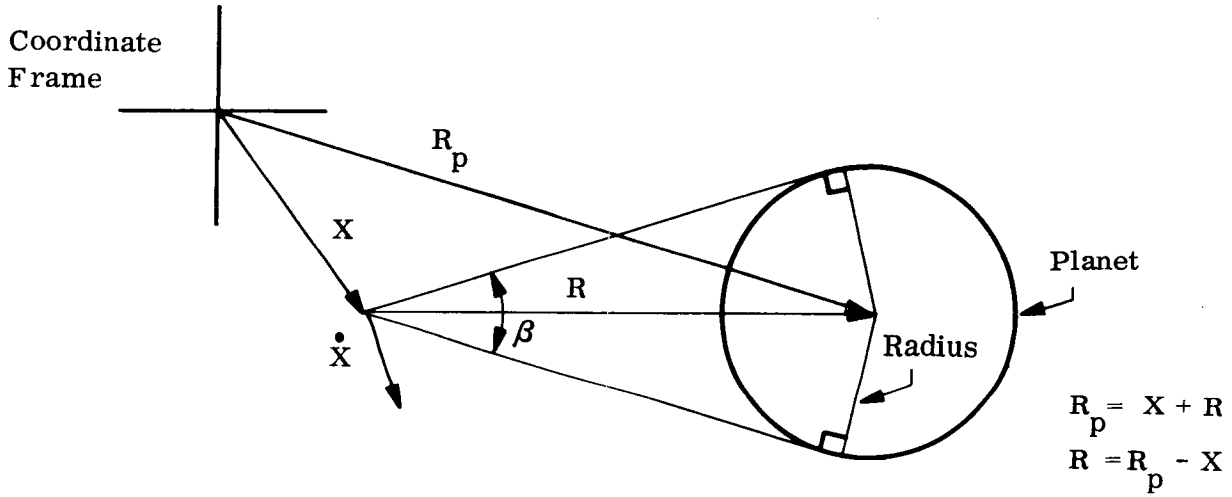

X = Position of Vehicle

$\dot{X}$ = Velocity of Vehicle

R_p = Position of Planet

R = Position of Planet WRT Vehicle

Figure B-4 Subtended Angle Geometry

APPENDIX C

INTERPLANETARY TRAJECTORIES

This appendix presents a description of the four interplanetary trajectories which have been used in this study. The trajectories are: (1) Nominal high-energy Earth-Mars, (2) Direct-return Mars-Earth, (3) Low-energy Earth-Mars, and (4) Venus Swingby return. The data which are shown are in Earth equator and equinox of 1950 coordinates. Ecliptic projections of the trajectories are shown in Figures C-1 through C-4.

C.1 NOMINAL HIGH-ENERGY EARTH-MARS TRAJECTORY

This trajectory (Figure C-1) has a launch date of 10 February 1975, 1 hours, 32 minutes, 28.629 seconds, with a park orbit length of 1736.518 seconds.

	Earth-Centered Conic (Injection)	Sun-Centered Conic (Patch)	Mars-Centered Conic (Patch)
Date	10 February 1975	10 February 1975	10 October 1975
Fractional Date	$2^h1^m25.147^s$	$23^h43.^m24.812^s$	$21^h35^m48.596^s$
x (km)	-0.51940523+04	-0.11441701+09	-0.44850600+06
y	-0.33714096+04	0.84261958+08	0.27226599+06
z	-0.21758862+04	0.36545250+08	0.20978100+06
$\dot{x}$ (km/sec)	0.97623321+01	-0.95000336+01	0.43146753+01
$\dot{y}$	-0.11540529+02	-0.27582250+02	-0.26728354+01
$\dot{z}$	-0.5422576+01	-0.1185094+02	-0.20487671+01

The trajectory has a radius of closest approach at Mars of 38600 km (500 km altitude). It passes Mars on the Sun light side near the ecliptic plane. The flight time is 235 days.

C.2 DIRECT-RETURN MARS-EARTH TRAJECTORY

This trajectory (Figure C-2) is the return trajectory which leaves Mars 40 days after the arrival of the nominal high-energy trajectory.

	Mars-Centered Conic (Injection)	Sun-Centered Conic (Patch)	Earth-Centered Conic (Patch)
Date	12 November 1975	13 November 1975	3 September 1976
Fractional Date	$10^h47^m26.241^s$	$19^h41^m18.707^s$	$5^h4^m57.839^s$
x (km)	-0.34075300+04	0.91568038+08	-0.88066700+06
y	-0.18867350+04	0.18887866+09	0.27005599+06
z	-0.66730232+03	0.84164875+08	0.84061749+05
$\dot{x}$ (km/sec)	0.32159301+01	-0.17725844+02	0.99308927+01
$\dot{y}$	-0.48195511+01	0.80037536+01	-0.30949005+01
$\dot{z}$	-0.32001703+01	0.3498172+01	-0.10445975+01

The trajectory has a perigee radius of 6442 km (76 km altitude). Perigee is at a latitude of -59.98 degrees and longitude of 223.06 degrees. The flight time is 296 days 18 hours.

C.3 LOW-ENERGY EARTH-MARS TRAJECTORY

This trajectory (Figure C-3) has a launch date of 16 September 1975, 15 hours, 43 minutes, 45.774 seconds with a park orbit length of 2108.507 seconds.

	Earth-Centered Conic (Injection)	Sun-Centered Conic (Patch)	Mars-Centered Conic (Patch)
Date	16 September 1975	18 September 1975	13 March 1976
Fractional Date	$16^h18^m54.280^s$	$22^h25^m58.745^s$	$8^h52^m50.544^s$
x (km)	0.29018053+04	0.14996085+09	0.16526200+06
y	-0.36250747+04	-0.11305100+08	0.51892199+06
z	-0.46386877+04	-0.45878474+07	-0.15034200+06
$\dot{x}$ (km/sec)	0.10323948+02	0.31401292+01	-0.14043786+01
$\dot{y}$	0.54134400+01	0.30343401+02	0.45550116+01
$\dot{z}$	0.22277772+01	0.14721659+02	0.12999684+01

The trajectory has a radius of closest approach at Mars of 3866 km (506 km altitude). It passes Mars on the sun light side near the ecliptic plane. The flight time is 180 days.

C.4 VENUS SWINGBY RETURN TRAJECTORY

This trajectory (Figure C-4) is the return trajectory which uses Venus as an intermediate body. The trajectory is presented in two parts -- Mars-Venus and Venus-Earth.

MARS-VENUS TRAJECTORY

	Mars-Centered Conic (Injection)	Sun-Centered Conic (Patch)	Venus-Centered Conic (Patch)
Date	17 March 1976	18 March 1976	2 October 1976
Fractional Date	$1^h49^m57.120^s$	$9^h34^m43.369^m$	$10^h11^m6.046^s$
x (km)	0.17969313+03	-0.14681165+09	-0.37369350+06
y	-0.35024405+04	0.17784405+09	-0.43777800+06
z	-0.16125196+04	0.85612638+08	-0.21971449+06
$\dot{x}$ (km/sec)	0.67743930+01	-0.13848957+02	0.66815886+01
$\dot{y}$	0.17013941-01	-0.10114000+02	0.75653162+01
$\dot{z}$	0.32651396-00	-0.39254735+01	0.38212271+01

The trajectory has a radius of closest approach to Venus of 7478Km. It passes the planet near the ecliptic on the dark side. The trajectory has a flight time of 200 days.

VENUS-EARTH TRAJECTORY

	Venus-Centered Conic (Closest Approach)	Sun-Centered Conic (Patch)	Earth-Centered Conic (Patch)
Date	3 October 1976	3 October 1976	9 March 1977
Fractional Date	$1^h50^m10.583^s$	$17^h24^m48.435^s$	$20^h53^m6.529^s$
x (km)	0.68684836+04	-0.18490072+08	-0.58701999+05
y	-0.29227867+04	-0.97547584+08	-0.84728450+06
z	-0.44976045+03	-0.42663465+08	-0.36641487+06
$\dot{x}$ (km/sec)	0.55811975+01	0.35807143+02	0.35199869-00
$\dot{y}$	0.10396058+02	0.40184393+01	0.45016639+01
$\dot{z}$	0.80025092+01	0.17794444+01	0.18674508+01

The trajectory has a perigee radius of 6402 km. Perigee is at a latitude of -16.2 degrees and a longitude of 270 degrees. The flight time is 160 days.

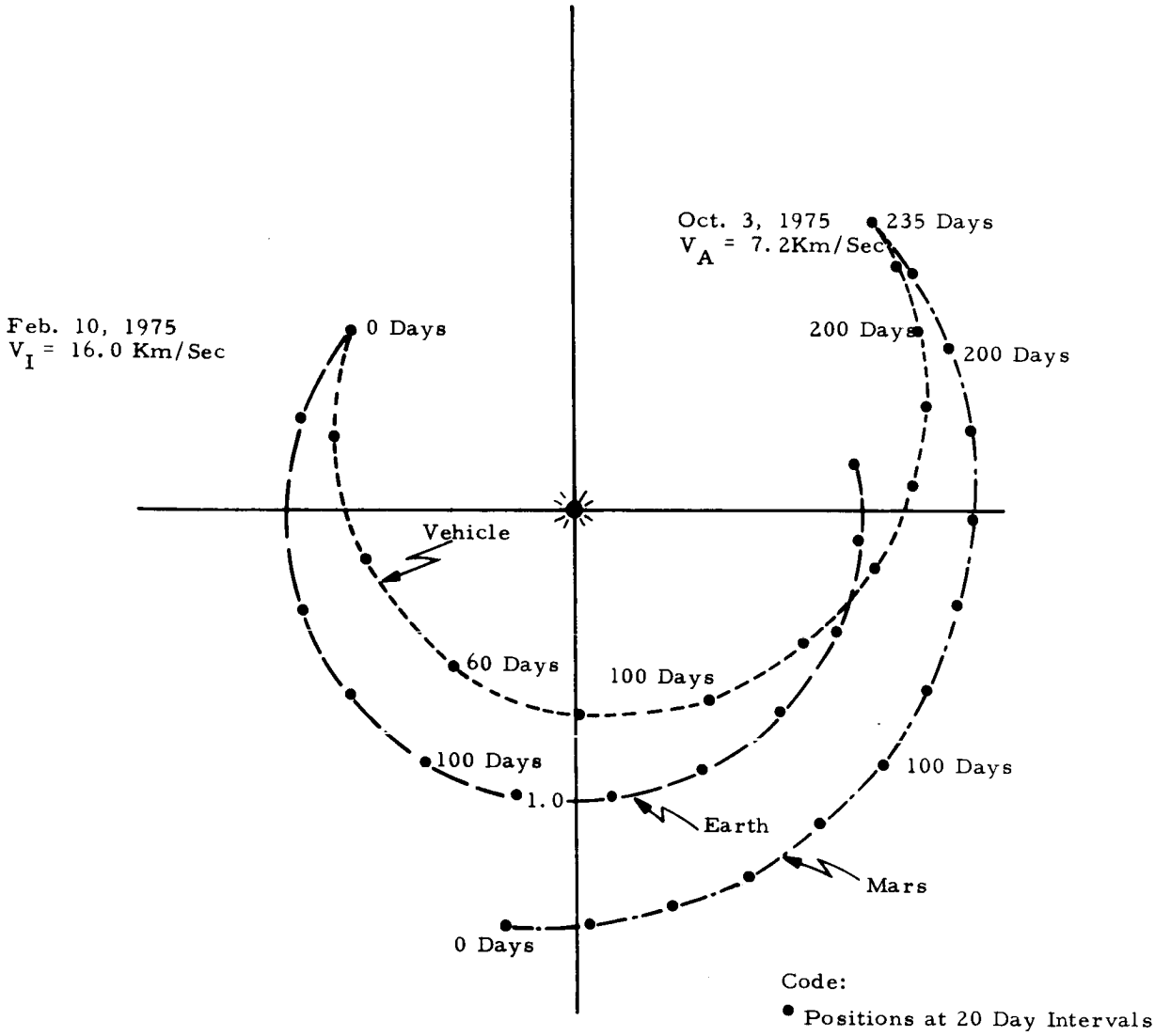

Figure C-1 Ecliptic Projection, Earth-Mars Trajectory

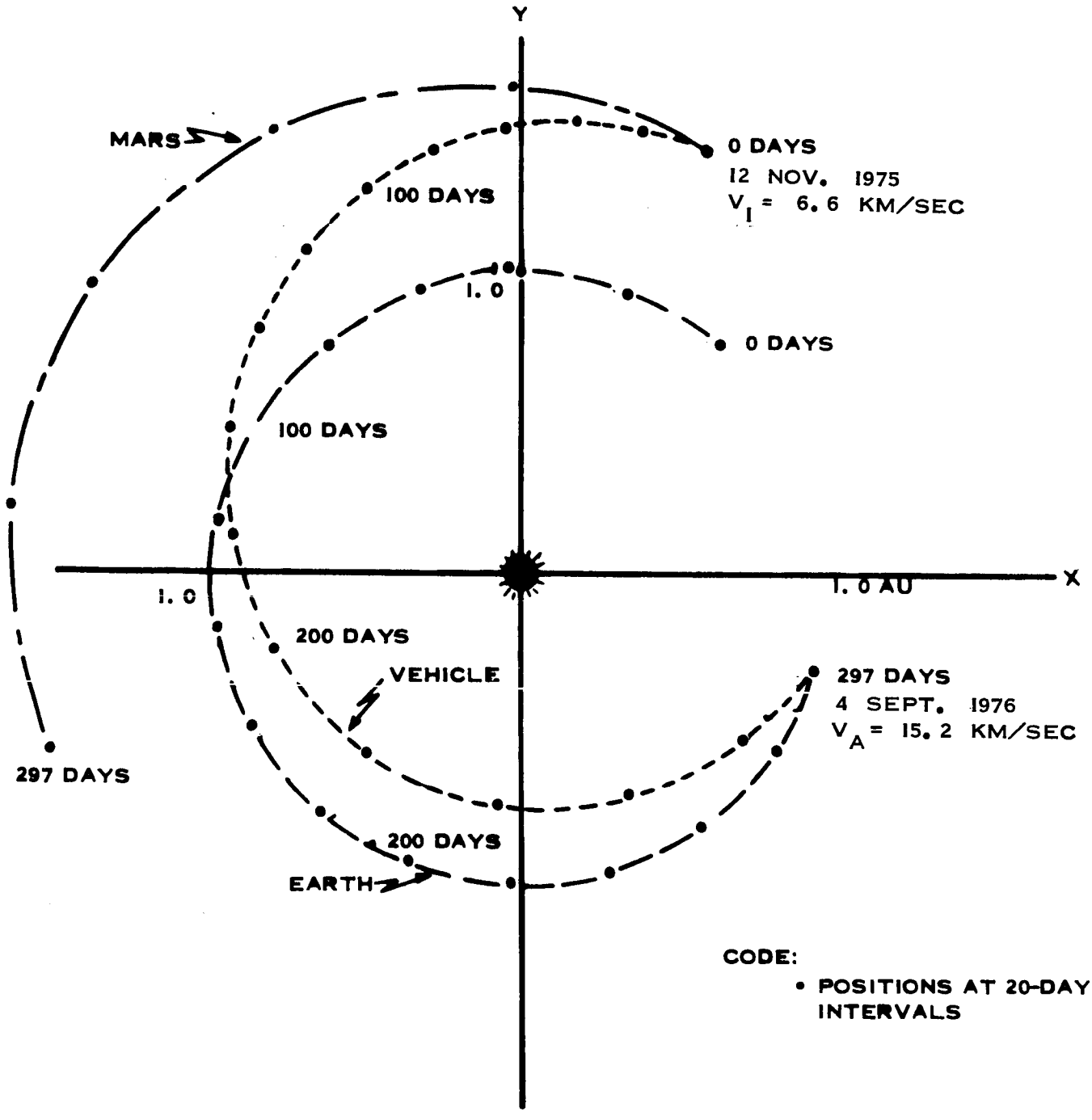

Figure C-2 Ecliptic Projection, Mars-Earth Trajectory

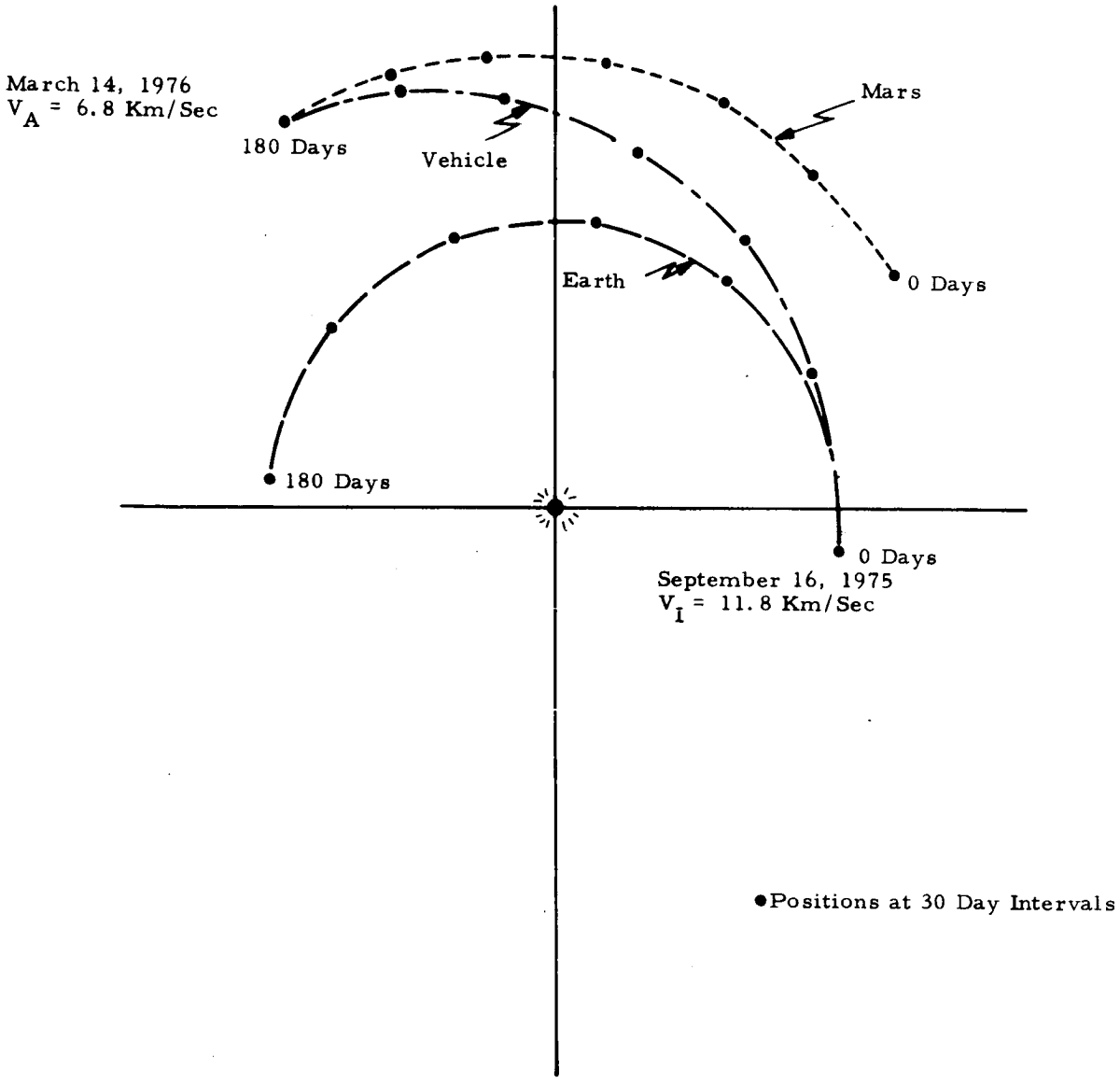

Figure C-3 Ecliptic Projection, Earth-Mars Trajectory

Ecliptic of Date
Coordinates

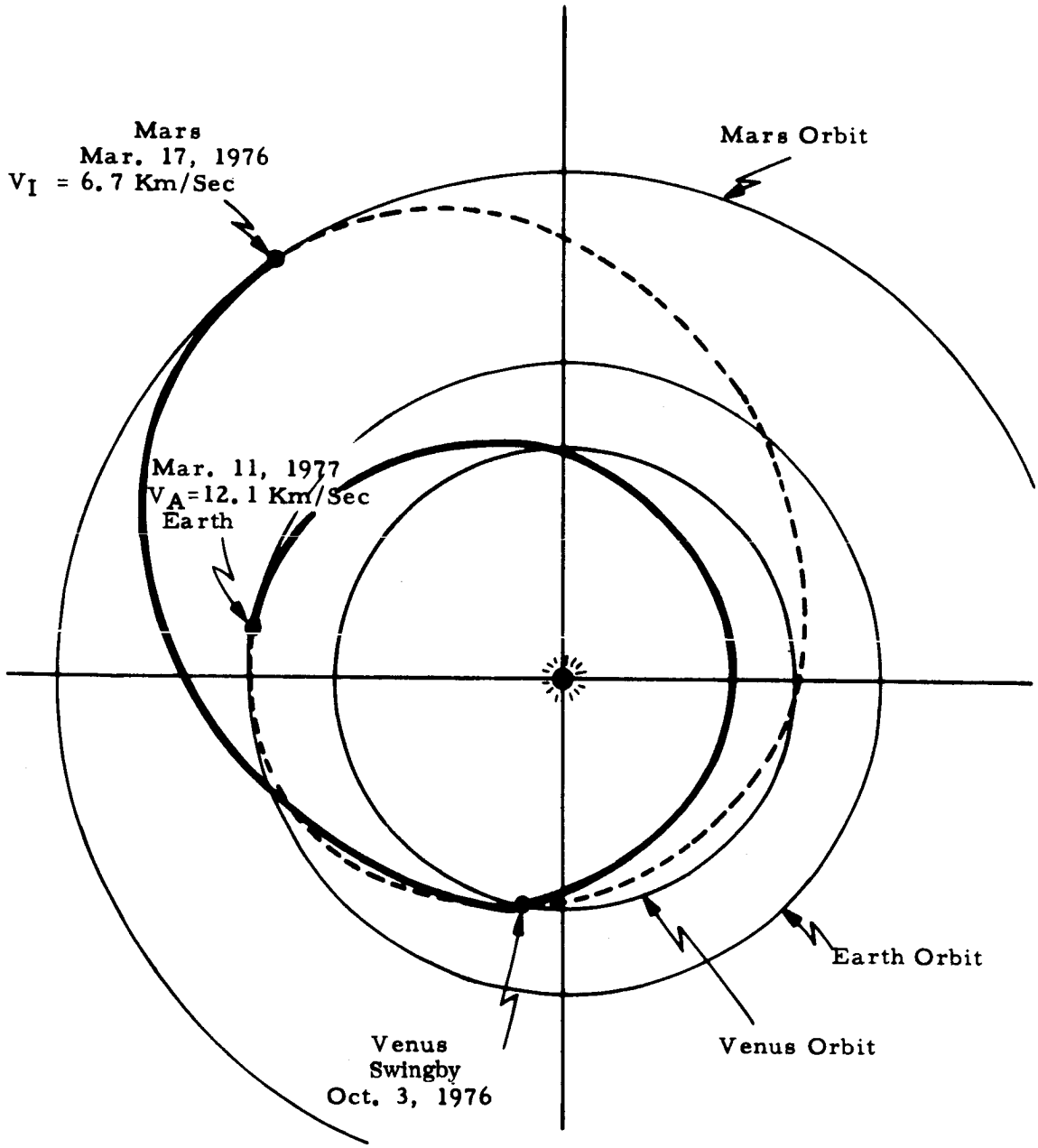

Figure C-4 Ecliptic Projection, Mars-Venus-Earth Trajectory

APPENDIX D

DERIVATION OF ORBITAL ELEMENT GRADIENTS

This appendix contains the derivation of the orbital element gradients with respect to position and velocity state space. The orbital elements considered are those used in the PCEP Program: a, e, q, Ω, i, and ω. The gradients for a, e, and q are identical to those listed in Reference 1 (IEPP). The gradients for Ω, i, and ω have been re-derived.

All gradients are listed below:

$$H^T(e) = \frac{1}{\mu^2 e}\begin{bmatrix} C_3V^2R\left[I-\hat{V}\hat{V}^T\right]R + \frac{h^2\mu}{R^2}\hat{R} \\ \hline h^2V\hat{V} + C_3R^2\left[I-\hat{R}\hat{R}^T\right]\hat{V} \end{bmatrix}$$

$$H^T(q) = \frac{1}{\mu e}\begin{bmatrix} V^2R\left[I-\hat{V}\hat{V}^T\right]\hat{R} - \mu\frac{q^2}{R^2}\hat{R} \\ \hline R^2V\left[I-\hat{R}\hat{R}^T\right]\hat{V} - q^2V\hat{V} \end{bmatrix}$$

$$H^T(a) = \begin{bmatrix} \frac{2a^2}{R^2}\hat{R} \\ \hline \frac{2a^2}{\mu}\hat{V} \end{bmatrix}$$

$$H^T(\Omega) = \begin{bmatrix} -\frac{V}{\beta}\left[\hat{V}\otimes\right]\hat{\beta} \\ \hline \frac{R}{\beta}\left[\hat{R}\otimes\right]\hat{\beta} \end{bmatrix} = \begin{bmatrix} \left[\nabla\Omega\right]^T \\ \hline \left[D\Omega\right]^T \end{bmatrix}$$

$$H^T(i) = \begin{bmatrix} \frac{V}{h}\left[\hat{V}\otimes\right]\left[\hat{h}\otimes\right]\hat{\beta} \\ \hline -\frac{R}{h}\left[R\otimes\right]\left[h\otimes\right]\hat{\beta} \end{bmatrix}$$

$$H^T(\omega) = \begin{bmatrix} \frac{1}{e}\left[\nabla\bar{P}\right]^T \left[\hat{h}\otimes\right]\hat{P} + \cos i \left[\nabla\Omega\right]^T \\ \hline \frac{1}{e}\left[D\bar{P}\right]^T \left[\hat{h}\otimes\right]\hat{P} + \cos i \left[D\Omega\right]^T \end{bmatrix}$$

where

$$H^T(e) = \begin{bmatrix} \left[\nabla\bar{P}\right]^T \hat{P} \\ \hline \left[D\bar{P}\right]^T \hat{P} \end{bmatrix}$$

ϕ = True Anomaly: $R = \dfrac{\frac{h^2}{\mu}}{1 + e\cos\phi}$

where: $C_3 = -\dfrac{\mu}{a} = V^2 - 2\dfrac{\mu}{R}$

$\bar{\beta} \triangleq \left[Z\otimes\right]\bar{h} = \left[Z\otimes\right]\left[R\otimes\right]\bar{V}$

$\hat{\beta} \triangleq \dfrac{\bar{\beta}}{|\bar{\beta}|}$ A unit vector along the line of ascending node

$\hat{P} = \dfrac{Vh}{e\mu}\hat{N} - \dfrac{1}{e}\hat{R}, \quad e\hat{P} = \bar{P} = \dfrac{\bar{V}\times\bar{h}}{\mu} - \hat{R}$

Gradient operations are defined as

$$\nabla = \left[\frac{\partial}{\partial R_1}, \frac{\partial}{\partial R_2}, \frac{\partial}{\partial R_3}\right]$$

$$D = \left[\frac{\partial}{\partial \dot{R}_1}, \frac{\partial}{\partial \dot{R}_2}, \frac{\partial}{\partial \dot{R}_3}\right]$$

where $\bar{R} = R_1\hat{1} + R_2\hat{2} + R_3\hat{3}$

and $\dot{\bar{R}} = \dot{R}_1\hat{1} + \dot{R}_2\hat{2} + \dot{R}_3\hat{3}$

$\hat{X}$, $\hat{Y}$, $\hat{Z}$ are unit vectors defining the reference coordinate system.

$\hat{V}$ is a unit vector in the direction of the velocity vector.

$\hat{R}$ is a unit vector in the direction of the radius vector.

The quantity $[\otimes]$ is defined to be the skew-symmetric cross-product matrix. For example: $[R\otimes]$

$$R\otimes = \begin{bmatrix} 0 & -R_3 & R_2 \\ R_3 & 0 & -R_1 \\ -R_2 & R_1 & 0 \end{bmatrix}$$

REFERENCES

1. Interim Study Report on Navigation and Guidance Analysis for a Mars Mission, Philco WDL Guidance and Control Systems Engineering Department, WDL-TR2359, Palo Alto, California 4 December 1964.

2. Schmidt, S.F., WDL-TR4, The Application of State Space Methods to Navigation Problems, Philco WDL Guidance and Control Systems Engineering Department, Palo Alto, California, July 1964.

3. Kizner, W., A Method of Describing Miss Distance for Lower Interplanetary Trajectories, JPL Publication No. 674, 1 August 1959.

4. Battin, R.N. Astronautical Guidance, McGraw Hill Book Co., 1964.

5. Kalman, R.E., "A New Approach to Linear Filtering and Prediction Problems," J. of Basic Engr., ASME Trans., Vol. 82 D, March 1960.

6. Smith, G.L., Schmidt, S.F., and McGee, J.A., Application of Statistical Filter Theory to the Optimal Estimation of Position and Velocity Onboard a Circumlunar Vehicle, NASA Technical Report R-135, Ames Research Center 1962.

7. Mc Lean, J.D., Schmidt, S.F., and McGee, J.A., Optimal Filtering and Linear Predictions Applied to a Midcourse Navigation System for the Circumlunar Mission, Technical Report D-1208, NASA Ames Research Center, March 1962.

8. Schmidt, S.F., "State Space Techniques Applied to the Design of a Space Navigation System," JACC Conference Paper, 1962.

9. Pfeiffer, C.G., "A Procedure for Approximating the Statistical Description of Errors Resulting from Multiple Midcourse Maneuvers", JPL Internal Memorandum T.M. 312-128.

10. Programers Manual for Quick-Look Mission Analysis Program, Philco WDL-TR2217, Palo Alto, California, 24 January 1964.

11. User's Manual for Quick-Look Mission Analysis Program, Philco WDL-TR2218, Palo Alto, California, 24 January 1964.

12. Advanced Error Propagation Program Under Development for NASA Goddard Space Flight Center, Contract No. NAS 5-9700.

13. Holdridge, D.B., Space Trajectories Program for the IBM 7090 Computer, JPL Technical Report No. 32-223, 2 March 1962.

14. Programer's Manual for Interplanetary Error Propagation Program, Philco WDL-TR2184, Palo Alto, California, 15 November 1963.

15. User's Manual for Interplanetary Error Propagation Program, Philco WDL-TR2185, Palo Alto, California, 15 November 1963.

16. Pines, S., Wolf, H., Goddard Minimum Variance Orbit Determination Program, X-640-62-191, Goddard Space Flight Center, Greenbelt, Md., 18 October 1962.

17. Rohde, P.J., The Scheduling of Measurements for Analysis of an Onboard Navigation System, WDL-TR2600, October 1965 (To Be Published as NASA Contractor Report).

18. Manned Mars Mission Study, Report for NASA Ames, Contract No. NAS Z-1409, By TRN, STL Redondo Beach, California, 28 March 1964.

19. A Study of Manned Mars Exploration in the Unfavorable Time Period (1925-1985), General Dynamics FZM 4039, 4 Volumes, Forth Worth, Texas, February 1964.

20. "Definition of Injection Errors", Unnumbered Memo from MSFC.

21. Victor W.K., Stevens, R., Golomb, S.W., Radar Exploration of Venus: Goldstone Observatory Report for March-May 1961, JPL Technical Report No. 32-132.

22. "Results on Physical Constants and Related Data from the Radio Tracking of Maneuver (Venus) and Ranger II - VII Missions", W.L. Sjogner and D.W. Trask, Journal of Spacecraft and Rockets, Volume 2, Number 5 September-October 1965.

23. Anderson, J.D., Null, G.W., and Thornton, C.T., "The evaluation of certain astronautical constants from the radio tracking of Manier II," AIAA Progress in Astronautical and Aeronautics, Vol. 14.

24. MIT Experimental Astronomy Laboratory TE-5. Appendix O. May 1963.

25. Deerwester, J.M. "Initial Mass Savings Associated with the Venus Swingby Mode of Mars Round Trips", AIIA Paper 65-89, 2nd Aerospace Science Meeting, New York, N.Y. 25-27 January 1965.

26. Battin, R.H., "A Statistical Optimizing Navigation Procedure for Space Flight," ARS Journal, 1681-1696, November 1962.

27. Battin, R.H., "A Comparison of Fixed and Variable Time of Arrival Navigation for Interplanetary Flight", Volume 3, Ballistic Missile and Space Technology, Academic Press, New York, p. 3, 1960.

28. Hartwell, J.G., Danley, J.M., Jones, A.L., Planetary Approach Navigation, Honeywell Aero Document R-ED 28137, 30 April 1964.

29. Harry, D.P., Friedlander, A L., An Analysis of Error and Requirements of an Optical Guidance Technique for Approaches to Atmospheric Entry with Interplanetary Vehicles, NASA TR R-102, 1961.

30. Friedlander, A.L., Harry, D. P., A study of Statistical Data-Adjustment and Logic Techniques as Applied to the Interplanetary Midcourse Guidance Problem, NASA TR R-113, 1961.

31. Carroll, J.E., Lillestrand, R.L., "Error Contours in Interplanetary Navigation", Navigation" Journal of the Institute of Navigation, Vol. 11, No. 2, P. 145, Summer 1964.

32. Smith, G.L., "Secondary Errors and Off-Design Conditions in Optimal Estimation of Space Vehicle Trajectories," NASA TN D-2129, January 1964.

33. Denham, W. F., Speyer, J.L. Optimal Measurement and Velocity Correction Programs for Midcourse Guidance, Raytheon Report BR-2386, 24 April 1963.

34. White, J.S., Callas, G.P., Cicolani, L.S., "Application of statistical Filter-theory to the Interplanetary Navigation and Guidance Problems, NASA Technical Note D-2697, Ames Research Center, 3 February 1965.

35. Study and Analysis of Advanced Spacebourne Detection, Tracking and Navigation System, NAS W 460 Westinghouse Air Arm Division, December 1962.

36. Complication Report for Advanced Spacehouse Detection, Tracking and Navigation Systems Study and Analysis, NAS 8-11205, Westinghouse Defense and Space Center, Aerospace Devision, Baltimore, Maryland, 6 July 1964.